Addis Ababa University

Addis Ababa Institute of Technology

School of Mechanical & Industrial Engineering

Design and Optimization of Solar Thermal Vapor Absorption Refrigeration System Integrated With Phase Change Material for Cold Room Application

By: Firehiwot Matewose (BSc. 2019 G.C)

A Thesis Submitted to the School of Graduate Studies of Addis Ababa Institute of Technology, Addis Ababa University in partial fulfillment for the Degree of Master of Science in Mechanical Engineering (With Specialization Thermal and Energy System Engineering)

Advisor: Dr. –Ing Demiss Alemu

Co – advisor: Demiss Molawerk (PhD candidate)

Addis Ababa, Ethiopia

June, 2023

Addis Ababa University
Addis Ababa Institute of Technology
School of Graduate Studies
School of Mechanical and Industrial Engineering

Design and Optimization of Solar Thermal Vapor Absorption Refrigeration System Integrated With PCM for Cold Room Application

By: Firehiwot Matewose

Approved by the Board of Examiners:

_____	_____	_____
Advisor Name	Signature	Date
_____	_____	_____
Internal Examiner	Signature	Date
_____	_____	_____
External Examiner	Signature	Date
Dr. Araya Abera	_____	_____
School Dean	Signature	Date
Dr. Sosina Mengistu	_____	_____
Associate Director For PG Program	Signature	Date

Declaration

I hereby declare that the work which is being presented in this thesis entitled "Design and Optimization of Solar Thermal Vapor Absorption Refrigeration System Integrated with PCM for Cold Room Application" is original work of my own, has not been presented for a degree of any other university and all the resource of materials used for this thesis have been duly acknowledged.

Firehiwot Matewose	Date

This is to certify that the above declaration made by the candidate is correct to the best of my Knowledge.

Dr-Ing Demiss Alemu	Date
Demiss Molawork	Date

DEDICATION

I dedicate this work to my father Matewose Mada, my mother Mame W/Michael, My big brother Million, my little brother Bereket, my spiritual Father Aba Samuel, my spiritual mother Emahoy welete Mikael and my best friends Issayias and Fikere Mikael

And finally I dedicate this work to my husband who is not alive now Ato Taddese Abera.

Upon whose advice and loving support I drew
courage strength and patience.

ACKNOWLEDGMENT

Prior to rest of the acknowledgements, I would like to thank God for providing me the health and patience to finish this thesis work successfully, as well as for giving me strength during difficult times in my life.

I would like to express my heartfelt appreciation to my advisor, Dr.Ing Demiss Alemu, for sharing his wealth of knowledge and making himself available for guidance at various stages of this work. I'd also like to thank my co-adviser, Mr. Demis Molawerk, for his friendly approach and invaluable material and idea support.

My thanks also go to the Mechanical Engineering Department staffs, particularly Mr. Tamirat Agonafir. I admire everyone who helped me with technical support during my difficult life until this work was completed.

Above all, I owe a lifetime of gratitude to my family and friends, whose love and understanding made all of this possible.

ABSTRACT

Now a day many cooling systems are used in order to keep the food product in the conditioned room. For this cooling effect, mostly conventional compression refrigeration system is applicable which has high-energy consumption and the working fluid of it that is HFCC causes the environmental degradation and ozone layer depilation. Using renewable energy is a promise-able technology to solve the above problem but its energy source is not pretty much. For energy of low quality source absorption-based cooling system is compatible what if it requires energy storage system. This thesis emphasizes optimizing the vapor absorption refrigeration system of performance 7.772 kW. Material that undergoes phase change (PCM) is combined utilizing solar thermal energy to provide cooling capacity, allowing the system to function at night as a backup thermal energy storage system. The cooling load was calculated for 6500 kg of fish is to be stored in 4x2x2.5 m size of the room. By using ASPEN plus software, the vapor absorption refrigeration for this load was optimized and modeled. Ammonia, which is created by distilling an ammonia-water (NH3-H2O) solution in the generator, serves as the refrigerant for the VAR system. The obtained Coefficient of Performance was 0.7, this is a typical performance for a vapor-absorbing system. The power source of VAR system was solar based heat energy where solar radiation is under Hawassa weather conditions. This solar thermal heat energy supplied for 6 hours for VAR system and the remaining 18hrs is provided by PCM storage system. The size of the CPC collector was 28.26 m^2. Additionally, the system's performance is examined in MATLAB integrating with ASPEN plus software. The charging and discharging temperature variation with respect to time for thermal storage is 3.5 and 9.5 hours for minimum solar radiation and 1.5 and 15.5 hours for maximum solar radiation respectively.

Key words: - COP, Cooling load, solar thermal, cold room, PCM, optimization, ASPEN plus, MATLAB, absorption

TABLE OF CONTENTS

LIST OF FIGURES

LIST OF TABLES

LIST OF ABREVATION AND ACRONYMS

ARS	Absorption refrigeration system
COP	Coefficient of performance
CPC	Compound Parabolic Collector
EES	Engineering Equation Solver
EOS	Equation of State
ETC	Evacuated Tube Collector
FPC	Flat Plate Collator
HCFCs	Hydro chloro floro carbons
HCs	Hydrocarbons
HPG	High Pressure Generator
HTF	Heat Transfer Fluid
IIR	International refrigeration institute
LCPUFA	Long Chain Poly Unsaturated Fatty Acid
LHS	Latent heat storage
LPG	Low Pressure Generator
MOGA	Multi-Objective Genetic Algorism
PCM	Phase change material
PR-BM	Peng Robinson-Boston Mathias
PUF	Poly Urethane Foam
PV	Photo Voltaic
R&D	Research & Development
SASCHCS	Solar Absorption Sub Cooled Hybrid Compression System
STARS	Solar thermal absorption refrigeration system
TES	Thermal energy storage
VARC	Vapor absorption refrigeration Cycle
VCRS	Vapor compression refrigeration system
VLE	Vapor-Liquid Equilibrium

Nomenclature

Symbol	Meaning	SI Unit
C_p	Specific heat capacity	kJ/kgK
L,X	Length, thickness	m
K	Thermal conductivity	W/mK
R	Thermal resistance, Universal gas constant, radius	$\frac{m^2K}{W}, \frac{J}{Kmol}, m$
Q	Load	kW
A	Surface Area	m^2
T	Temperature	℃ or K
P	Pressure	bar
V	Volume	m^3
u	Overall heat transfer coefficient	W/m^2K
h	Heat transfer coefficient	kJ/kg
m	Mass	kg
t	Time	sec
d, D	Diameter	m
H	Height	m
$\dot{m}, m_f$	Mass flow rate	kg/s
$\bar{V}$	Molar volume	m^3/mol
N_u	Nusselt number	-
F	Fraction	-
F'	Collector efficiency factor	-
F_R	Heat removal factor	-
C	Concentration ratio	-
Q_u	Useful energy	kW
U_L	Collector heat loss coefficient	W/m^2K
I	Irradiance	W/m^2

Acronyms

θ	Angle
τ	Transmissivity
α	Absorptivity
γ	Correction factor , liquid volume fraction
ε	Emissivity
ρ	Density, (kg/m^2)
η	Efficiency

Superscript

in	Inlet
Out	Outlet
P	Product , pump
max, min	Maximum, Minimum
T	Tank , Total
L , l	Liquid
S	Solid
i, o	Inner , Outer
Melt	Melting

CHAPTER ONE

1. INTRODUCTION

1.1 Background of the Study

Fish is a mainstay in many parts of the world due to its high-quality animal protein source, vital fatty acids, and micronutrients, which are found in far higher concentrations in fish than in diets derived from terrestrial animals [1]. However, it is a delicate food; it spoils easily and can become unsafe. According to a study by the International Refrigeration Institute (IIR), 23 % of perishable goods in underdeveloped nations went bad because they weren't kept in coolers [2]. In many African countries, including Ethiopia, there is a lack of facilities to properly store, transport and consume fish. According to the available information, Ethiopian fisheries do not appear to be managed, however some stocks (such as niletilapia perch in certain lakes) (Hawassa and chemo) exhibit signs of overfishing [3]. Even if there is overfishing, inadequate storage, preservation, and transportation facilities provide the biggest marketing limitation for fish, resulting in a 22 % loss in sales. According to the available information, Ethiopian fisheries do not appear to be managed, however some stocks (such as tilapia and nile perch in certain lakes) (Hawassa and chemo) exhibit signs of overfishing [4]. Many market participants that are interested in owning sizable cold storage facilities and refrigerated transportation also show cash limits. Therefore, it must be refrigerated from the time it is caught until it reaches a consumer’s stove. Otherwise, producers lose their stock and consumers should have to face health problems.

Since it protects the physiological qualities, cold storage is the most popular method for long-distance preservation, storage, and transportation of aquaculture products. By regulating the temperature and relative humidity within the cold storage, it is best approach to keep perishable goods in a natural and healthy condition for a long duration of time. The preservation of perceptual characteristics, the reduction of spoiling, and the extension of shelf life have all benefited from recent advancements in the cold storage of perishables. These advancements are the result of collaboration between physiologists who determined fish require and cooling experts who designed and operated refrigeration equipment to meet those requirements. As a result, since it prevents product waste, refrigeration inside cold room emerge to be a cost-effective investment and operation option [5].

Refrigeration mean an evaporation of refrigerant liquid, which have absorbed heat from the product to make a cooling effect. Food that has to be preserved quickly might benefit from refrigeration. Refrigeration provides significant economic value in addition to halting degradation. The immediate refrigeration processing (cooling and/or freezing) following the harvest, as well as the storage and transit in a low temperature environment, are advised for perishables in order to retain the highest quality of food. Before the invention of mechanical cooling systems , mankind chilled their food using ice and snowpack, which they either collected locally or transported from the mountains [6].

It is necessary to thoroughly examine many specifications and criteria in order to choose the system that is best appropriate for the desired application. When choosing a refrigeration system, some chilled space-related aspects must be taken into account, including the necessary interior humidity, the length of the process, and the temperature at which the product will be stored [7]. Additionally, the packing inside (box, bulk, plastic tray, or cardboard) is one more aspect which needs to be considered. When choosing a refrigeration system, important considerations include product variety and quantity, storage times, investment prices, and operational costs of various technologies [5]. As per the researchers depending on the power source basically the type of refrigeration systems classified in to two: vapor compression and vapor absorption. The absorption-based cooling system uses low grade power source such as solar, geothermal, biomass and waste heat energy from various power plants.

Making the cold room solar driven system is an attractive solution as sun energy is the massive prevalent origin of energy on globe. Ethiopia also receives a lot of solar insolation, with about 365 days of sunlight annually. Through cooling processes that are either powered by electricity or by solar heat energy may be utilized to provide a cooling effect [8]. The electrically powered system uses a photovoltaic (PV) solar energy system, in which the sun energy is first transformed to electrical energy and at that time applied to creating the cooling effect in a manner similar to traditional techniques. The thermal system uses solar heat energy to run an absorption refrigeration system's generator. This solar thermal system is not available at most time of the day so energy backup system is required for the rest time application.

Thermal energy storage is the non-permanent storage of heat energy in the form of hot or cold storage substances. [9]. A thermal storage system typically consists of a medium for storing energy and tools for adding and removing heat from the medium. The researchers identifies that sensible heat storage, latent heat storage, and thermochemical thermal storage are the three ways that heat energy is kept [10].

Many researchers are conducted on this storage method for thermal energy for different applications. Even though solar thermal storage systems for cold rooms have been the subject of extensive research, there are still no firm conclusions regarding the total effectiveness of the ARS with thermal storage in definite cooling circumstance. With this in mind, the purpose of this research is to contribute definitive remarks on the efficacy of the ARS with hot storage PCM under the climatic conditions of Hawassa in Ethiopia using the numerical model.

1.2 Drawbacks of Current Refrigeration Systems

The following table provides a brief summary of existing ARS and their shortcomings.

Table 1-1 Existing absorption refrigeration system and their drawbacks

No	Power source for ARS cold storage	Working principle and	Draw back	Reference
1	Conventional type of compression refrigeration system for cold storage	This type of refrigeration system uses the mechanical compressor in order to do this heat must be moved from a low to a high temperature which utilizes high power consumption. It has a good performance.	• The increasing global energy demand and CO_2 emission is expected to increase. • causes 65% of CO_2 emissions • The large amount of energy needed to run the compressors	[11], [12]

2	Absorption refrigeration system for cold room	This type of heat driven refrigeration system uses low-quality energy sources include biomass, geothermal, solar and squander heat energy from thermal systems. They are regarded as having minimal overall costs and operating in an environmentally beneficial manner. The refrigerants used in absorption systems are not greenhouse gases and do not deplete the ozone layer.	•Lower performance coefficient than the traditional system; • Compared to the typical system, the startup time is longer; • The usage of ammonia might generate a foul odor as a result of system leakage.	[13] [14], [15].
3	solar charged VAR system for cold room application	This kind of cold storage uses a solar-assisted vapor absorption refrigeration (VAR) system, which passes heat-carrying HTF through a collector that collects solar energy. The VAR generator is then given heat in order to keep the system running.	• The size of system will be very large • This system is not applicable at solar radiation is not available during night time.	[16], [7]
4	Hybrid powered absorption refrigeration system for cold room	The two type of power source is used in this type of cold room. For instance the solar thermal-	• The system size is very large	[17]

		photovoltaic power cold storage is presented in the literature. In order to run the system's several components in the hybrid system is crucial. The solar thermal operates the generator of ARS and the PV operates the pump and fan unit of the system		

1.3 Statement of problem

Traditional cooling methods that employ toxic refrigerants use more energy and result in peak loads, which have an adverse effect on the environment. Regarding energy diversification and environmental protection, vapor-compression cooling cannot compete with absorption refrigeration technology. A low-quality heat source, such as geothermal, biomass, solar, or process/waste heat, is often used to drive an absorption refrigeration system. Utilizing solar energy is appealing mostly because of supply and demand issues in practical applications. The period of solar radiation is constrained inside a day, however the absorption system ought to be used all through the day. To get around fragmentary behavior of solar energy and fluctuating cooling requires, thermal storage technologies are crucial. Several simulations, experiments, and review research have been done on solar driven absorption system integrating with TES device to get a cost and energy-effective, continuous operation, environmentally responsible and small in size absorption system. Most of the research rely on the incorporation of absorption system with hot thermal energy storage system, combined different system, cascading system, cycle modification, multiple effect system, and use of different working fluids to enhance the performances of cooling system. But compared to more connected vapor compression systems, absorption cooling methods are not seen as competitive, because of lower coefficient of performance, massive size, high initial price, and intermittent operation and difficult to gain steady COP. In Ethiopia also whatever several studies are conducting in this sector but still it needs more study on it. To fill this gap further research need to be performed

like optimization of generator temperature and COP of the ARS, exploring further study on usage of thermal energy storage, accurately sizing the TES, modifying the cycle etc.

1.4 Objective of the Study

1.4.1 General Objective

The main goal of this investigation is to design and optimize a hot storage PCM-integrated solar thermal vapor absorption refrigeration system for use in cold rooms.

1.4.2 Specific Objective

The particular aim of this study: -

- Designing of cold room and cooling load calculation
- Thermodynamic analysis and optimization of Vapor Absorption Refrigeration System by make use of ASPEN plus to determine maximum COP of the system
- Develop mathematical model for solar collector and PCM storage system and simulate with MATLAB interface and integrating with ASPEN plus
- Performance analysis of charging and discharging of hot storage PCM using MATLAB

1.5 Relevance of the Study

The results of this research will directly assist the government, angler, and investors around the lake, loges and the user by reducing post harvesting losses and spoilage due to the lack of storage. It is also important for the user to keep their healthiness and to serve to them fresh fish. Implementing the renewable energy source, improves the fish storage systems which is very important and promising technology. This renewable energy can provide a variety of advantage on environmental, economic, healthy and other benefits for the country.

Beside that this paper will make an opportunity for the researchers to do further detail and modification on the absorption-based cooling system and also for the cold room application.

1.6 Scope and Limitation

This study will intended to find solar thermal vapor absorption refrigeration for cold room with objective of performance analysis with non-grid power system and PCM at nighttime, which is eco-friend to the environment. This research focus on performance analysis of the VARS integrated with solar thermal and PCM. This cold room will simulated only by focusing the sunshine is available. The cold room operating during summer season will be future work.

The thermal solar energy source is used to operate of the generator as well as the PCM but the power source for the pump and fan coil unit has no determined yet in this research. This may the future work for further detail of this topic.

In order to make simplify the system the used method is quasi dynamic simulation because of the ARS is steady state condition but remain one is dynamic or transient system simulation.

CHAPTER TWO

2. METHODOLOGY

The approaches used to accomplish the research project's goal are covered in this chapter. The thermal storage of hot storage PCM powered by a solar collector with ARS for cold room application are computationally simulated and modeled. The performance analysis will then be examined in relation to PCM's charging and discharging operation. The simulation of ARS with thermal storage will be put into practice to deal with these tasks. As a result, the methods listed below will be used.

2.1 Literature Review

The literature on working principle of absorption refrigeration system and its types will be reviewed. The various forms of energy production will be examined, with a focus on solar energy for ARS whether or not thermal energy storage is used. We'll review the materials utilized as heat transfer fluids and storage medium.

2.2 Collection of Data

The mentioned information will gathered from the accessible literature and other sources.

- Data on sun radiation and surrounding temperatures will be gathered from the Ethiopian Metrological Agency for Hawassa.
- Storage capability (cached fish per day) required by anglers around the lake Hawassa(Amora gedel)
- From reliable sources, the physical and chemical characteristics of heat transfer fluid and storage material will determined.
- Data among experiments on PCM capsules and an absorption refrigeration system

Storage materials (PCM) and insulating materials have been chosen as the two key material categories. Materials used to store heat can be chosen based on factors such as thermal conductivity, heat capacity, availability in area, etc.

Selection of insulating materials will made according to their less heat conductivity and accessibility in the area. Additionally, the availability, reflectivity, and absorbance of solar irradiance will be taken into account while choosing the materials for compound parabolic solar collectors integrated

to absorbers. Additionally, the cold room's construction materials will be chosen depending on their thermal conductivity and accessibility.

2.3 Physical Model

After sizing each component according to the amount of energy that must store to reach the requirements, a schematic design of the system integration will be shown in the physical concept. Then will discuss about the charging and discharging process's system flow and operating theory.

2.4 Mathematical Model

For heat transfer fluid and storage channel, energy transfer equations of the system that combines a CPC collector and PCM storage are developed. That is, PCM capsules in liquid and heated storage. The absorption system that integrates thermal storage also has an energy equation included.

2.5 Computational Model

Aspen Plus platform will do thermodynamic study of absorption-based cooling system because it has been chosen for process simulation optimization. The PCM storage system and the compound parabolic solar concentrator that fuel the ARS generator will be modeled using MATLAB software. The energy balance in space and time will be discretized using the finite difference approach. In addition to simulating the geographical and temporal phases of charging and discharging scenarios, the computer model will also depict the transient temperature distributions of PCM and HTF. The quantity of stored energy during the course of solar thermal storage will be roughly estimated.

2.6 Computational Model Validations

By comparing simulation results to published experimental findings, the accuracy of the results will be confirmed. The ARS model will be validated with experimental work.

2.7 Findings and Discussions

Under this heading, the computational model's findings will be presented and discussed. We'll talk about the temperature distributions in the storage during charging and daytime ARS operation. There will be presentations of the thermal storage efficiencies, COP of ARS, and overall efficiency. We'll investigate the melt portion of PCM thermal storage.

CHAPTER THREE

3. LITERATURE REVIEW

3.1 Invention of Cold Storage Room

Charles started the invention of fish storage in cold room at 1957 in United States department of interior fish and wild life service. They have construct the cold-storage plant that had freezing, handling and storage rooms fisheries goods of several kinds [18]. This cold storage facility is made up of a building enclosed in an insulating and moisture-proofing shell. With a capacity of 2,000,000 cubic feet of chilled space at -5^{o}F to -10^{o}F, the design of a single store warehouse includes a rectangular building that is more than 400 feet square. They have used diesel driven compressor of variable speed to held the temperature at -5^{o}F for the cold storage. This plant consumes high energy and requires large space.

The need for a better lifestyle and more comfort has grown significantly since the industrial revolution. A growing number of energy-intensive technical items and equipment are being introduced virtually daily to meet these demands. Fossil fuels such as: coal and natural gas are currently used in majority of power plants due to their widespread availability and low cost, particularly in Gulf region. But these systems generate dangerous gases like CO2 and NOx, etc., which are bad for the environment and all living things [15]. By constructing typical energy-hungry vapor-compression cycles, the greatest amount of energy in grid of nations located either hot or cold regions employed to offer cooling or heating, respectively. For the compressor to function during these cycles and provide the system's essential cooling or heating, a significant quantity of energy is used. This excessive energy usage has an impact on both the environment and the individual in terms of operating costs. Therefore, it is more important than ever to develop air conditioning, cooling, and refrigeration systems that are more cost effective, more environmentally friendly, and can be powered by low-grade heat sources, like solar, geothermal, biomass, as well as process/waste heat.

3.2 Absorption Refrigeration System

3.2.1 System Description

A cooling system that uses absorption principle is referred to as absorption refrigeration. Due to the launch of absorption process to cooling industry, it is now feasible to build cooling system using less electrical energy than with conventional vapor-compression cooling systems. Because absorption cooling technology is widely employed in practical applications, several absorption refrigeration cycles with high performance have been developed for both home and commercial uses [15].

Solar, geothermal, and industrial waste heat all can be used in environmentally friendly absorption refrigeration system. As result, there is ongoing work and plenty of research and development (R&D) in the literature to make even more advancements. These R&D can be split into different classification, including arrangement types, energy and exergy analysis, thermo-economic analysis, effects of phase change materials, and alternative fluids [19]–[22]. This research have studied on the performance of ARS and effect of phase change materials on it.

3.2.2 Working Principle

As seen in the Figure 3-1 below, the components of a simple absorption cooling system include generator, absorber, condenser, evaporator, pump, and two expansion valves presented by Dincer [15]. The generator receives heat before the strong solution arrives at state 2. On basis of difference in saturation temperatures between refrigerant and absorbent, refrigerant is separated from a solution by heating this strong solution. In states 3 and 4, the generator releases the vaporized refrigerant and the weak solution, respectively. Following its entry into condenser, where it rejects heat to cooling fluid, the vaporized refrigerant at state 3 eventually exits at state 5 as a saturated mixture. The saturated mixture then moves to condition 6 and enters the evaporator after passing through

expansion valve, which causes sudden drop in pressure to enhance saturated mixture's vapor concentration. The saturated refrigerant mixture is in the evaporator.

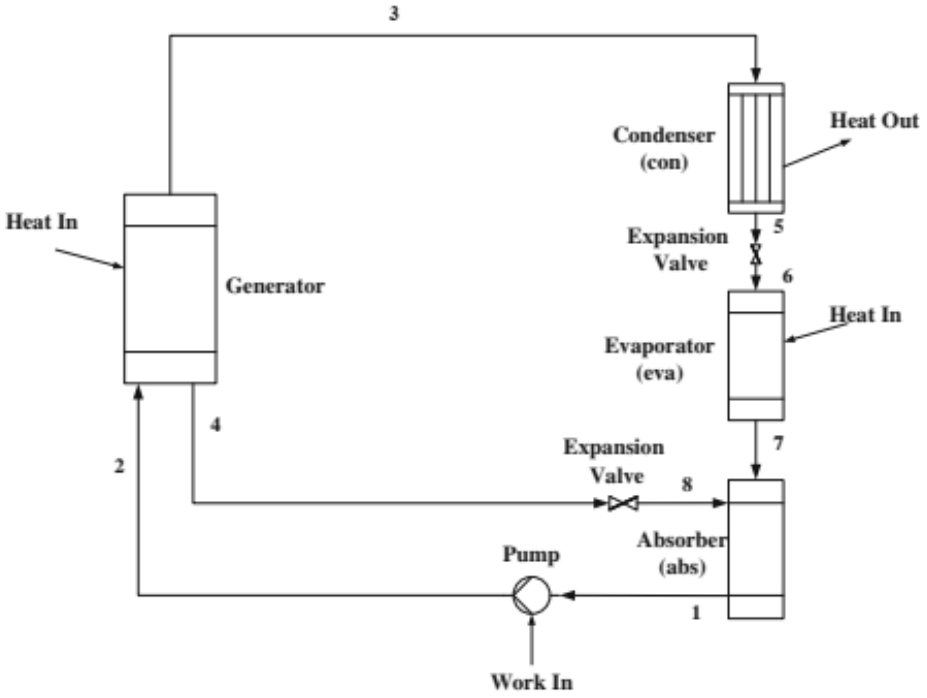

Figure 3-1 A schematic for a simple absorption cooling system [15]

3.2.3 Types of Absorption Cooling System

The creation of a cooling system uses low-grade energy and can reduce amount of power required for cooling or heating. The absorption refrigeration system is one such cooling method. According to Figure 3-2, three different types of absorption refrigeration systems are: single effect, half effect, and multiple effect. Based on number of generators employed and how they are interconnected, this classification is made [15]. Different type of absorption refrigeration system is well studied in the literature.

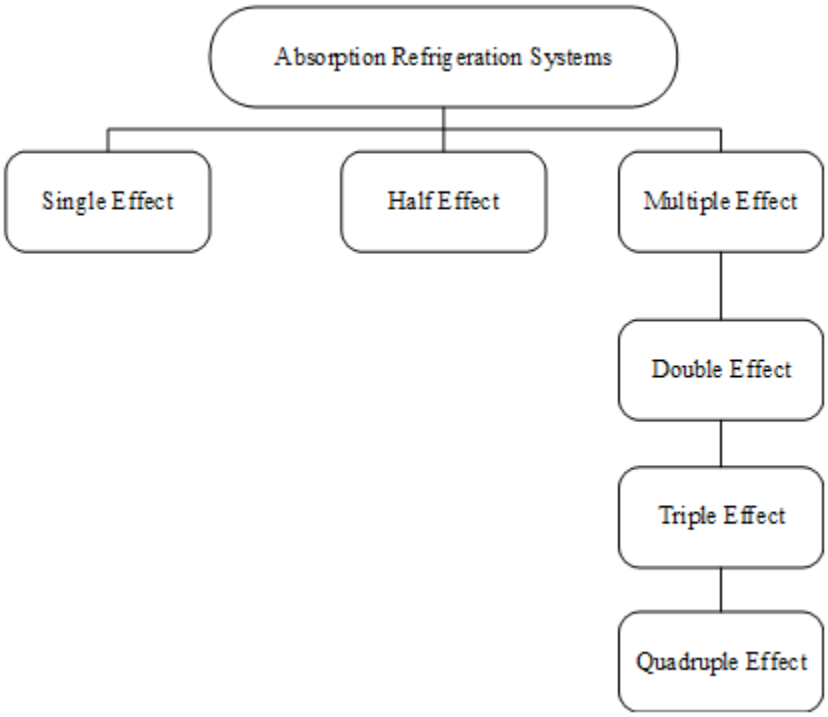

Figure 3-2. Classification of absorption refrigeration systems

3.2.3.1 Single Effect Absorption Refrigeration System

Most basic type of single effect absorption refrigeration system includes an expansion valve set, generator, condenser, absorber, evaporator and pump. According to the application and the available space, these components may be set up either in series or in parallel. For instance Ketafi et.al have demonstrated Water-lithium bromide pair was used in a thermodynamic study of single stage absorption refrigeration system, and theoretical cycle results were reported and compared with another mathematical model. It has contain a single components as shown in Figure 3-3. In the context of this investigation, a simulation software using Matlab was also created. According to the simulation outcomes, the cycle's COP rises as the temperatures of the generator and evaporator rise while falling as they rise for the condenser and absorber. With generator temperature of Tg = 92 °C, which is close to figure provided by Yazaki manufacturer, the system's COP reached its maximum value of 0.77.

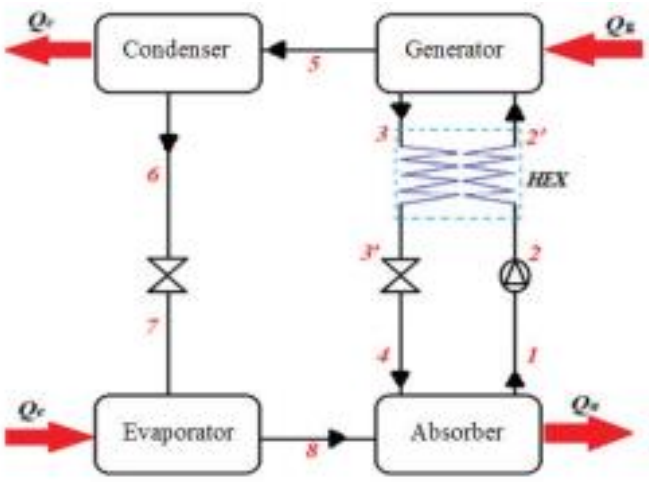

Figure 3-3. Simple effect Absorption cooling cycle [23]

3.2.3.2 Double Effect Absorption Refrigeration System

According to Figure 3-4, a double effect absorption refrigeration system features two generators and more than two heat recovery heat exchangers compared to a single effect absorption refrigeration system. The thermodynamic simulation of using a dual-effect series flow absorption system with water and lithium bromide as working fluids and a variety of heat sources was discussed by [20]. To compare the result of operating temperatures on High Pressure Generator's (HPG) heat capacity and exergy destruction, system's coefficient of performance (COP), and mass flow rate of three different heat sources (hot water, hot air, and steam), a parametric study is being carried out. The outcome demonstrates that when temperatures of heat sources rise, energy destruction likewise rises, while needed flow rates of the sources fall. Compared to hot air, hot water requires less flow. Increases in HPG's operating temperatures reduce HPG's exergy destruction. At lowest source temperature, lowering amounts to 40 percent for hot air, 42.8 percent for steam, and around 45.6 percent for hot water. In order that hot air applications show highest exergy destruction value.

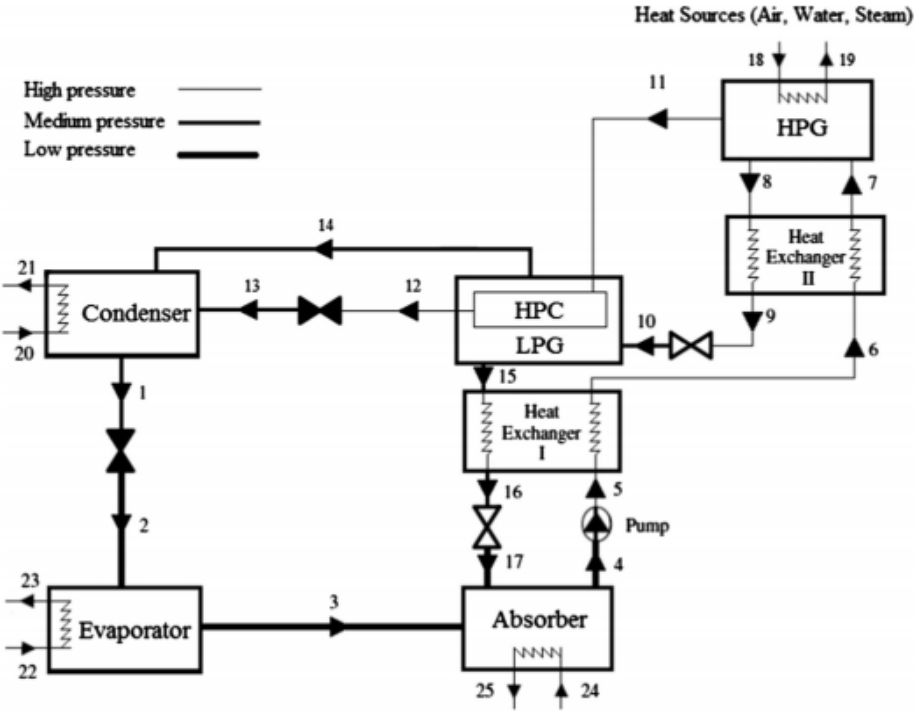

Figure 3-4. Flowchart for double effect series flow absorption refrigeration system [20]

3.2.3.3 Refrigeration systems with triple and quadruple effect absorption

A triple effect absorption refrigeration system has four energy retrieval heat exchangers, two expansion valves, a pump, three generators, absorber, condenser, and evaporator. The research on multiple effect absorption cooling systems—beyond the triple effect—has been prompted by a recent development in the field of absorption refrigeration systems. A quadruple effect absorption refrigeration system is one such system. It comprises of four generators, absorber, condenser, evaporator, two expansion valves, pump, and five heat recovery heat exchangers [15].

3.2.4 Required Amount of Heat Sources

An absorption cooling system functions primarily as heat-driven cooling system of low quality, means the amount of cooling it can generate depends on the system's operating temperature. A single effect absorption refrigeration system has temperature operating range of 80 to 150 °C and may produce cooling of 1 to 100 tons. For double effect absorption refrigeration system may produce cooling of 1 to 1000 tons and requires a working temperature that is somewhat higher than single

effect system, ranging from 120 to 230 °C. A triple effect absorption refrigeration system, has temperature range of 150–230°C, is a more sophisticated absorption refrigeration system that is currently undergoing lab-scale experimental examination. A triple-effect absorption cooling system can handle huge [15].

3.2.5 Working fluids of Vapor Absorption Refrigeration System

The system of absorption refrigeration, the working fluid is referred to as the "absorbent" or "refrigerant". According to absorption refrigeration systems, the refrigerant is a combination of two fluids that is employed in a way which makes one fluid's saturation temperature lower than the other. On the basis of the combination being utilized and working environment, the fluid with lower saturation temperature is chosen. The other fluid serves as absorbent which absorbs lower saturation temperature fluid, which works as refrigerant, in absorber. As illustrated in Figure 3-5, there are five groups of refrigerants utilized in absorption refrigeration systems: halocarbons, hydrocarbons, inorganic compounds, azeotropic mixes, and nonazeotropic mixtures.

An absorption refrigeration system uses a number of working fluids, including ammonia-water, lithium-bromide-water, Tridroxide-water, and Alkitrate-water. Among these, ammonia-water and lithium-bromide-water are the most often utilized. Due to its high performance coefficient and simplicity of management, lithium-bromide-water solution is chosen for domestic air-conditioning applications. The high operational expenses that result from corrosion and crystallization problems at working temperatures over 473.15 K, however, are a significant disadvantage of the LiBr-water system. Lithium-bromide-water working fluid's working temperature constraint prohibits it being employed on broad scale, and pricey salt required in system to address the corrosion problem raises the system's operating costs. Comparatively speaking, the ammonia-water system [15].

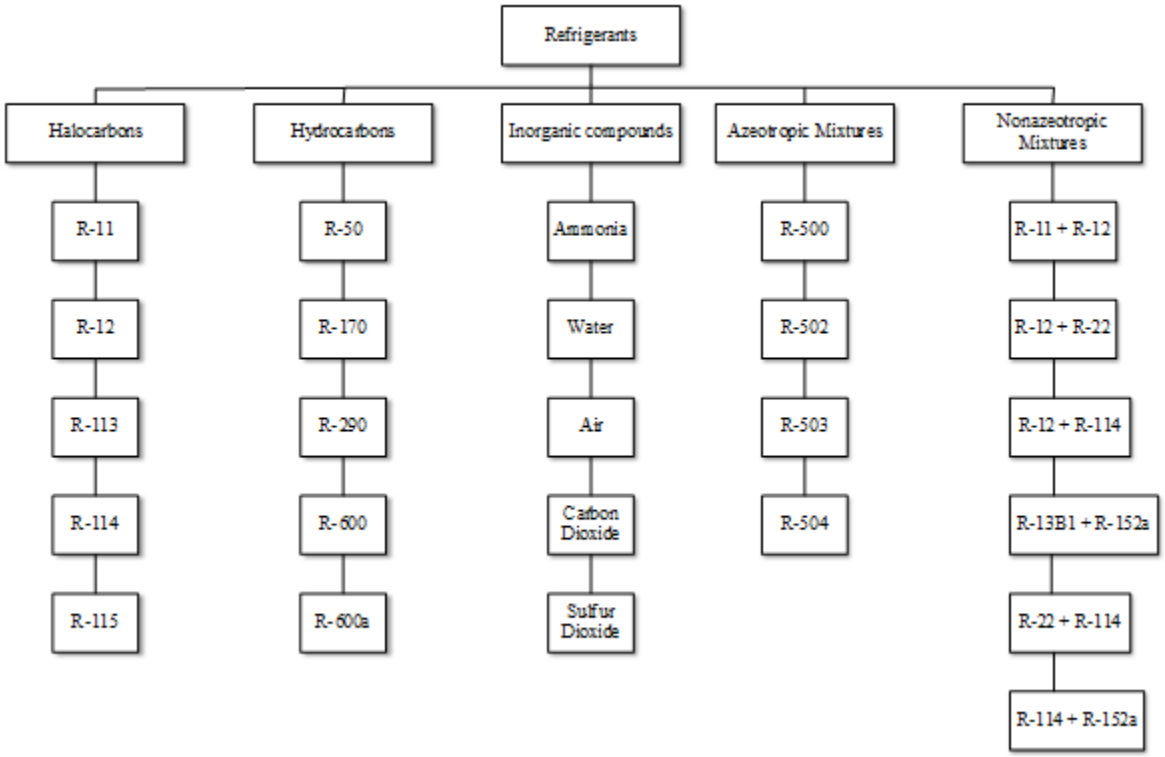

Figure 3-5 Refrigerant classification for varied applications

3.3 Energy source for the absorption cooling system

Absorption cooling systems is strong candidates to integration with waste energy and renewable energy sources because of their relatively low-grade heat-dependent characteristics. Several energy sources include:

3.3.1 Geothermal Energy

The geothermal source temperature is more than 90 °C, geothermal energy sources may also utilized to heat absorption refrigeration systems.

3.3.2 Power Plant Waste

Absorption refrigeration systems may be connected with other industrial units, such as power plants, to recover low-grade waste heat in addition to using renewable energy sources. Megawatt-scale

steam power plants reject heat from their condensers at high temperatures, which can be utilised to supply substandard heat to the absorption cooling system. By using less energy, poor-quality waste heat from power plants may be recovered and used to provide cooling that can support the demands of the facility. This can help the facility become more efficient and cost-effective.

3.3.3 Solar Energy

Solar energy is most alluring energy source for absorption refrigeration systems. Almost all types of solar thermal systems, including concentrated flat plate, evacuated tube, parabolic trough, and parabolic dish, can supply a required operating temperature for absorption cooling system. This makes it a particularly appealing source of energy.

3.3.3.1 Classification of solar energy

Solar energy can classified in to two based on mode of energy conversion which is electrical and thermal energy as shown in Figure 3-6.

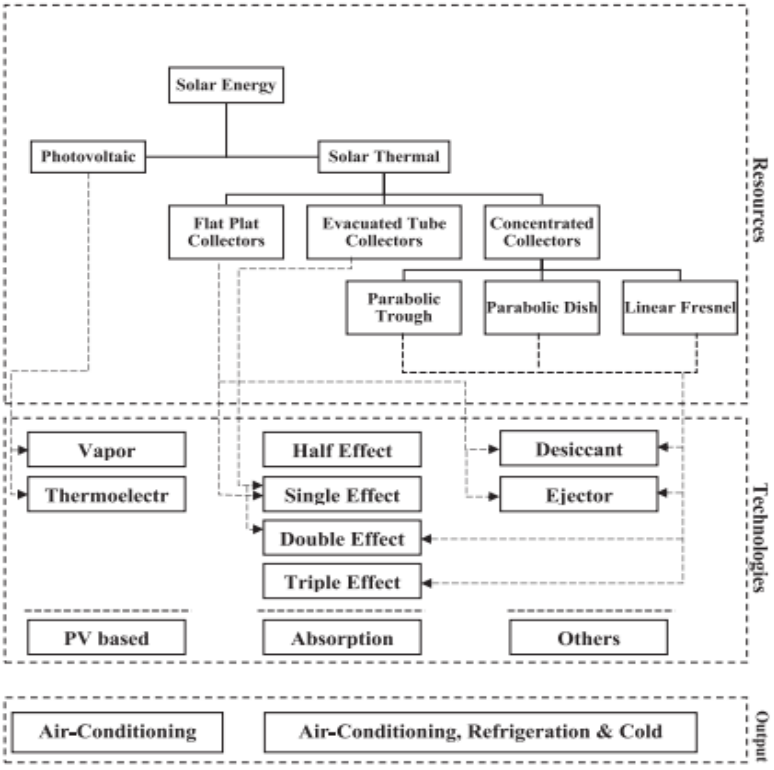

Figure 3-6 Different combinations solar integrated cooling technologies [24].

3.3.4 Other Sources

Nuclear power facilities, which reject low-grade heat at comparatively high temperatures and may employ a portion of that heat to provide huge cooling from triple effect and quadruple effects absorption cooling systems, are another extremely appealing heat source for absorption refrigeration systems.

3.4 Other Researchers Work

Hmida et al. discuss a cold storage room energy improvement study that was done. In this room, an ammonia/water absorption system is employed to supply necessary refrigeration capacity. The mathematical model is developed to study a behavior of cold storage areas while taking into account regional climatic factors and interior cold room temperature. Fruits are first pre-cooled in an adjacent room with an indoor temperature of 6°C in order to prevent the cooling load variance, as demonstrated in Figure 3-7. The Matlab program R2016a is used to calculate the monthly cooling load. A fair agreement between the experimental and numerical findings was achieved with a relative error of 1.5% when modeling thermal behavior of a cool room with a usable volume of 98 m3 and a capacity of 40 tons. With an 8 kW cooling load and an ideal coefficient of performance (COP) of around 0.74, the required heat flux in generator is roughly 11 kW [7].

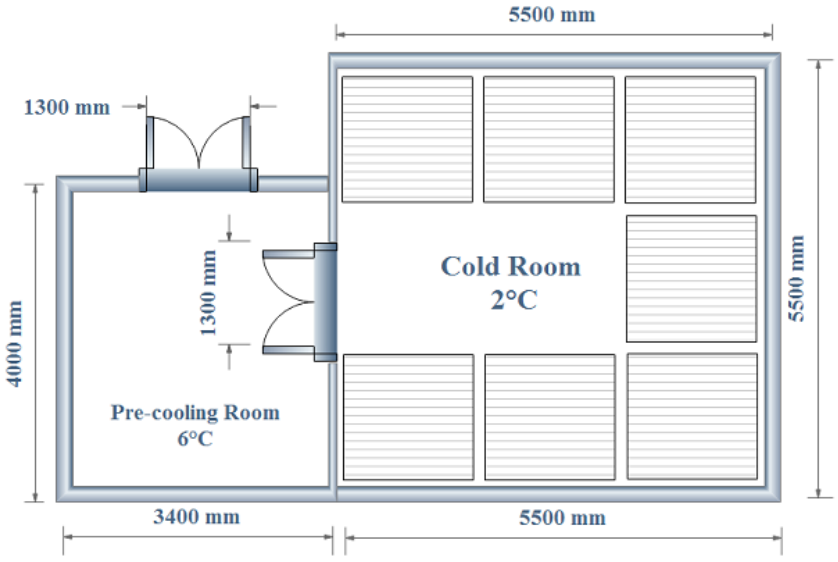

Figure 3-7. Cold room dimensions [7]

For further improvement of cooling capacity of cold storage Yongrui et al presented a cost effective energy-saving option for the cold storage cooling system is solar absorption-subcooled compression hybrid cooling system. It has been shown in Figure 3-8 that in order to reduce the effort required by the compressor, through a closed water cycle, the absorption subsystem's cooling power cools the refrigerant of compression subsystem. When the top layer of storage tank reaches a temperature greater than 60 °C, hot water pump 2 is turned on to drive the absorption subsystem. Pump 3 of the closed water cycle begins when pump 2 turns on, delivering the absorption subsystem's cooling output to compression subsystem's sub-cooler. Pumps 2 and 3 are turned off if the top layer of storage tank's temperature is less than 55 °C since the hot water's temperature won't be high enough to operate absorption subsystem. Only the compression subsystem is in use in this situation to fulfill cooling requirements for cold storage. An approach for resolving both confined and unconstrained optimization issues is to use genetic algorithms. The optimization is subject to the restriction that the collector area be no more than 4000 m^2. It is established that for the scenario when the collector area (2000 m^2) is half available area, the ideal design is as follows: an absorption subsystem size of 0.04-0.06 kW/m^2 with a storage tank volume of 40-60 L/m^2. 68.8 kWh/m^2 is the maximum yearly electric energy savings. The minimal payback period for solar absorption-subcooled compression hybrid cooling system is 4.96 years, and it is commercially feasible for cold storage without any subsidies.

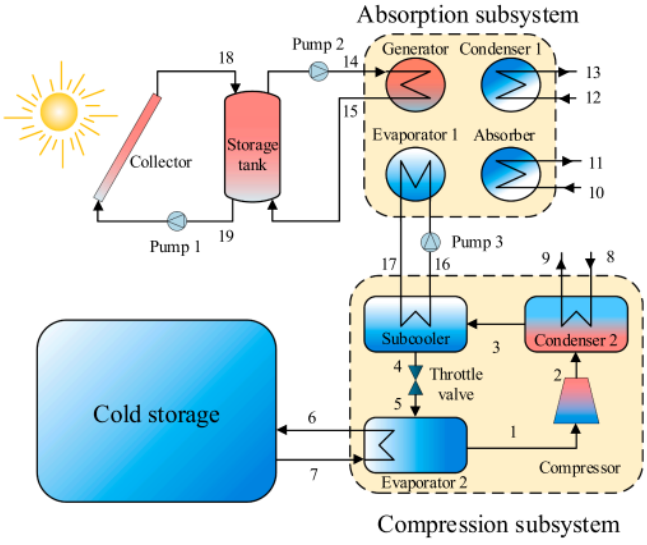

Figure 3-8. Schematic diagram of SASCHCS [25]

Boris Huirem et al uses first and second principles of thermodynamics, 17.5 kW lithium bromide-water (LiBr-H2O)-based vapor absorption refrigeration system has been provided. The condenser and absorber of a machine, where cooling water is cycled for rejecting the heat load, are connected by a square fiber reinforced plastic (FRP) counter flow cooling tower with honeycomb-type PVC infill. As seen in the Figure 3-9 below, a cooling chamber is connected to machine's evaporator where chilled water is created and cycled to create cold air within the chamber for chilling stored fruits. Additionally, it has a control panel where temperature, concentration, and flow rate of the working fluid (LiBr-H_2O) are all recorded and shown during the process. Using Design Expert-12 software, model assessed vapor absorption system's ideal performance metrics, such as COP, ECOP, TED, etc., for uses such as fruit and vegetable transit storage or on-farm chilling.

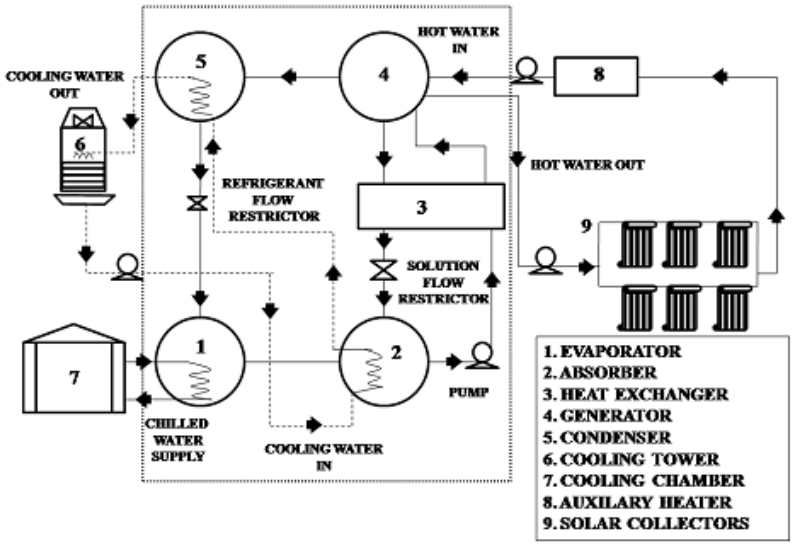

Figure 3-9. A schematic illustration of a solar-assisted single effect LiBr - H2O vapor absorption refrigeration system [18]

Basu and et al. presented in Figure 3-10, generator and evaporator temperatures for VARS are set at 75°C and 10°C, respectively, with a storage temperature of 10°C. The average chiller COP was determined to be 0.8 for cooling area and chilling the water, compared to 1.3 for creating ice alone. At T_{gen}=120^oC, with average condenser and evaporator temperatures of 34.5^oC and -2.2^oC, respectively, maximum COP (0.8) was discovered [17].

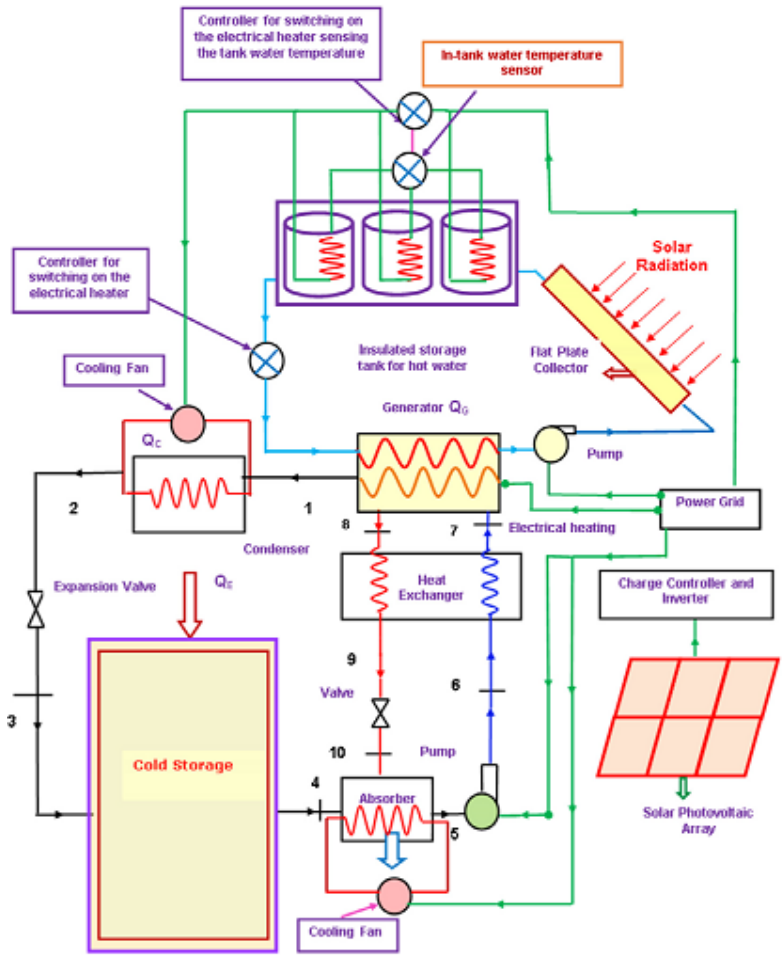

Figure 3-10. Schematic of potato cold storage driven by solar thermal photovoltaics [17]

Absorption chillers powered by solar energy can provide continuous cooling, Mohammed et al. considered two additional storage units that are connected with the primary chiller come in form of cooled water and ice. Depending on the needs for cooling, the system can operate in a variety of modes. Experimental testing of the system is done using different storage units, and the findings are then reported. The average chiller COP was determined to be 0.8 for cooling area and chilling water, compared to 1.3 for creating ice alone.

3.5 Thermal Energy Storage

The biggest drawback of solar energy is mismatch between energy supply and energy demand since it is time-dependent. In solar vapor absorption systems, solar collector's energy is used to provide

heat to generator; as a result, it must provide a steady heat input to the absorption chiller during whole process. Thermal energy storage (TES) may therefore become a significant concern when energy is available but cannot be supplied to the operation. Due to its potential for load reduction, energy savings, and capacity to overcome the drawback of intermittent energy supply and demand, TES is a well-studied and utilized technology.

Because of its high energy storage density and long-term storage capacity, absorption thermal energy storage is desirable for the use of solar energy, waste heat, off-peak power, and other renewable energy sources. In recent years, there has been a thorough investigation of absorption thermal energy storage using thermodynamic cycles, working pairs, and system designs for a variety of purposes [10]. In general, the mismatching could be corrected by utilizing thermal energy storage, which is critical for future low-grade energy and off-peak electricity consumption.

3.5.1 Material Properties for Solar Thermal Energy Storage

The qualities of the selected thermal energy storage materials affect how well TES systems function. In accordance with specified criteria of the application domains, thermos-physical characteristics of thermal energy storage materials should be stated in the following aspects [29].

- Melting point: The melting point of phase change materials should be close to the operating temperature range of the TES system. Density: High density improves energy storage density, resulting in a smaller TES system volume.
- Latent heat of fusion: The latent heat of fusion of phase transition materials ought to be quite high. The system's energy storage density is improved by high latent heat of fusion.
- Specific heat (Cp): High specific heat should characterize sensible heat storage materials. The system's energy storage density is improved by high specific heat.
- Thermal conductivity: High thermal conductivity accelerates required pace of thermal charging and discharging.
- Super cooling: Super cooling should be kept to a minimum while freezing phase shift materials. At a temperature as near as feasible to its freezing point, storage material should totally freeze.

- Cost and availability: Lower storage material prices result in lower capital and operating costs. They should be widely available.
- Thermal stability: High temperatures shouldn't cause them to disintegrate. This increases the material's ability to store energy and provides a broader working temperature range. Even after prolonged thermal cycles of heating and cooling, a material's characteristics should remain constant.
- Chemical stability: Longer lifespan of energy storage facility due to storage materials with a high chemical stability. Volume change: The volume of phase-change materials should only slightly vary during the process. Low thermal expansion coefficient is another need for material. The size of the container is increased by significant volume changes. Phase segregation problems are also brought on by large densities differences between two phases.
- Non-toxic: They shouldn't be hazardous to the environment.
- Non-corrosive: Due to container corrosion, thermal energy storage materials that corrode severely shorten the life of energy storage plants.
- Flammability: They should not explosive or flammable.
- Vapor pressure: In the range of working temperatures, they ought to have little vapor pressure. High temperature pressure confinement is necessary for high vapor pressure. It also calls for pricey insulation.

3.5.2 Types of Thermal Energy Storage

Thermal energy is stored in three ways: sensible heat storage, latent heat storage, and thermochemical heat storage [30].

In **sensible heat storage**, a material's heat capacity, which depends on the volume of medium and temperature variation, stores thermal energy. Due to their large thermal mass, liquid or solid storage media (such as water, oil, molten salts, rocks, metals, and others) are frequently utilized. [29], [31]. Sensible heat storage has a wide range of applications, but it has a poor storage capacity and substantial sensible heat loss, necessitating a large system volume and insulation for long-term storage. Additionally, because its output temperature is lower than its intake temperature, additional external methods, such as heat pumps, must be used to raise it. [32].

In **latent heat storage,** enthalpy of melting, vaporization, and sublimation i.e., when substance transforms from solid to liquid, liquid to gas, and solid to gas are stored when a material undergoes a phase change at a certain temperature. The solid to liquid phase change is preferred despite the fact that enthalpy of melting is lower than other method since it often results in a minimal change in volume. [33], [34]. Additionally, a variety of phase transition materials may provide melting temperatures over a wide range, making latent heat storage useful for thermal energy storage under various operating situations [29]. In this context, a wide range of substances, including as ice, hydrated salts, parafn waxes, fatty acids, and eutectics of organic and inorganic chemicals, have been used in solid-liquid phase shift [35], [36]. Latent heat storage has a larger energy storage capacity (5–14 times) than sensible heat storage and a more constant heat output temperature [36]. However, because to poor heat transmission, significant heat losses, and super-cooling, its application is constrained [37].

In contrast to the first two techniques, **thermochemical heat storage** relies on the concepts of physical or chemical bonding and a binary working pair to store thermal energy. The two parts of this approach are sorbent and adsorbate, where the sorbent is typically either a liquid or a solid and the adsorbate is a gas or vapor. A chemical reaction or reversible sorption process that includes charging (heat storage) and discharging (heat release) phases stores thermal energy. [29], [38].

3.5.3 Phase Change Materials

The use of phase-change materials is a viable method of storing solar thermal energy (PCMs). PCMs can function in a wide range of temperature settings and provide higher density energy storage due to their isothermal nature. Additionally, PCM systems exhibit isothermal behavior throughout both the charging and discharging operations and have large energy storage capacities. Heat energy may be stored via a variety of methods:

- External heat storage:
    - Storing hot energy to supply the generator.
    - Storing of produced cool energy.
- Internal heat storage:

The heat transfer fluid (HTF) from solar collectors might pumped to hot thermal storage tank in external thermal storage systems to store energy for later use.

PCMs may be divided into four categories based on their phase change: solid-solid, solid-liquid, solid-gas, and liquid-gas as shown in Figure 3-11.

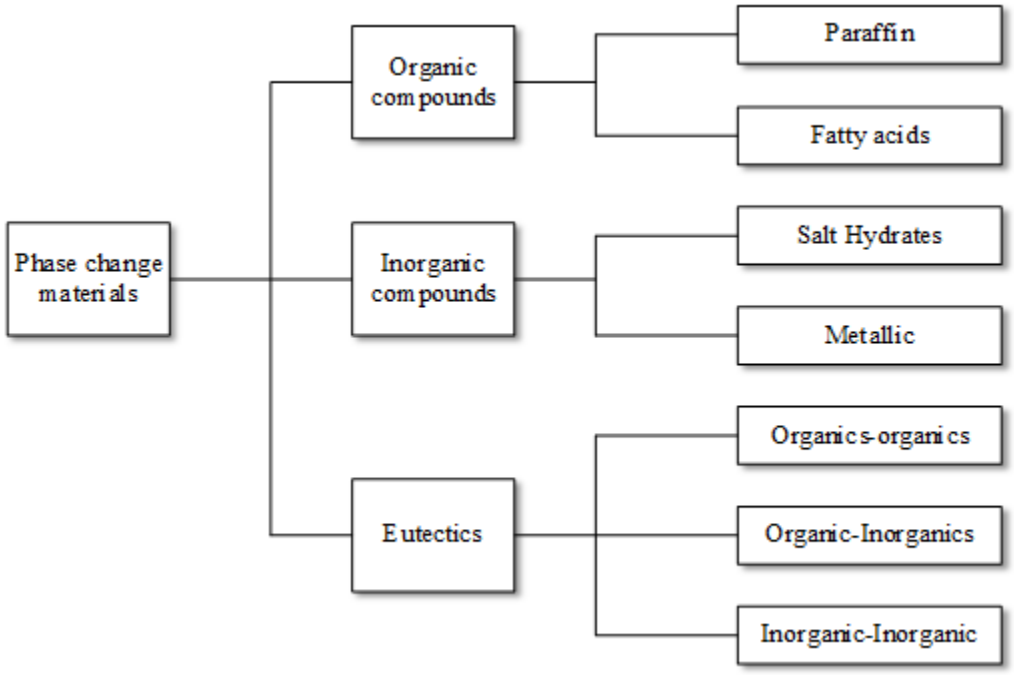

Figure 3-11 Phase change materials (PCMs) classification.

The thermos-physical characteristics of the materials under consideration must be thoroughly and completely understood. Included in this are melting point, fusion heat, density, thermal conductivity, and stability of thermal characteristics across repeated heating and cooling cycles. Based on the heat of fusion and melting temperature, visual representation of PCMs was in Figure 3-12. As shown in this figure in contrast to chlorides, carbonates, and fluorides, which need a high melting temperature, paraffin wax, fatty acids, salt hydrates, and their eutectic combination have a low melting temperature. Based on their melting point and material characteristics, these materials can be used in a variety of applications.

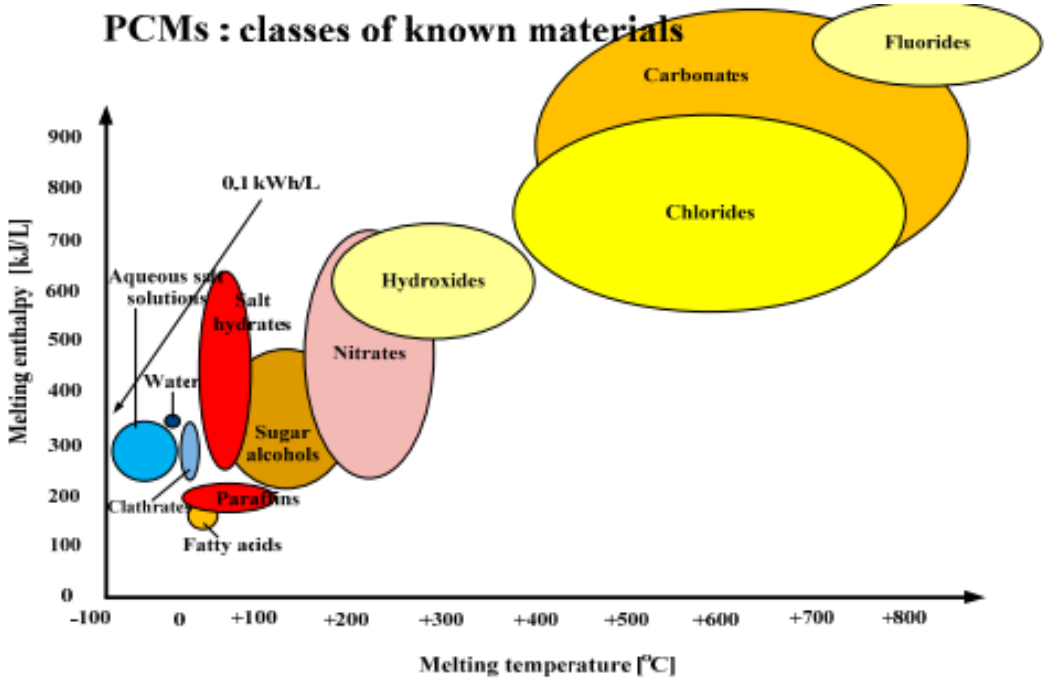

Figure 3-12 Classes of existing PCMs [39]

3.6 Solar collector

A unique type of heat exchanger known as a solar collector converts sun radiation energy into heat. Solar collector is different from more traditional heat exchangers in a number of ways. The solar collector is an apparatus that collects some of sun's energy, transforms it into heat, and then transmits the heat to a fluid that is passing through the collector (often air, water, or oil). These later systems utilize radiation and quick heat transfer to facilitate fluid-to-fluid exchange. Solar energy is collected and transmitted from circulating fluid to the hot water or air conditioning system directly or to a thermal energy storage tank where it may be recovered for use at night or on cloudy days. The non-concentrating collector class includes three distinct types of solar collectors: flat plate, evacuated tubes, and concentrated solar collectors, depending on outlet temperature of HTF.

Table 3-1 Solar energy collectors [40]

Collector type	Absorber type	Concentration ratio	Temperature range (°C)
Flat plate collector (FPC)	Flat	1	30-80
Evacuated tube collector (ETC)	Flat	1	50-200
Compound parabolic collector (CPC)	Tubular	1-5	60-240

Flat Plate Collector

A flat plate collector captures solar energy and converts it to thermal energy using water as the working fluid. The most basic and extensively researched technology for solar-powered household hot water systems is undoubtedly flat plate collectors. It has a wide variety of uses in medium temperature range of almost 100°C, from home to industrial preheating.

Evacuated Tubes Collector (ETCs)

ETCs are commonly constructed with parallel rows of twin glass tubes, each with a metal heat pipe connected, to limit conductive and convective heat loss. ETCs have a temperature limit of 200 °C. Common uses include industrial process heat, space heating and cooling, and water heating for residential and commercial buildings. Because of the curved curvature of the tubes, evacuated solar collectors are less sensitive to the sun's angle and orientation than flat plate solar collectors. In cold areas, ETCs often outperform flat plate collectors because their efficiency does not decline as quickly as flat plate collectors' does when the outside air temperature drops.

Compound Parabolic Collectors (CPC)

By transferring heat from the absorber to the fluid , CPC solar collectors combine many cutting-edge technologies to enable the production of heat from radiant sun energy. Given that it doesn't need tracking, the compound parabolic concentrator (CPC) is a very intriguing solar collector technology for a variety of low-concentration applications.

3.7 Optimization of Solar thermal VARS for Cold Room with PCM using Aspen plus

Optimizing intended objectives is necessary to improve the performance of single effect ARS. According to the results of an ARS thermodynamic analysis, there is an optimum temperature for the generator, condenser, and evaporator at which the COP and exergetic efficiency are at their highest levels [13]. A single-effect ARS simulation employing solar and natural gas as the energy sources is carried out in another work by Gormi [41]. He discovered that for a particular condenser temperature, an ideal generator temperature may be calculated. This generator temperature is crucial because it produces the highest COP and exergetic efficiency while requiring the fewest solar collectors. According to these two research, there can be a generator temperature where the COP and the exergetic efficiency are both at their highest levels. The highest COP and exergetic efficiency are attained at various generator temperatures for the same condenser temperature, according to Samanta and Basu study that optimized single-effect ARSs from an energy and exergetic point of view [42]. The referenced research are constrained by improper optimization and the formulation of such criteria.

The solar absorption-subcooled compression hybrid cooling system for cold storage is methodically developed. According to YOngrui Xu et al. work the modeling of typical days, and an optimization may be achieved for an economically feasible energy saving solution. The genetic algorithm performs global optimization.

The most recent studies on ARS thermodynamic optimization are discussed here. Using a multi-objective, multi-variable genetic algorithm, investigated on the effects of various parameters on a single-effect lithium bromide/water absorption cooling system and optimized system under various operational conditions to maximize exergetic and energetic efficiencies. For the purpose of determining correlations between design factors and operational parameters, the Group Method of Data Handling neural network technique is used. The results show a maximum increase energy and exergetic efficiency of around 9.1% and 3.0%, respectively. The mean temperature of generator is lowered by 6.2 ºC, while the mean temperature of evaporator is raised by 1.6 ºC, to accomplish this improvement. They have come to the conclusion that using low-grade heat, such that from the sun, improves thermodynamic performance while also lowering generator temperature.

Pumps, centrifuges, filters, splitters, and evaporators are just a few of the pre-existing libraries that are available to Aspen Plus users. These libraries contain product blocks with pre-defined parameters. Another choice offered by the program is a user-defined unit operation block, which designates a process that isn't recorded or can't be represented using the items in the existing library.

3.8 Summary of Literature Survey

The conclusion can be drawn from the above literature on solar absorption refrigeration are mentioned below:

- Solar absorption cooling has been studied, resulting in a wealth of theoretical and experimental literature. .
- The average COP and average generation temperature used to drive the singe effect solar absorption cycle vary 0.255-0.855 and 50-140 °C respectively.
- Nearly all studies on PCM based absorption cooling system use hot thermal energy backup system to close the energy supply-demand gap.
- There is no universal principle for sizing a thermal energy storage system. .

Table 3-2 Summery from the literature review

Reference	Generator temperature	Working fluid	COP	(thermal energy storage)TES	Types of work	Software	Solar collector
[44]	-	Helium	21%	PCM(water solution at eutectic concentration)	Simulation with prototype	DeltaEC, DSTAR	Parabolic trough
[19]	120	NH_3/H_2O	0.8	Ice and chilled water	Experiment		CPC-18 evacuated tube
[45]	167 °C	ammonia-water-hydrogen	0.159	-	Simulation and Experiment	ASPEN plus	
[7]	-	NH_3/H_2O	0.74	-	Simulation and Experiment	Matlab and Comsol Multiphysics	
[23]	92°C	$LiBr–H_2O$	0.77	-	Simulation	Matlab	FPC and ETC
[46]	90°C	$LiBr–H_2O$	0.66	Erythritol	Experimental	-	-
[47]	140°C	NH_3/H_2O	0.69	Ice	Experimental	-	ETC

CHAPTER FOUR

4. SOLAR DATA ANALYSIS AND DESIGN OF COLD ROOM WITH COOLING LOAD CALCULATION

4.1 Study Area and Site Selection

Lake Hawassa was chosen as the research location since it is one of Ethiopia's prospective fish harvesting areas. This study is being undertaken for the fish storage cold room application. Lake Hawassa (Figure 4-1) is situated between 06°58°-07°14°N latitude and 38°22°-38°28°E longitudes, 1685 m above sea level, and is 275 km south of the country's capital, Addis Abeba. The region has 950 mm of annual precipitation on average, and the average ambient temperature of the air is 19.8 °C.

One of the most significant commercial fish caught in Africa and other tropical regions is the Nile Tilapia, Oreochromis niloticus. More than 60% of all annual landings take place in Ethiopia as a result. It even reaches more than 85% in Lake Hawassa, is the one rift valley lake in our country. [50]. It was tested how long tilapia (Oreochromis niloticus) could be kept in ice at various temperatures. The fish had a 15-day shelf life in ice and a 12-hour shelf life at room temperature.

Figure 4-1 Situation in Lake Hawassa in Ethiopia

4.2 Solar Data Analysis

The main goal is evaluating the solar radiation that is available in the chosen location to evaluate and analyze the amount of the sun energy for study purpose. Determining how much solar energy is taken in by the solar collector is the major objective of this investigation. The local meteorological conditions at the location have an impact on the area's potential for solar energy. The Ethiopian metrological organization collects the solar data for Hawassa, which is situated at 07°14′ N latitude and 38°28′ E longitude. Kalogirou proposed a solar radiation representative days for each month as shown in Table 4-1.

Table 4-1 Recommended Average Days for Months and Values of n by months

Month	n for ith day of the month	For average day of month		
		Date	n	δ
January	i	17	17	-20.9
February	$31 + i$	16	47	-13.0
March	$59 + i$	16	75	-2.4
April	$90 + i$	15	105	9.4
May	$120 + i$	15	135	18.8
June	$151 + i$	11	162	23.1
July	$181 + i$	17	198	21.2
August	$212 + i$	16	228	13.5
September	$243 + i$	15	258	2.2
October	$273 + i$	15	288	-9.6
November	$304 + i$	14	318	-18.9
December	$334 + i$	10	344	-23.0

Note: Form Klein (1977). Do not use for $|\phi| > 66.5^{o}$.

4.2.1 Monthly Average Hourly Global Solar Irradiance for Hawassa

In Figure 4-2 is possible to study the Hawassa average hourly total solar radiation for the 2021 data.

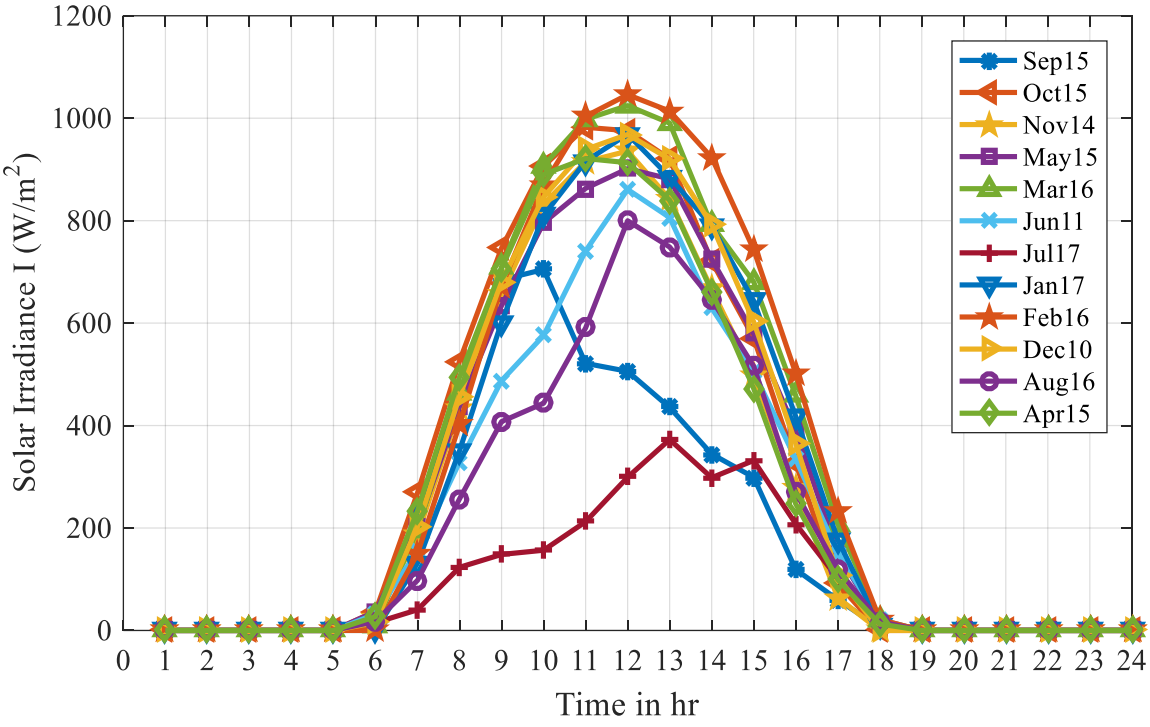

Figure 4-2 Hawassa's hourly average solar radiation for the suggested days in the months

4.2.2 Calculation of Monthly Mean Hourly Diffuse and Beam Solar Radiation on Flat Surface

The ratio of hourly diffuse to daily diffuse radiation, determined by Liu and Jordan correlations, as a function of time and day length:

$$r_d = \left(\frac{\pi}{24}\right)\frac{cos\omega - \cos\omega_s}{\sin\omega_s - \frac{2\pi\omega_s}{360}cos\omega_s} \quad 4\text{-}1$$

Where ω is hour angle and ω_s is sunset hour angle and can determined by

$$\omega = (ST - 12) * 15°\,,\ \omega_s = \cos^{-1}(tan\phi tan\delta) \quad 4\text{-}2$$

Where the hourly diffused radiation to daily diffuse radiation ratio is given by

$$r_d = \frac{I_D}{H_D} \quad 4\text{-}3$$

Average monthly hourly beam solar irradiance on a horizontal surface

$$\overline{I_B} = \bar{I} - \overline{I_D} \quad 4\text{-}4$$

Where Monthly average hourly global solar irradiance on flat surface in W/m2 given

$$\bar{I} = \frac{r_t \bar{H}}{3600} \qquad 4\text{-}5$$

Where $\bar{H}$ monthly average daily global radiation on horizontal is surface in J/m^2 and r_t is the ratio of hourly total to daily total radiation as a function of day length (n)

The total, beam, and diffuse sun irradiance of Hawassa for the days of 16 February and 17 July are shown in Figure 4-3.

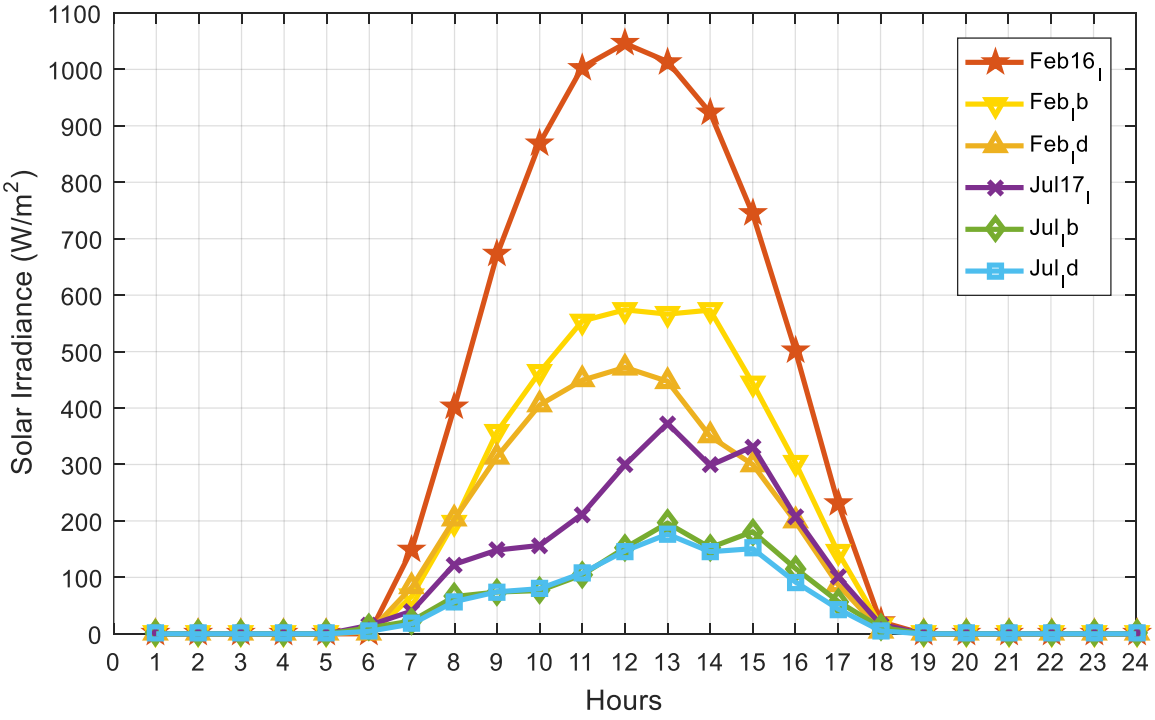

Figure 4-3 Hawassa total, beam, and diffuse solar radiation for the represented days of 16 February and 17 July.

4.2.3 Calculation of Atmospheric Temperature Variation on an Hourly Basis

One of the required inputs in the calculation of cooling load is air temperature. Figure 4-4 depicts the hourly change in outdoor temperature as predicted by using the minimum and highest daytime temperatures of mathematical expression. The data was gathered from the Ethiopian Metrological Agency.

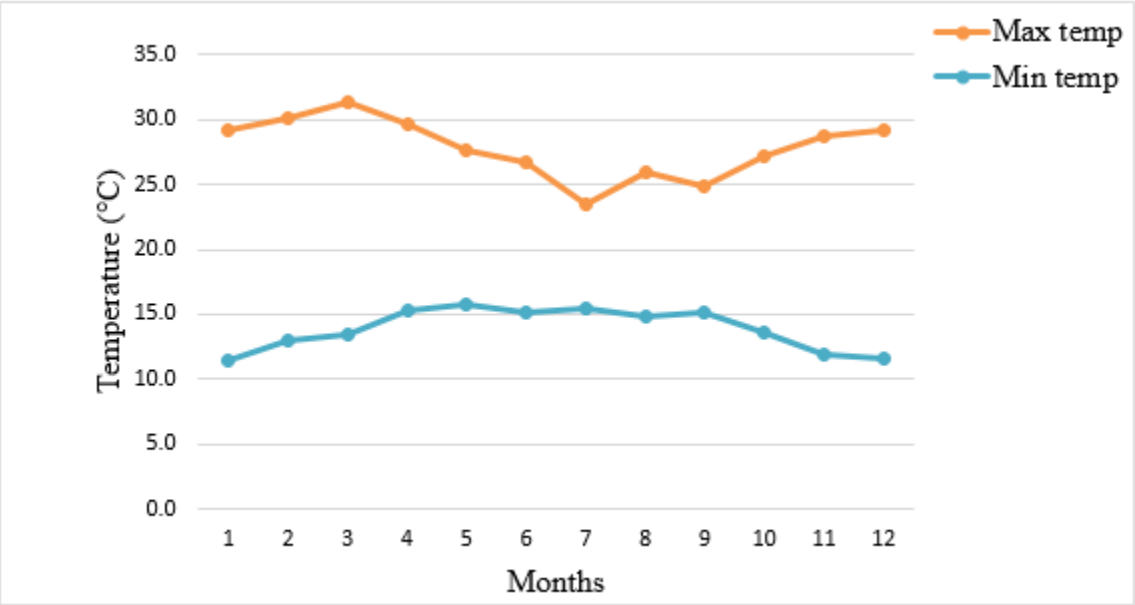

Figure 4-4 Temperature maximum and minimum variations on a monthly basis (2021)

4.3 Design of Cold Room

A room that is kept at a low temperature is referred to as a cold room (as for refrigeration). Fish are kept in the cold room that is being designed. The perishability must be avoided to maintain the advantages (nutritional value, quality, color), and it's also necessary to regulate a number of other factors, including cooling load, moisture, and ventilation. The product is kept at a temperature below the surrounding air in the positive cold room. Cooling considerably lowers the rate of fish degradation in these spaces. Thus, the product's storage life is lengthened [7].

4.3.1 Design Considerations and selection of Cold Room

Before the cold storage is built, there are a few factors that need to be established. In order for the system and units to operate with great efficiency over many years and to prevent rising energy consumption, these characteristics must be precisely specified.

1- Determining the sort of cold storage: - It's important to consider the use that will be made of the cold storage.
   - ❖ In this case cold room chamber (0°C).

2- Products that should be stored: - Only one type of product should be kept in a single room. If the product is in enclosed packaging and the storage temperatures are compatible, different items may be kept together.

   - ❖ In this case, we are going to store only fishes.

3- Temperature and relative humidity for product storage: - The sort of items to be stored is taken into account while building a cold room. The shelf life and storage of the items may be reduced as a result of the wrong temperature being chosen.

   - ❖ According to prior research, Oreochromis niloticus was discovered in ice storage in eatable state for 15 days [49]. Therefore, the cold storage is only used to store the product at temperature of 0°C and relative humidity of 98% according to FAO.

4- Entry temperature of the product to the room: - It's crucial to know what temperature the items are brought to the cold room to calculate the cooling capacity.

   - ❖ Since fish is collected from lake Hawassa the outside temperature of product is to be considered as taken the more recursive temperature of analyzed year is 31.3°C in March.

5- Daily admission quantity to the items' cold room: - The amount of items entering the cold room determines the number of forklifts, staff, vehicles, truck parking area, etc.

   - ❖ In this case, two people work inside the cold room for handling purposes for four hours per day on average is estimated.

6- Products can be packaged in a variety of ways, depending on how they will be stored: in a carton box, a package, a pallet, a chassis, or stacked.

   - ❖ Since the fish is wet, the plastic crate is used for packaging. In addition, the crate rack material is aluminum due to it has no corrosion.

7- Cold storage room dimensions are governed by the desired capacity, the topography, and the zoning status.

   - ❖ In this case, Y. Alemu et.al, has mentioned the weight of catch fishes per day is 1266.9 kg with 5620 number of fishes. Let us assume this is the 20% of the total cold room capacity which is exchanged daily, then the total room capacity will be 6,334.5 kg of fish storage capacity of cold room has taken.

8- Geographical features of the site where the cold storage will be constructed: - The accurate calculation of the cooling load to be estimated for the product to be computed in the cold room must take into account factors like the outside weather conditions and relative humidity.
    - ❖ The storage room is located in Hawassa (southeast of Ethiopia), which is identified by a maximum temperature is 31.3°C and an average relative humidity of 60%.
9- Construction materials of cold storage: Cold storage can be composed of steel or reinforced concrete. To lessen heat gain from the floor, walls, and ceiling, the rooms must be insulated.
    - ❖ [7], [51], [52] have used concrete block with insulation material for room construction similarly in this research the cold room will build using such type of room.
10- Doors in cold storage, heat gain generation, and cost are some of the deciding considerations for door type. Consequently, it's important to choose the right kind of door.
    - ❖ *Sliding door:* Used as the door of the cold rooms. It must be at the height and width that the forklift can pass. It's height is 2m and width is 1.3m [7]

4.3.2 Sizing of Cold Room

As we have mentioned the number of catches fish per day is 5620 with the weight of 1266.9 kg. From this, the average weight of single fish will be 0.225 kg. Since we have estimated the 20 % of the fish is exchanged per day, the overall number of fish stored will be 28,100 (6335 kg of fish) at standard this product should cover 2/3 of the room volume which means 65% of the room is cover by product with its packing material. From this using the Helpman software the total inside volume of the room is determined as 20 m^3.

Assumption of internal dimensions is taken according to total capacity of fishes to be stored, are given as: Length = 4 m, Width = 2 m and Height = 2.5 m.

4.4 Cooling Load Calculation

For cooling load in a cold room calculations transmission, product, occupancy, lighting, equipment, infiltrations loads are requires to consider. In the following sections all loads are calculated.

4.4.1 Transmission Load

The dimensions of our warehouse type cold storage room is 4 m long 2 m wide and 2.5 m high. It has four panels so we should calculate U (heat transfer coefficient) value for each across the cross sectional area.

The best technique to keep the required storage temperature constant is through thermal insulation. It reduces heat transmission between adjacent spaces and conserves energy. The material properties of a cold room are provided on Table 4-2 because selecting the right material is crucial when creating one.

Selection of cold room Insulating Materials

- Insulation made of polyurethane spray or polyurethane foam (PUF) is versatile in the surfaces it may be applied to and used to stop heat from moving from a warm exterior room into a cold refrigerator. The insulating substance has a low heat conductivity [7]. For this study, **Polyurethane foam** is taken as room insulation material since it has high thermal resistance as shown in table below.

Table 4-2 Cold Room Material Characteristics

	Characteristics of the materials			
Material	**Type of material**	**Thickness (L) (m)**	**Thermal conductivity (k)(W/mK)**	**Thermal resistance (R=1/K)(m^2 K/W)**
Ceiling				
Asphalt shingles	Roofing	0.15		0.08
Expanded Polyurethane, extrude	Insulation	0.1	0.026	27.7
Stainless steel	Interior	0.03	0.0625	
Wall				
Concrete block lightweight aggregate	Exterior	0.15		0.29
Asbestos Cement plaster	Sheathing	0.03	0.58	1.73
Expanded Polyurethane, extrude	Insulation	0.1	0.026	27.7
Stainless steel	Interior	0.03	0.0625	
Floor				
Concrete lightweight	Exterior	0.2	0.1	
Polyethylene sheet (low density)	Vapor retarder	0.03	0.33	
Expanded Polyurethane, extrude	Insulation	0.05	0.026	27.7
Stainless steel	Interior	0.03	16	
Door				
Stainless steel	Interior	0.0015	16	
Polyurethane foam	Insulation	0.077	0.03	
Stainless steel	Interior	0.0015	16	

The weighted maximum temperature air for Hawassa is 31.3^{o}C at 60% RH, the internal air should 0^{o}C at 98 % RH, the wall, and roof and flour are all insulated with 100mm polyurethane with a U value of 0.18 W/m^2.

4.4.1.1 Transfer of Heat through the Walls

Figure 4-5 shows that both convection and conduction Heat transfer involves passing through a wall, we will use to calculate the transmission load equation 4.6;

$$Q = \frac{A \times U \times (T_{out} - T_{in})}{1000} \qquad 4.6$$

Where Q= load in Kw, A = surface area of insulated wall in m^2, U = the overall heat transfer coefficient in w/m^2, T_{out} = max temperature at outside of cold room in ^{o}C, T_{in} = required min temperature inside cold room ^{o}C, 1000 = conversion from watts to kilowatts (1kw = 1000 watts)

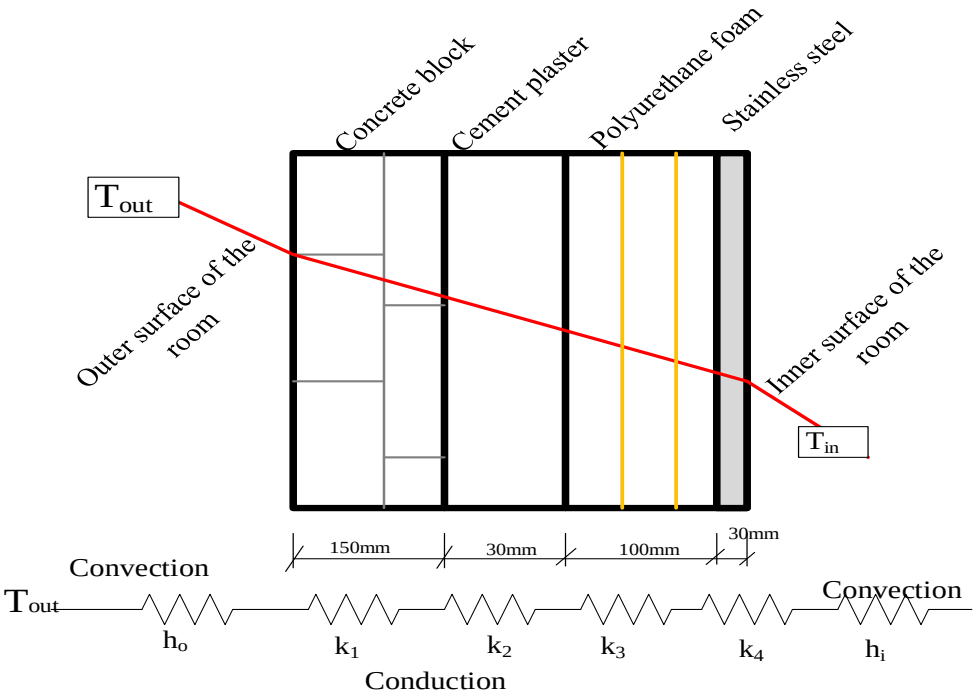

Figure 4-5 Heat transfer network diagram for wall of the room

The overall heat transfer coefficient is given by:

$$u = \frac{1}{\frac{1}{h_o} + \frac{x_1}{k_1} + \frac{x_2}{k_2} + \frac{x_3}{k_3} + \frac{x_4}{k_4} + \frac{1}{h_i}} \quad 4.7$$

Where, h_o --- heat transfer coefficient on the outer surface, h_i --- heat transfer coefficient on the inner surface, X_1, X_2, X_3, X_4 --- Thickness of wall materials respectively (m), K_1, K_2, K_3, K_4 --- Thermal conductivity of wall materials ($W/m^2\,^oC$).

When the wall is thick and the conductivity is low, the resistance X/K reduces U to such a small value that $1/h_i$ and $1/h_o$ have little effect and can be omitted from the calculation [51].

Therefore, heat transfer coefficient through the wall as a whole is:

$$u = 0.214\ \frac{W}{m^2 k}$$

The orientation of the cold room is shown in the Figure 4-6 below.

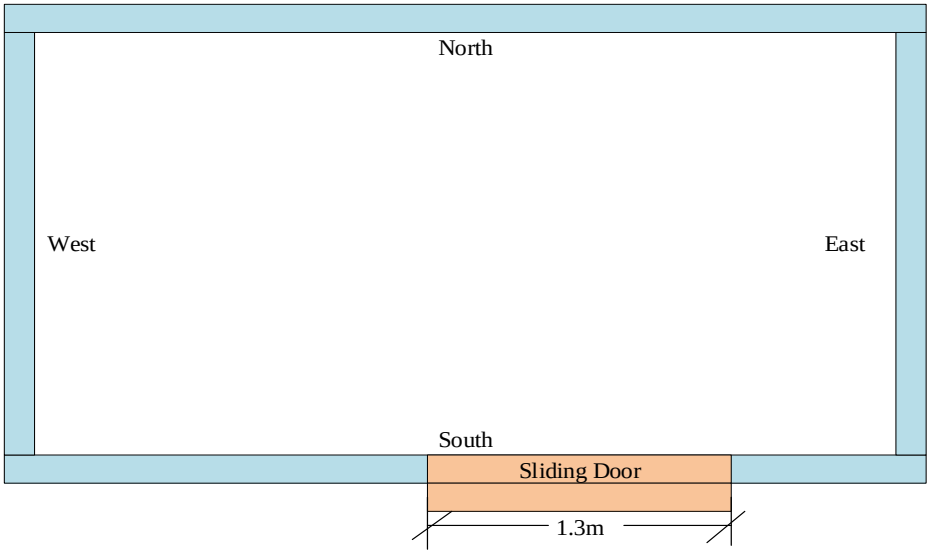

Figure 4-6 Direction of cold room dimension

The heat load of the one side (north wall) load with the area of (4m x 2.5m) is calculated as:

$$Q_1 = 0.067\text{kW}$$

The heat load of the one side (east and west wall) load with the area of (2m x 2.5m) is calculated as:

$$Q_2 = 0.0335\ \text{kW}$$

The heat load of the one side (south wall) load with the area of (4m x 2.5m) minus the area of the door (2m x 1.3m) is calculated as:

$$Q_3 = 0.0496\ \text{kW}$$

Total heat load trough the walls is

$$Q_{wall} = Q_1 + Q_2 + Q_3 = 0.15 \text{ kW}$$

3.1.1.1 Through the Roof

The overall heat transfer coefficient trough roof is:

$$u = 0.227 \ \frac{\text{W}}{\text{m}^2\text{k}}$$

The heat transfer through ceiling is calculated as

$$Q_{ceiling} = 0.0568 \text{ kW}$$

3.1.1.2 Through the Floor

The overall heat transfer coefficient trough floor is:

$$u = 0.253 \ \frac{\text{W}}{\text{m}^2\text{k}}$$

The heat transfer through floor is calculated as

$$Q_{floor} = 0.0634 \text{ kW}$$

3.1.1.3 Through the Door

The overall heat transfer coefficient trough floor is:

$$u = 0.390 \ \frac{\text{W}}{\text{m}^2\text{k}}$$

The heat transfer through floor is calculated as

$$Q_{door} = 0.032 \text{ kW}$$

The total transmission heat transfer is calculated as

$$Q_{Total\ transmition} = Q_{wall} + Q_{celiing} + Q_{floor} + Q_{door}$$

$$\boldsymbol{Q_{Total\ transmission} = 0.873 \text{ kW}}$$

4.4.2 Product Load

Product load is relates with product exchange on every day basis in cold storage. It means every new product comes with additional heat gain, thus it automatically affecting cold storage load. As we

have assumed the percentage of goods changed, each day is 20% of the product. Since we are storing the fish, the specific heat for fish is 0.93 Wh/kg.K above freezing as shown in the

Table 4-3 [7].

Table 4-3 Product specific heat

Products	Specific heat above freezing (Wh/kg.K)	Latent heat (Wh/kg.K)
Meat	0.87	64
Fish	0.93	67
Vegitable and fruits	1.04	80
Dairy products	1.05	80
Cheese / butter	0.76	47
Drink	1.1	87
Bred	0.52	37

Regarding to the collected data from Lake Hawassa the fish is harvested at nighttime, at which the weather condition reaches the ambient temperature. Since that, we are taking the average ambient temperature, from metrological data in Hawassa 28^{o}C. In this case let us take this product is cooled through the solar irradiance is available by considering this is most likely avail for 6 hrs, and by taking the cooling load is constant trough this time. Therefore, the sensible heat gain from the product is computed by equation 4.8:

$$Q_p = \frac{mc_p(T_{enter} - T_{store})}{1000 \times 6hrs} \qquad 4.8$$

Here, Q= product load in Kw, C_p = specific heat of product in KJ/kgK, m = mass of the product exchanged per day in kg, T_{enter} = temperature of products (fish) when outside in ^{o}C, T_{store} = temperature required for fish to be keep inside ^{o}C

$$Q_p = 5.49\ kW$$

4.4.3 Occupancy Load

Internal loads generated by people working inside the room will then be calculated since we need to take into consideration the heat that people produce. We'll assume there are three people working in the business for 4 hours each day. Based on the temperature outside, we can look up and estimate that they generate around 273 watts of heat inside.

The equation below determines the amount of heat a worker releases:

$$Q_{occupancy} = \frac{q \times N \times t}{1000 \times 24} \qquad 4.9$$

Where: Q = heat released by the person, q = heat emitted per individual (watt), N = workers' number, t = time spent inside the cold room (hrs.), 1000 just converts the watt into kW

The data offered in the literature was used to determine how much heat a person emits [7]. Table 4-4 demonstrates how the type of job affects the amount of heat emitted. With heavy labor, the heat emitted in a 0°C cold room may reach 372 W; with normal physical effort, it is closer to 273 W, and with little work, it is closer to 233 W.

$$Q_{occupancy} = 0.137\ kW$$

Table 4-4 Heat emitted by a person

Cold room temperature	Heat released by person q (W)		
	Hard work	Average work	Light work
+10 °C	372	2244	186
+7 °C	372	250	198
+4 °C	372	256	209
+2 °C	372	267	221
0 °C	372	273	233
-7 °C	384	314	279
-12 °C	365	337	291
-18 °C	407	372	326
-23 °C	419	407	349

4.4.4 Lighting Load

Depending on standard lighting installation, we have assumed the gap between two lamps is 2.5m the number of lamp required is 6 with 40 watt for each. Let us take the lamp is used for 4 hour per day during a door opening. This is heat produced by the lamps inside cold storage, for that we can use the formula mention below:

$$Q = \frac{No.of\ lamps\ \times time\ \times wattage}{24 \times 1000} \quad 4.10$$

Where: Q = Kw, Lamps = lamp number, Time = usage hour per day, lamp wattage power rating in watts, 1000 converts the watts to Kw.

$$Q_{light} = 0.04\ kW$$

4.4.5 Equipment Load

Now that we know how much heat the evaporator's fan motors produce, we can compute it. In order to do this, we may utilize the formula:

$$Q_{fan} = \frac{fans\ \times time\ \times wattage}{1000 \times 24} \quad 4.11$$

Where: Fans = fan number, Time = usage of hour per day, the fan's wattage power rating in watts multiply by 1000 to converts watts to Kw.

Two 250W fans will be used by the evaporator in this chilly room, and it is anticipated that they would run for 20 hours each day. Consequently, the calculation's outcome will be

$$Q_{fans} = 0.42\ kW$$

4.4.6 Infiltration Load

We must now determine the heat load caused by air intrusion. Air infiltration during door opening is also taken into account as an additional source of heat load. The following calculation yields this load:

$$Q_{infiltration} = \frac{changes \times volume \times energy \times (T_{out} - T_{in})}{3600} \quad 4.12$$

Where: Changes = volume air change per day, Volume = volume of cold storage, Energy = energy of fish per cubic meter per degree Celsius, T_{out} outside temperature and the T_{in} is inside temperature. Let's assume there will be 5 volume air changes every day since the door is open. The room's volume is 20 m^3, and each new cubic meter of air delivers 2 kJ/°C. The outside air is 31.3 °C, while the air inside is 0 °C.

$$Q_{infiltration} = 0.264kW$$

4.5 Over All Cooling Load of the Cold Room

The all values of loads in percentage on the cold room is depicted in Figure 4-7. As shown the major heat is gained by products (76%). Finally, to calculate the overall load we will add all the above loads.

$$\boldsymbol{Q_T = \sum Q_i} \quad 4.13$$

$$Q_T = Q_{transmission} + Q_p + Q_{occ} + Q_{light} + Q_{fan} + Q_{infiltration}$$

$$\underline{\boldsymbol{Q_T = 7.223\ kW}}$$

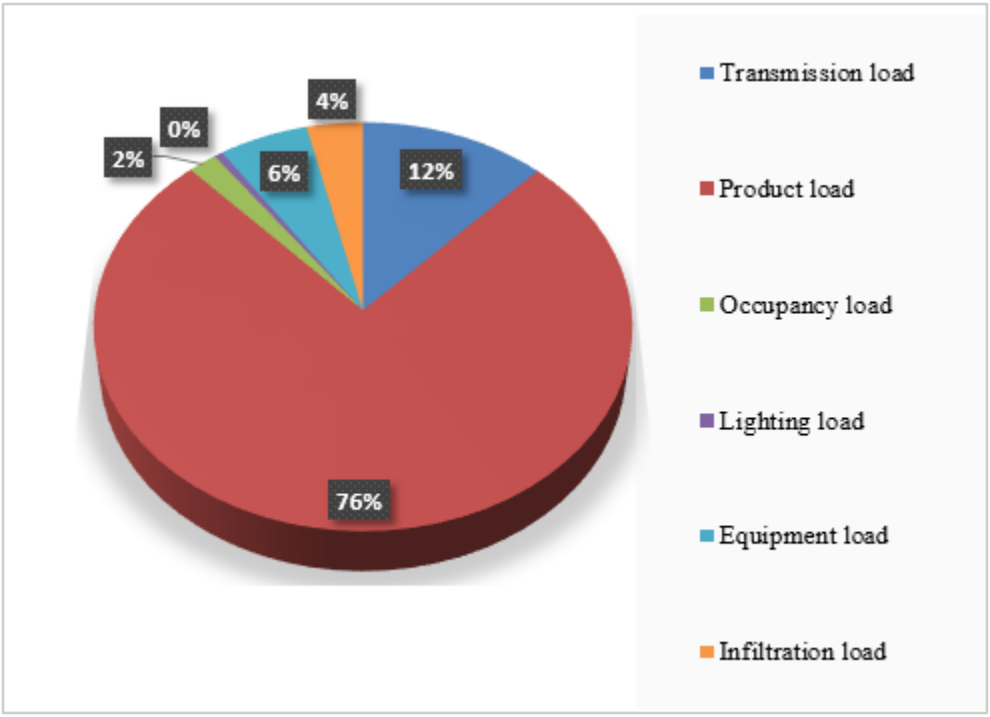

Figure 4-7 Cooling load distribution of cold storage

The HELPMEN determination for the cooling load calculation and manual calculation has to be compared as shown in the Figure 4-8 in order to validate cooling load. The result discrepancy of overall load is 2.286% which is most likely small and acceptable.

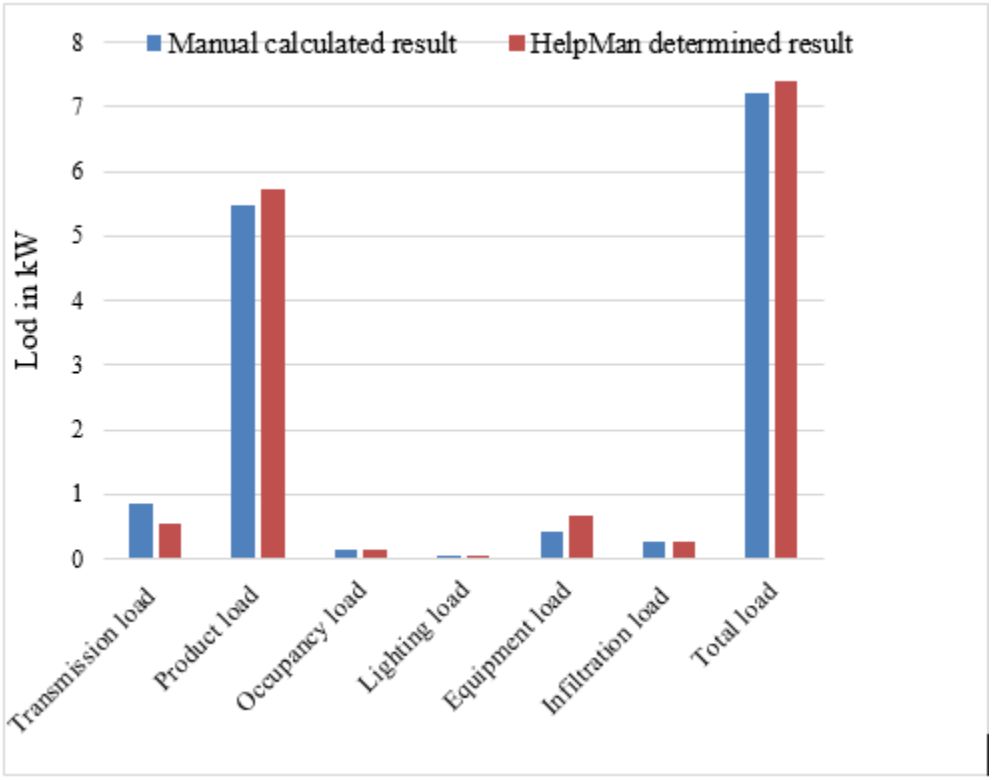

Figure 4-8 Comparison of cooling load calculation using Helpmen and manual calculation

Furthermore, thermal load caused by packaging and pallets accounts for approximately 10% of preserved product thermal load [7]. Therefore, overall room's cooling capacity is **7.772 kW**. This load is equal to the evaporator cooling capacity so, $Q_{eva} = 7.772\ kW$.

This cooling load is taken to be cooled within 6hrs during the solar radiation is available since we are considering the product, occupancy, light and infiltration loads is occurred during this time. For the remaining 18hrs, the cooling load will be **1.137 kW** since we are considering only the transmission load and equipment load available at night time. Therefore, thermal energy storage (PCM) will design for this cooling load. Therefore the detail parameters of the cold storage are listed in the Table 4-45 below.

Table 4-5 Cold room design parameters

Parameter	Value
Length	4m
Width	2m
Height	2.5m
Type of insulation	Polyurethane foam
Thickness of insulation	0.1m
Type of product	Fish
Total maximum mass of product	6,500kg
Storage temperature	0°C
Number of workers	2
Working hours of workers per day	4hrs
Daily operation time of light	4hrs
Mass loaded	20%
Overall cooling load at day time (6 hrs.)	7.772 kW
Overall cooling load at night time (18 hrs.)	1.137 kW

CHAPTER FIVE

5. ANALYSIS OF THE THERMODYNAMIC PERFORMANCE AND OPTIMIZATION OF THE COLD ROOM'S VAPOR ABSORPTION REFRIGERATION CYCLE

5.1 Absorption Refrigeration System Selection

First type of absorption system should identify and its working fluid around the system. Selection of ARS is done by considering the size of cold room with cooling capacity and estimated that the size to be 2.5 m in height, 2m wide and 4m long with a total volume of 20 m^3 and the cooling load is to be 7.772 kW (2.207 tons of refrigeration). From the above literature summery, we have selected single stage ARS since it can be requires generator with in temperature range of 80-150 °C and has a cooling capacity of 1 to 100 tons of refrigeration [15].

5.1.1 Absorption refrigeration systems' working fluid

From the literature survey the system requires a high latent heat of vaporization for ammonia (NH_3) operate well. Since NH_3 has a freezing point of -77°C, it can be used in low-temperature applications. Due to the volatility of both NH_3 and water, a cycle needs a condenser to condense the water that would otherwise evaporate with NH_3. Without this additional condenser, water would build up in the evaporator and harm the system's efficiency. The system's other drawbacks include its more pressure, toxicity and corrosive nature toward copper and copper alloys. However, water–NH_3 is eco-friend and economic it is used as working fluid in this research [65].

5.2 Modeled System Description and Working Principle

Systems for producing cooling that depend on thermal energy to produce the necessary output are known as absorption refrigeration systems. As indicated in Figure 5-1, an absorption refrigeration system typically consists of eight fundamental subsystems: pump, expansion valve, heat exchanger,

evaporator, condenser, and generator. Each of these components must effectively complete a specific duty in order for the absorption refrigeration system to function.

Ammonia/water combination heated inside generator using thermal energy from solar thermal heat energy in order to desorb the refrigerant. The ammonia-rich solution that is on its way to generator and has therefore been heated cools the refrigerant vapours (7) as they travel to the rectifier. This partially condenses water vapors, further cleaning ammonia vapors. These go to condenser that uses air cooling, where they liquefy. The refrigerant heat exchanger follows, followed by the refrigerant expansion valve, where liquid refrigerant (10) flows. The refrigerant is delivered into the evaporator (11) when its pressure is reduced, where it absorbs heat from the food product to evaporate. The ammonia-poor solution returning from the generator absorbs refrigerant vapour in two stages: first, in heat exchanger, where the absorbed heat is used to hot ammonia-rich solution as it pass to generator (3); and second, in air-cooled absorber, where absorption process is completed.

5.3 Mathematical Modeling of Absorption Refrigeration System

Mathematical model is developed and simulated according to the following assumptions:

- Absorption refrigeration system operates at steady state conditions.
- At the condenser and evaporator outlet refrigerant is saturated liquid and saturated vapor respectively.
- Pressure drop in pipelines and heat exchangers is negligible.
- All of absorption refrigeration system's components maintain a constant internal temperature. As a result, the temperature of each outflow stream is the same as the component of the ARS it is coming from.
- The reference ambient conditions of air in Hawassa are 31.3 °C and 1 bar.
- All expansion processes are isenthalpic.
- Except the generator, evaporator, condenser, and absorber, there is no heat transmission to or from the system to environment.

We ignore pump work, pressure loss in the lines and components, and we provide the states 1, 4, and 10 and 12 saturation conditions in order to make the issue simpler (Figure 5-1).

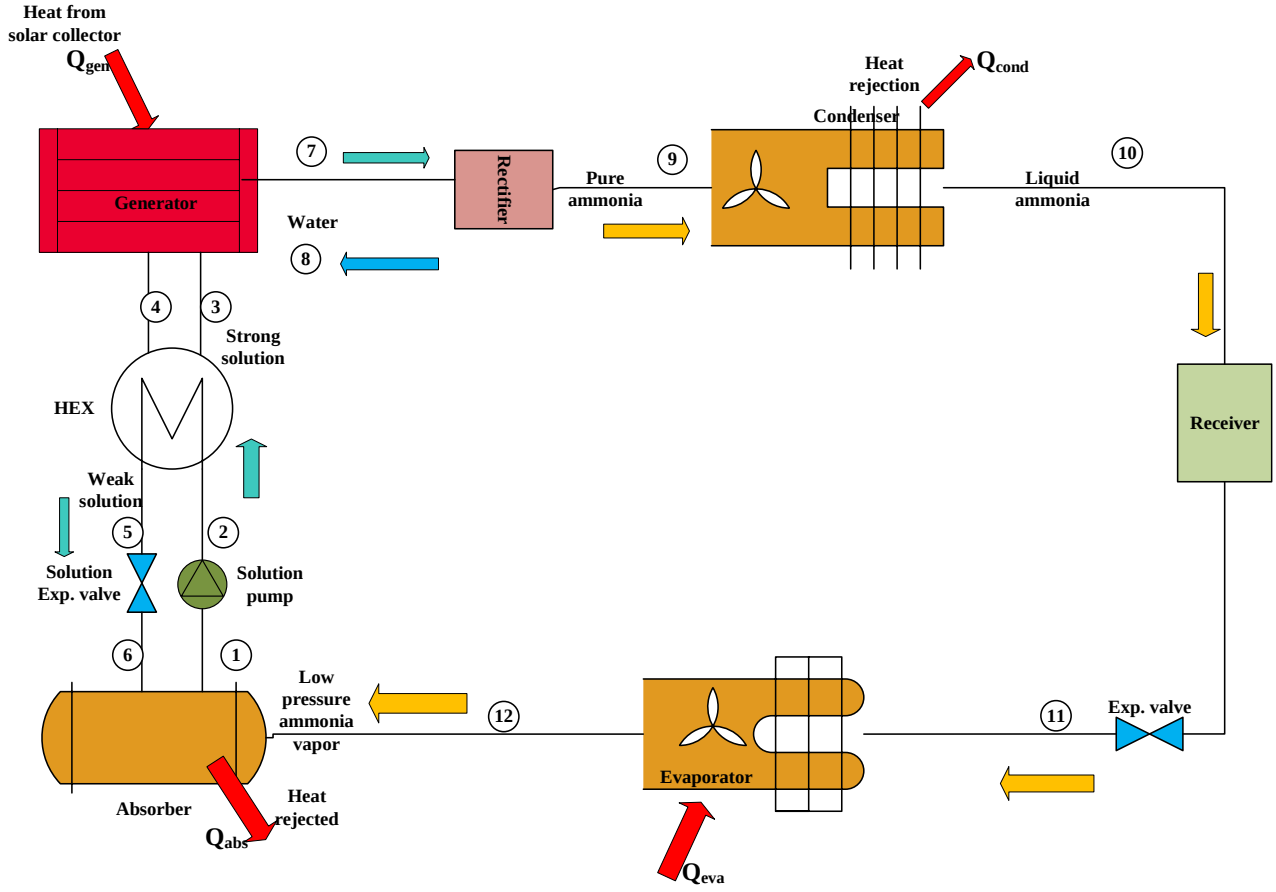

Figure 5-1 Simple refrigeration cycle based on vapor absorption

The thermodynamic cycle has four steps, just like the vapor compression cycle, and they are as regard to:

- Isothermal heat supply at the evaporator
- Chemical compression in a pump, generator, and absorber assembly
- Condenser isothermal heat rejection of produced refrigerant
- Condensed refrigerant expands adiabatically in the expansion valve.

The following formula is used to determine theoretical cycle performances and it is derived from the total energy balance [55].

$$Q_{abs} + Q_{cond} + Q_{rect} = Q_{gen} + Q_{evap} + W_p \qquad 5\text{-}1$$

We have information on the mass balance in absorber or generator.

$$m_s X_{abs} = (m_s - m_r) X_{gen} \quad 5\text{-}2$$

Where the subscripts *gen* and *abs* refer to generator and absorber solutions and X indicates mass proportion of absorbent in the solution, and m_r and m_s are gaseous refrigerant mass flow rate and tabsorber-exit solution mass flow rate (or solution pumping rate), respectively.

Mass flow of refrigerant is equal to:

$$\boldsymbol{m_r = \frac{Q_e}{(H_8 - H_7)}} \quad 5\text{-}3$$

For calculating system performance, the following formula is applied to compute mass flow rate of strong and weak solution [55],

$$f = \frac{m_s}{m_r} = \frac{x_g}{(x_g - x_a)} \quad 5\text{-}4$$

The following equations describe energy balance surrounding generator, absorber, condenser, and evaporator:

Generator rate of heat addition

$$Q_{gen} = m_7 \times h_7 + m_4 \times h_4 - (m_3 \times h_3 + m_8 \times h_8) \quad 5\text{-}5$$

Heat rejection rate on rectifier is determined as the following equation

$$Q_{rec} = \dot{m}_7 h_7 - (\dot{m}_9 h_9 + \dot{m}_8 h_8) \quad 5\text{-}6$$

The condenser's rate of heat rejection

$$Q_{cond} = m_9 \times (h_9 - h_{10}) \quad 5\text{-}7$$

The evaporator's capacity to absorb heat

$$Q_{evap} = m_{12} \times (h_{12} - h_{11}) \quad 5\text{-}8$$

The absorber's capacity to reject heat

$$Q_{abs} = m_{12} \times h_{12} + m_6 \times h_6 - m_1 \times h_1 \quad 5\text{-}9$$

An energy balance of heat exchanger's hot side

$$Q_{shx\_h} = m_4 \times (h_4 - h_5) \quad 5\text{-}10$$

Likewise, an energy balance of heat exchanger's cold side

$$Q_{shx\_c} = m_3 \times (h_3 - h_2) \quad 5\text{-}11$$

If, then the heat exchanger's overall energy balance is met.

$$Q_{shx\_c} = Q_{shx\_h} \times eshx \quad 5\text{-}12$$

Where: $eshx$ is the solution heat exchanger effectiveness which is give as.

$$eshx = \frac{T_4 - T_5}{(T_4 - T_2)} \quad 5\text{-}13$$

The solution pumping power by small pump

$$swp = V_1 \times \frac{(P_2 - P_1)}{etap} \quad 5\text{-}14$$

$$W_p = m_1 \times swp \quad 5\text{-}15$$

Where: $etap$ is isentropic efficiency of pump.

Coefficient of performance (COP)

$$COP = \frac{Q_{evap}}{Q_{gen} + W_p} \quad 5\text{-}16$$

Since we have neglected pump work, COP of the absorption system will

$$COP = \frac{Q_{evap}}{Q_{gen}} \quad 5\text{-}17$$

5.4 Sample Calculation of COP for Ammonia Water ARS

Figure 5-1 is used as a reference for the calculation. Basis: The vapor absorption system has a cooling capability of 7.772 kW under the subsequent operational circumstances (all are outlet temperatures): Condenser Temperature = 39.8 °C, Evaporator Temperature = 0 °C, Absorber Temperature = 35 °C and Generator Temperature = 80 °C.

The following information is required: - C_p of water = 4.187 kJ/kg-K , C_p of ammonia = 2.2 kJ/kgK

To determine absorber and generator temperatures, we must first determine the value of saturation pressure from ammonia p-h chart for condensing temperature 39.8 °C and evaporating temperature 0 °C from APENNDIX A.

$P_E = P_A$ = saturated vapor pressure at 0°C = 4.296 kPa

$P_C = P_G$ = 1547 kPa

Doing energy balance around the evaporator

Heat load on evaporator $Q_{evap} = 7.772\ kW$

By using $T_E\ and\ P_E$ can be determined from an ammonia p-h chart , $h_{12} = 1265\ kJ/kg$.

Using $T_c \; and \; P_c \, , h_{10} = \; 189.3 \; kJ/kg$

As know, h_{10} and h_{11} are equal via expansion valve

From equation 5-8, we can calculate

$$m_{12} = 0.00662 \; kg/sec$$

For the system $m_{12} = m_{10} = m_9 = 0.00662 \; kg/sec$

Using $T_E \;\; and \; P_E$ from the ammonia-water solution enthalpy-concentration diagram in APPENDIX A to determine the concentration of ammonia

$$x_{12} = x_{10} = x_9 = 0.9996 \; \cong 1$$

1. **For absorber**

Weak and strong solution mass balancing

$$m_1 = m_{12} + m_6$$

$$x_1 m_1 = x_{12} m_{12} + x_6 m_6$$

In APPENDIX A the figure shows an enthalpy-concentration chart for an ammonia-water solution with ammonia in saturated liquid. $T_A \; and \; P_A \, , h_1 = 179.96 \frac{kJ}{kg} and \; x_1 = 0.81$ and also at $T_G \; and \; P_G, \; h_4 = 371.43 \; kJ/kg \; and \; x_4 = \; 0.49$

$x_4 = \; x_5 = x_6 = 0.49$

Therefore, doing the mass balance around generator or absorber,

Mass flow ratio, f = 1.25

$m_s = m_6 = \; 0.0071 \; kg/sec$

$m_1 = \; m_6 + \; m_{12} = 0.0137 \; kg/sec$

In this system

$x_1 = x_2 = x_3 = 0.81$

Using P_G and x_3 ammonia-water solution enthalpy-concentration diagram $h_3 = 132.6 \; kJ/kg$ and using equation

$h_2 = h_1 + SWP$

$swp = V_1 \times (P_2 - P_1)/etap$

Where $V_1 = 0.001566 \frac{m^3}{kg} \; and \; \eta_{ip} = 0.75$

$h_2 = 179.98 \; kJ/kg$

Using energy balance at heat exchanger h_6 can be found

$m_2(h_3 - h_2) = m_4(h_4 - h_5)$

$h_5 = h_6 = 418.81\ kJ/kg$

Therefore heat rejected by absorber is find using equation 5-9.

$$Q_{abs} = 8.202\ kW$$

2. For generator

Heat input to generator was calculated using the equation 5-5. Using an enthalpy-concentration chart for an ammonia-water solution $T_7 = T_G$and P_G at saturated vapor $x_7 = 0.96$

Using the average concentration value $x_8 = 0.78$ can be get

Using mass balance

$m_7 = m_9 + m_8$, $x_7 m_7 = x_9 m_9 + x_8 m_8$

$m_8 = 0.00017\ kg/sec$ and $m_7 = 0.0058\ kg/sec$

Using $T_G$and P_G the saturated vapor the enthalpy-concentration chart for ammonia-water solution determine. $h_7 = 1430\ kJ/kg$ and also h_8 became $98 kJ/kg$ at P_8 and x_8 the solution in saturated liquid

$$Q_{gen} = 10.15\ kW$$

3. For rectifier

The rejected heat by rectifier is calculated using an equation 5-6.

Using P_C and x_9 the saturated vapor can be found using an enthalpy-concentration diagram for an ammonia-water solution. $h_9 = 1285\ kJ/kg$ where $m_9 = 0.00563\ kg/sec$

Therefore, $Q_{rect} = 1.34\ kW$

4. For condenser

The rejected heatfrom condenser was found using equation 5-7

$$Q_{cond} = 7.66 kW$$

5. For solution heat exchanger (hot side)

Applying equation 4.10, calculate the value of heat exchange from a weak solution to a strong solution is

$$Q_{shx_h} = -0.58\ kW$$

In the same manner, the energy balance on heat exchanger's cold side

$Q_{shx_c} = 0.58\ kW$

The solution pumping power by small pump

Using equation 5-15

$W_p = 0.00023\ kW$

Therefore, Coefficient of performance (COP) of ARS is

$$COP = 0.69$$

Energy balance of the cycle

Heat rejected

$$Q_{abs} + Q_{cond} + Q_{rect} = 17.202\ kW$$

Heat received

$$Q_{gen} + Q_{evap} + W_p = 17.21923\ kW$$

Thus, the energy balance checks very closely.

5.5 Aspen-Plus Software Introduction and System Modeling

5.5.1 Introduction of ASPEN

ASPEN is an engineering software used in process simulation, optimization as well as sensitivity analysis. ASPEN is a popular process modeling software platform. The choice to mimic absorption chillers in ASPEN as opposed to other programs was made largely due to two benefits. First, the ASPEN-produced chiller models can seamlessly connected with solar heat sources and plant cycle model. Second, ASPEN has a greater capacity for optimization than other software [56].

Aspen ONE is a complete collection of software solutions and expert services offered by Aspen-Tech with the aim of assisting process firms in achieving their operational excellence goals. Process organizations may boost operational effectiveness and profitability throughout their whole global enterprise by using the advantages of simulation models. Figure 5-2 depicts the four primary fields that Aspen-One covers: Chemical, Energy, Polymer, and Pharmaceuticals [55]. The aspen one software packages can perform different process simulations in various application, those packages are shown in Figure 5-3.

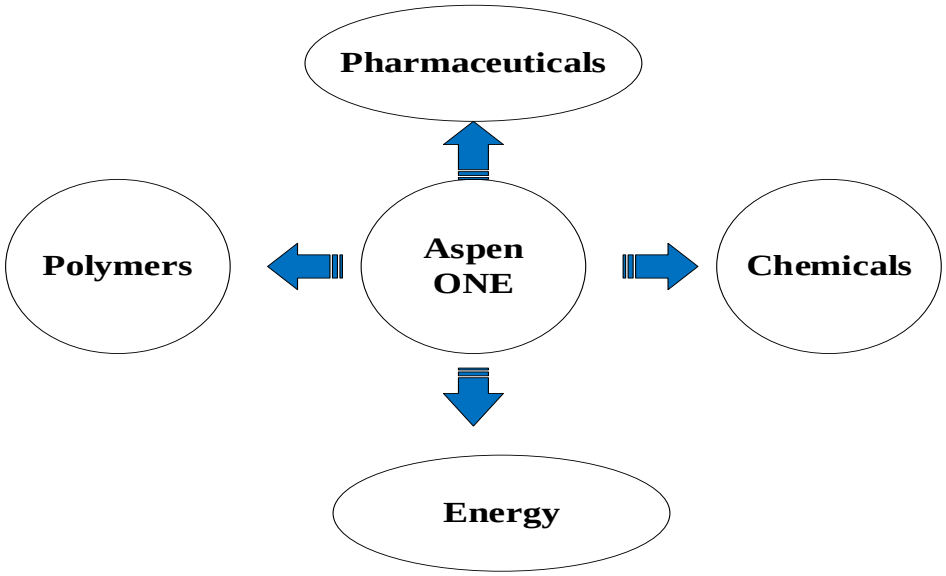

Figure 5-2 Aspen ONE's Industries and Business Areas

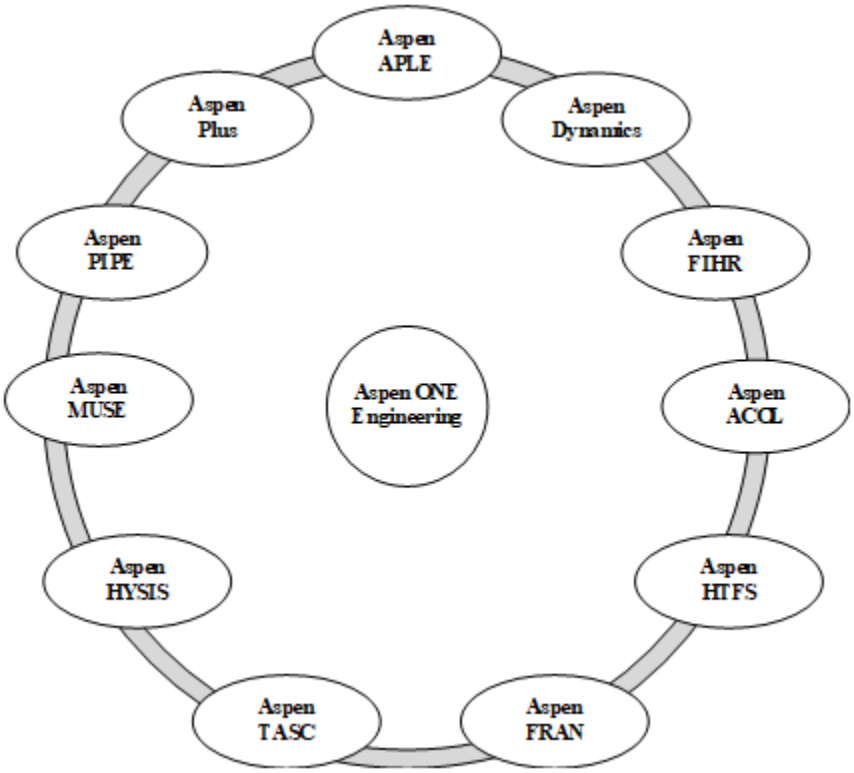

Figure 5-3 Engineering Classification of Aspen One

5.5.2 Aspen Plus

Aspen Plus is a market-leading process-modelling tool for conceptual design, optimization, and performance monitoring in the chemical, polymer, specialty chemical, metals and minerals, coal power, and absorption system sectors. With the use of the software program Aspen plus, a user may create a process model and then simulate it without having to perform laborious calculations [55].

Like other simulation software Aspen Plus, also have several steps for simulation and optimization task. Primarily, the property set up should be determined in this stage the process working fluids should be determine and the property method which can perform the simulation at the back of the software should be selected. To determine the physical condition of state of matter we should to use equation of state.

5.5.2.1 Property Method Selection

The absorption refrigeration cycle's performance will be examined and enhanced using the steady-state simulation model developed in the current study using the flow-sheeting program Aspen-Plus. One of the most crucial phases that might have an impact on modeling of absorption cooling cycles is the choice of an appropriate approach for determining thermodynamic parameters of working fluid. To estimate the mixture characteristics, Aspen-Plus has a sizable databank of thermodynamic property and transport models together with appropriate mixing rules.

ASPEN does not employ looks tables for property data, excluding particularly common fluids. Instead, a property approach must be chosen by the user depend on the operating environment and fluid properties. Consequently, much like with other property method based modeling tools, each model made in ASPEN has a built-in mistake. This is meant to serve as a caution to any prospective users that they should carefully consider the property technique while modeling in ASPEN because even look-up tables can occasionally include mistakes due to interpolation [56]. The operating circumstances and the fluids being modelled were taken into consideration in order to choose an appropriate property technique.

This paper investigates in depth the selection of ammonia/water mixture property model for use of modeling solar absorption chiller. To this purpose Rami [57] had conducted nine distinct approaches are pre-selected from software library and evaluated, but none of the methods accurately predicts vapor-liquid equilibrium (VLE). The equations of state (EOS) are then fitted to the VLE data to identify the related parameters of these models. The Peng-Robinson-Boston-Mathias equation of state (PR-BM), with fitted parameters, is the property method that Aspen-Plus implements that is most suitable for the prediction of the ammonia/water vapor-liquid equilibrium in examined temperature and pressure ranges, it can be concluded from these results [55], [56].

5.5.2.2 Equation of state

In thermodynamics, equation of state is a relationship among the system's intense and extended states. In more technical terms, an equation of state is a thermodynamic equation that describes the state of matter under a given set of physical conditions. It is a constitutive equation that depicts the relationship between two or more of a substance's state functions, such as temperature, pressure, volume, or internal energy. Using equations of state, it is possible to report the properties of fluids and fluid mixtures [55].

Peng-Robinson equation of state write [57]:

$$P = \frac{RT}{(\bar{V} - b)} - \frac{a}{\bar{V}(\bar{V} + b) + b(\bar{V} - b)} \quad 5.18$$

Where P is the pressure, $\bar{V}$, mixture molar volume, b, mixture co-volume, a, attraction term factor, and R universal gas constant. The mixture a and b are deduced from individual component constants a_i and b_i using mixing rules

$$b = \sum x_i b_i \quad 5.19$$

$$a = \sum_i \sum_j x_i x_j \sqrt{a_i a_j}(1 - k_{ij}) \quad 5.20$$

In these equation x_i is the mole fraction of component i in mixture and k_{ij} the binary interaction parameter of the components i and j. Usually it is supposed that:

$$k_{ij} = k_{ji} \tag{5.21}$$

This parameter is derived from vapor-liquid equilibrium (VLE) data by a regression procedure. To make an equation more flexible k_{ij} is written as function of the temperature:

$$k_{ij} = {k_{ij}}^{(1)} + {k_{ij}}^{(2)}T + \frac{{k_{ij}}^{(3)}}{T} \tag{5.22}$$

So that three parameters are fitted to VLE data: ${k_{ij}}^{(1)}, {k_{ij}}^{(2)}\ and\ {k_{ij}}^{(3)}$.

The constants a_i and b_i are determined by critical temperature and pressure of compound T_{ci} and P_{ci}, respectively:

$$a_i = \alpha_i(T)\left[0.45724\frac{R^2{T_{ci}}^2}{P_{ci}}\right] \tag{5.23}$$

$$b_i = 0.07780\frac{RT_{ci}}{P_{ci}} \tag{5.24}$$

In the $\alpha_i(T)$ function,

$$\alpha_i(T) = [1 + m_i(1 - \sqrt{T_r})]^2 \tag{5.25}$$

T_r is reduced temperature, $\frac{T}{T_{ci}}$, and m_i, a component specific parameter depending on acentric factor ω_i,

$$m_i = 0.37464 + 1.54226\omega_i - 0.26992{\omega_i}^2 \tag{5.26}$$

$\alpha_i(T)$ =1 at critical temperature.

Boston-Mathias modification of Peng-Robinson equation of state is as follow:

$$\alpha_i(T) = \ [\exp[c_i(1 - T_{ri}^{di})]]^2 \tag{5.27}$$

With

$$d_i = 1 + \frac{m_i}{2};\ c_i = 1 - \frac{1}{d_i} \tag{5.28}$$

5.5.3 The Absorption Chiller Model and Its Components in Aspen plus

5.5.3.1 Simulation Model

Figure 5-4 depicts the model created for the absorption machine. Aspen-Plus blocks for various machine parts, as well as input data utilized in these parts, are listed in Table 5-3 to run the simulation at ambient temperature. As indicated before Figure 5-1 shows state points in chiller, like pump exit

is state point 2, while absorber exit is state point 1. State point 4 denotes generator outlet that goes to the heat exchanger; state point 3 denotes heat exchanger exit that leads to the generator; and state point 11 denotes expansion valve 2 (DET2) exit that leads to the evaporator. The generator's vapor with some water exits at state point 7, the rectifier's return water liquid exits at state point 8, the ammonia vapor exits at state point 9, and the condenser exit is at state point 10. State point 5 is outflow of refrigerant heat exchanger, and state point 6 is the exit of refrigerant expansion valve 1 (DET1). State point 12 is evaporator outlet.

5.5.3.2 Validation of simulation model

To ensure that final model was accurate, the mathematical model was validated once it had been created. A benchmark example has been developed using Hmida's work (single effect model of NH_3-H_2O VAS was taken into consideration). Inputs value for single effect model with rectifier of NH_3-H_2O VAS are shown in Table 5-1 [7]. Table 5-2 compares the output of the current system produced by the mathematical model using the Aspen plus software (with inputs from Hmida) with the experimental outputs produced by Hmida.

Table 5-1 Aspen plus models Hmi da's input data

Parameter	Values
Generator temperature (°C)	120
Condenser and Absorber temperature (°C)	50
Evaporator temperature (°C)	2
Vapor phase composition	≥95
Heat exchanger pinch , (°C)	5
Heat absorbed by the evaporator (kW)	8

The results obtained for current model are comparable to those obtained for Hmida’s model.

Table 5-2 Comparison between results of current model and Hmida's model

Parameter	Hmida's experimental result	Present model result	Discrepancy
Heat supplied to evaporator, Q_{evap} (kW)	8	8	NA
Heat rejected from condenser, Q_{cond} (kW)	9.73	9.12	6.2%
Heat rejected from absorber, Q_{abs} (kW)	16	11.37	28.93%
Heat supplied to generator, Q_{gen} (kW)	10.86	10.22	5.89%
COP	0.74	0.78	5.41%

The performance of VAS is examined once the present model has been successfully validated. What if the some of the discrepancy is very large the basic components heat duty discrepancy is preferable. Therefore, Aspen plus simulates the performance of solar thermal powered ammonia-water absorption system.

It is possible to simulate generator temperature and (COP) of the reversible cycle by assigning values to evaporator, condenser, and absorber temperatures, respectively. Input parameters and presumptions from the simulation are discussed in the next subsection.

5.5.3.3 Simulation Procedure

Simulation model created in study initially sequential modular strategy in which each block is computed independently. In Table 5-3, the input data for each block is shown. The model takes into account a break point to input circumstances. At state 1, the entrance of the solution pump, this "break" point is added (Figure 5-4). Since the absorber's exit and the solution pump's inlet reflect the same state, state point 1 ought to have the same properties as the inputs provided at solution pump's intake after simulations have been conducted. This serves simulations' convergence condition. In a second stage, the simulations are conducted using EO (equation-oriented) methodology, in which governing equations of chiller model are simultaneously solved. This method is more successful at

tackling complicated issues. This method requires accurate starting estimates for all variables in order to achieve convergence. The simulation should then start in sequential modular mode, and when it has fully converged, the EO solution method should be initialized (synchronized) using the results of the sequential simulation.

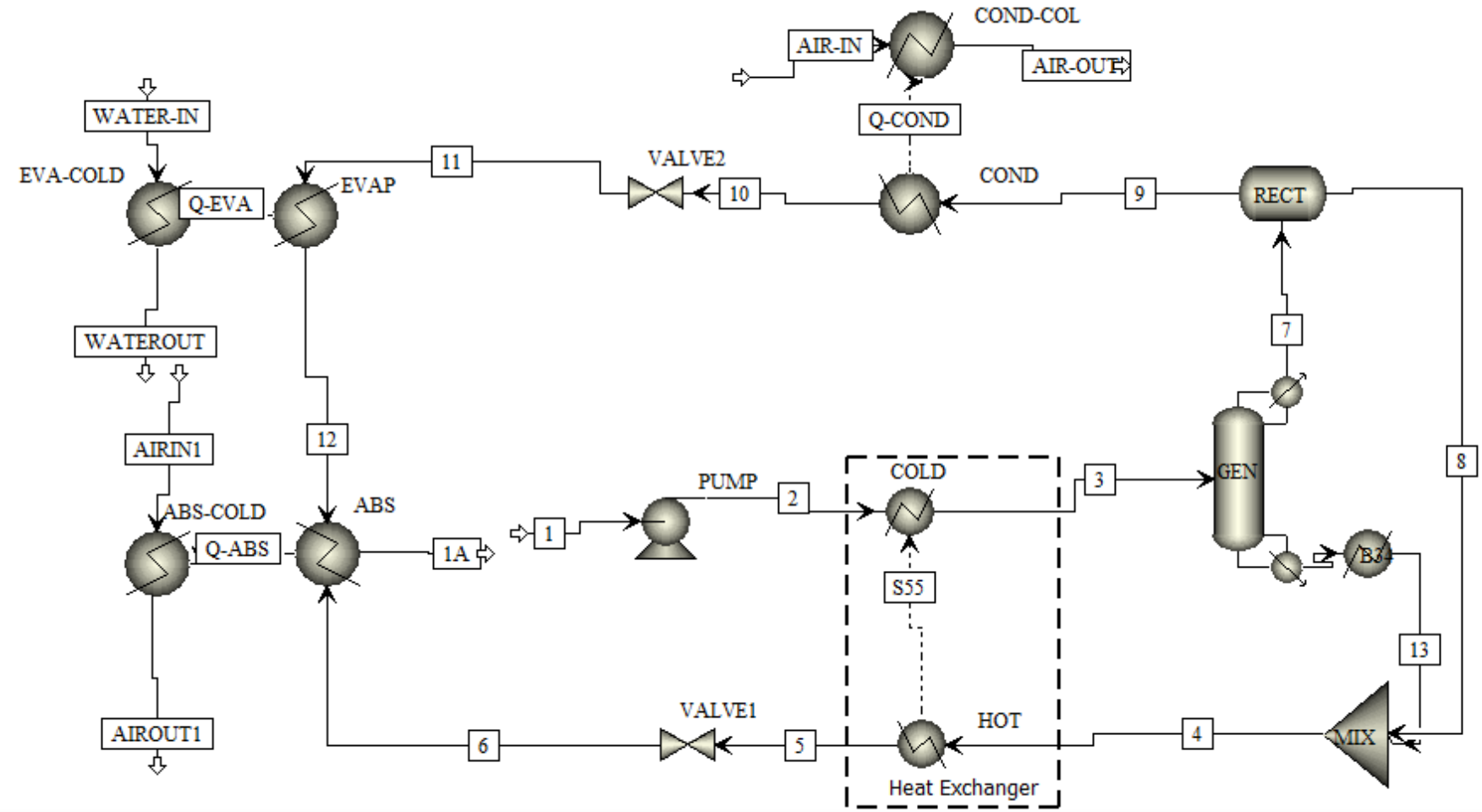

Figure 5-4 Absorption machine model in Aspen-Plus

Table 5-3 Aspen-Plus system components and models with corresponding input data

Machine elements	**Aspen-Plus block**	**Input value**
Condenser (COND)	HEATER block	Temperature = 39°C Pressure = 15.9 bar
Evaporator (EVAP)	HEATER block	Heat duty = 7.772 kW Pressure = 4.296 bar
Heat exchanger (COLD & HOT)	Two HEATER blocks	Hot side pressure = cold side pressure = 15.9 bar Hot side temperature change = 30°C
Absorber (ABS)	HEATER block	Pressure = 4.296 bar Vapor fraction = 0
Solution pump (PUMP)	PUMP	High pressure = 15.9 bar Isentropic efficiency = 0.75 **State 1** - Pressure = 4.296 bar - Total mass flow = 0.0137 kg/sec - Vapor fraction = 0 - NH_3 Mass fraction = 0.437 - H_2O Mass fraction = 0.563
Expansion valve 1(VALVE1)	VALVE	Outlet pressure = 4.296 bar
Expansion valve 2(VALVE2)	VALVE	Outlet pressure = 4.296 bar
	RADFRAC	Reflux mass ratio = 0.75 Mass flow rate at the bottom = 0.00741 kg/s
	HEATER	Pressure drop = 0 bar Exit temperature = 70°C
Rectifier (RECT)	FLASH block	Pressure = 15.9 bar Vapor fraction = 1

The calculation procedure used in the simulation for the different state points of the system is carried out at 31.3 °C of cooling air temperature are summarized in Table 5-4.

Table 5-4 Calculation procedure used for simulating of absorption system at 31.3 °C air cooling

States point	Calculation procedure
1	Saturated liquid; composition; total mass flow and pressure as input
2	Determined by the high pressure solution pump model
3	Determined by the SHX model
4 and 7	Saturated liquid and saturated vapor respectively, the mass flow rate ratio between state 4 and 7 is determined by the temperature of the waste heat available
5	Determined by the SHX model
6	Determined by the solution valve (VALVE1) model
8 and 9	Determined by the rectifier model base on a desired mass percent ammonia in state 9
10	Saturated liquid
11	Determined by refrigerant valve model
12	Vapor quality determined by evaporator pinch temperature

The proper selection of analogous blocks from software model-bank for primary elements of chilled machine is the foundation for modeling the process in ASPEN-PLUS.

A two-flow heat exchanger model is employed for the air-cooled condenser, absorber, evaporator, and solution heat exchanger. A distillation column is used to separate refrigerant in the generator. For the rectifier a simplified model flash column adapted to account for separation of remaining water vapor in this machine element. On one side, the generator's hot ammonia poor solution is mixed with evaporator's cold refrigerant vapors, resulting in partial absorption and a liquid/vapor mixture leaving for air-cooled absorber. On the other side, hot ammonia poor solution and heat produced to give partial absorption process heated ammonia rich solution as it passed to the generator.

5.5.4 Optimization for generator temperature and Coefficient of Performance

There are cases on which it is desired to simultaneously optimize two or more objective functions subject to the same set of constraints and variables. This is called multi-objective optimization. Two or more competing objectives must reduced or maximized while taking into account specific restrictions. This is known as a multi-objective optimization problem. The general form of a multi-objective optimization problem is as follows: [58]:

$$\begin{aligned} &Minimize/Maximize \quad f_m(x) \;\; m = 1,2,\dots,M \\ &\text{Subject to } \; g_j(x) \le 0 \;\; j = 1,2,\dots,J \\ &\qquad h_k(x) = 0 \qquad k = 1,2,\dots,K \\ &{x_d}^L \le \; x_d \le {x_d}^U \qquad d = 1,2,\dots,D \end{aligned} \tag{5-29}$$

The solution x is represented as $x = (x_1, x_2, x_3, \dots x_D)$ which is vector of D decision variables. The bounds of each decision variable are specified as the last set of constraints in Eq. (5-29) decides the structure of the D-dimensional variable space. The term $f_m(x)$ indicates the m_{th} objective in a total M number of objective functions, $g_j(x)$ represents the j^{th} inequality constraint and $h_k(x)$ is the kth equality constraint. In Eq. (5-29), J and K represent the total inequality and equality constraints, respectively.

In this work the objective of optimization is to maximize coefficient of performance of the ARS with 7.772 kW cooling capacity by optimizing its operating conditions in the presence of certain constraints. The COP is mainly depends on three variable on the component of condenser, absorber and generator while our evaporator specification is constant.

The optimization model includes three conflicting objective functions: the condenser sub cooling temperature, the heat exchanger change in temperature and the generator bottom mass flow rate and reflux mass ratio.

Result of optimization of ARS

Based on the three objective variables with in the given range the optimum generator temperature at the cooling load on the evaporator (Q_{eva} = 7.772 kW) is 101°C as shown in the Table 5-6 . The maximum COP of this system is 0.75. The stream results also present in the Table 5-5 below.

Table 5-5 Optimization result of the VARS for given objective function at 7.772 kW cooling load

State point	From	To	Pressure (bar)	Temperature (°C)	Vapor fraction	Mass flow rate (kg/hr)	NH3 Mass fraction (%)
1A	Absorber	Pump	4.296	37.52	0	48.24	44.9
2	Pump	SHX	15.9	37.75	0	48.24	44.9
3	SHX	Generator	15.9	60.05	0	48.24	44.9
4	Mixer	SHX	15.9	73.04	0	27.83	4.9
5	SHX	VALVE1	15.9	33.04	0	27.83	4.9
6	VALVE1	Absorber	4.296	33.28	0	27.83	4.9
7	Generator	Rectifier	15.9	100.89	1	22.14	96.14
8	Rectifier	Mixer	15.9	70.00	0	1.73	57.57
9	Rectifier	Condenser	15.9	70.00	1	20.41	99.4
10	Condenser	VALVE2	15.9	39.22	0	20.41	99.4
11	VALVE2	Evaporator	4.296	-0.39	0.14	20.41	99.4
12	Evaporator	Absorber	4.296	0	1	20.41	99.4
13	Generator	Mixer	15.9	70.00	0	26.10	0.014

Table 5-6 The optimum result of duty and COP of the ARS during charging process using hot storage PCM

Parameter	**Aspen-Plus prediction**
Q generator (kW)	10.26
Q condenser (kW)	8.69
Q evaporator (kW)	7.772
Q absorber (kW)	9.77
COP	0.75

As mentioned on chapter three at the night time (18 hrs.) cooling load of the system was 1.137 kW. Optimum generator temperature at the cooling load on the evaporator (Q_{eva} = 1.137 kW) is 87.9 °C as shown in the Table 5-7 . The maximum COP of this system is 0.64. The optimum result of duties also present in the Table 5-8 below.

Table 5-7 Optimization result of the VARS for given objective function at 1.137 kW cooling load

State point	From	To	Pressure (bar)	Temperature (°C)	Vapor fraction	Mass flow rate (kg/hr)	NH3 Mass fraction (%)
1A	Absorber	Pump	4.296	37.52	0	48.28	44.9
2	Pump	SHX	15.9	37.74	0	48.28	44.9
3	SHX	Generator	15.9	54.75	0	48.28	44.9
4	Mixer	SHX	15.9	74.67	0	26.63	8.5
5	SHX	VALVE1	15.9	45.67	0	26.63	8.5
6	VALVE1	Absorber	4.296	45.91	0	26.63	8.5
7	Generator	Rectifier	15.9	87.91	1	19.51	98.1
8	Rectifier	Mixer	15.9	50.00	0	1.86	80.5
9	Rectifier	Condenser	15.9	50.00	1	17.64	99.9
10	Condenser	VALVE2	15.9	39.22	0	17.64	99.9
11	VALVE2	Evaporator	4.296	-0.39	0.14	17.64	99.9
12	Evaporator	Absorber	4.296	0	1	17.64	99.9
13	Generator	Mixer	15.9	70.00	0	24.76	3.02

Table 5-8 The optimum result of duty and COP of the ARS during discharging process using hot storage PCM

Parameter	**Aspen-Plus prediction**
Q generator (kW)	1.789
Q condenser (kW)	1.163
Q evaporator (kW)	1.137
Q absorber (kW)	1.556
COP	0.64

CHAPTER SIX

6. SOLAR COLLECTOR AND HOT STORAGE PHASE CHANGE MATERIAL PERFORMANCE ANALYSIS INTEGRATED WITH VARS

6.1 Solar Thermal Collector with Hot Storage Phase Change Material on Absorption Refrigeration System

The most plentiful energy on our planet is solar energy. Systems for absorption refrigeration may be successfully combined with solar thermal systems since they are heated by heat. A day's worth of solar insolation is only available for a brief duration. As a result, without any form of energy storage, it is impossible to run an absorption system on solar energy for 24 hours. Thermal energy storage materials (TES) can be crucial in this situation for storing solar energy. In this case phase change material which is latent energy storage more beneficiary than sensible heat storage materials discussed in the literature.

Although solar-powered absorption systems are already in development, it appears that no more work has been done to integrate solar-charged phase change materials for absorption systems that operate at night. For day-night cycle operation, integration of the solar thermal collector and PCM storage with the absorption system has been given in this work. The evaporator of the absorption unit has been considered to keep a cold room with a capacity of 7.772 kW at 0 °C. This study has discussed the operational strategy of the developed system. The cooling demand determined the required PCM mass and CPC area.

In this study integration of solar energy and PCM as thermal storage to drive the absorption system is taken in two optional ways to analyze the performance of ARS. One of them is usage of hot thermal energy storage mount nearly to generator of absorption system (let it say system 1) which traps the thermal energy directly from the solar collector. And another one is usage of cold thermal storage mount on the evaporator of the absorption system (let it say system 2) that store the cold thermal energy and supply at night time. In this chapter the design and simulation of system 1 is investigated. The other system design and simulation will be present on the next chapter.

6.1.1 System Description

In this system, there are two cycles: the collection cycle captured and stored solar energy in a PCM storage tank, and the supply cycle heat is transferred from the PCM tank to the VARS generator. The schematic diagram of solar absorption refrigeration system (NH_3-H_2O) with solar charged hot storage PCM in collection cycle is shown in Figure 6-1. In this cycle from HTF storage tank (13) is pumped through the parabolic trough collector where it absorbs solar thermal energy (15) and passed through the flow separation valve in order to divide the coming high temperature HTF to PCM and generator to be applicable at the daytime. The thermal energy from the solar collector is supplied (18) to the PCM storage tank to charge the PCM through control valve. The temperature of PCM rises until it reaches the melting point, at which point it melts using the latent heat of fusion. The sensor gate valve closes when the PCM temperature rises to 10°C over the melting point, making the PCM suitable to heat the VAR generator (GEN). In parallel, the HTF is passed to generator directly from the CPC collector at the daytime. In the generator, the NH3-H2O solution's water evaporates, and the steam (9) then travels through the rectifier to completely separate the ammonia from the water before being sent to the condenser (CON), where it condenses. The condenser's liquid ammonia (10) is throttled in an expansion valve (REV), which lowers its pressure. At this pressure, the refrigerant (11), which evaporates while absorbing the latent heat of evaporation, flows through the evaporator (EVP). Following evaporation, the ammonia vapor (12) travels to the absorber, where the ammonia water solution absorbs it. Through the solution heat exchanger, the powerful NH3H2O solution (1) is fed to the VAR generator (SHX). The leftover weak ammonia solution (4) returns to the absorber after the ammonia evaporates in the generator while exchanging heat with the strong solution in the solution heat exchanger. The three-way valve locks the passage to the solar collector when solar radiation is not present, and the HTF passes via the PCM storage to get latent heat energy, which it then feeds to the generator as indicated in Figure 6-2.

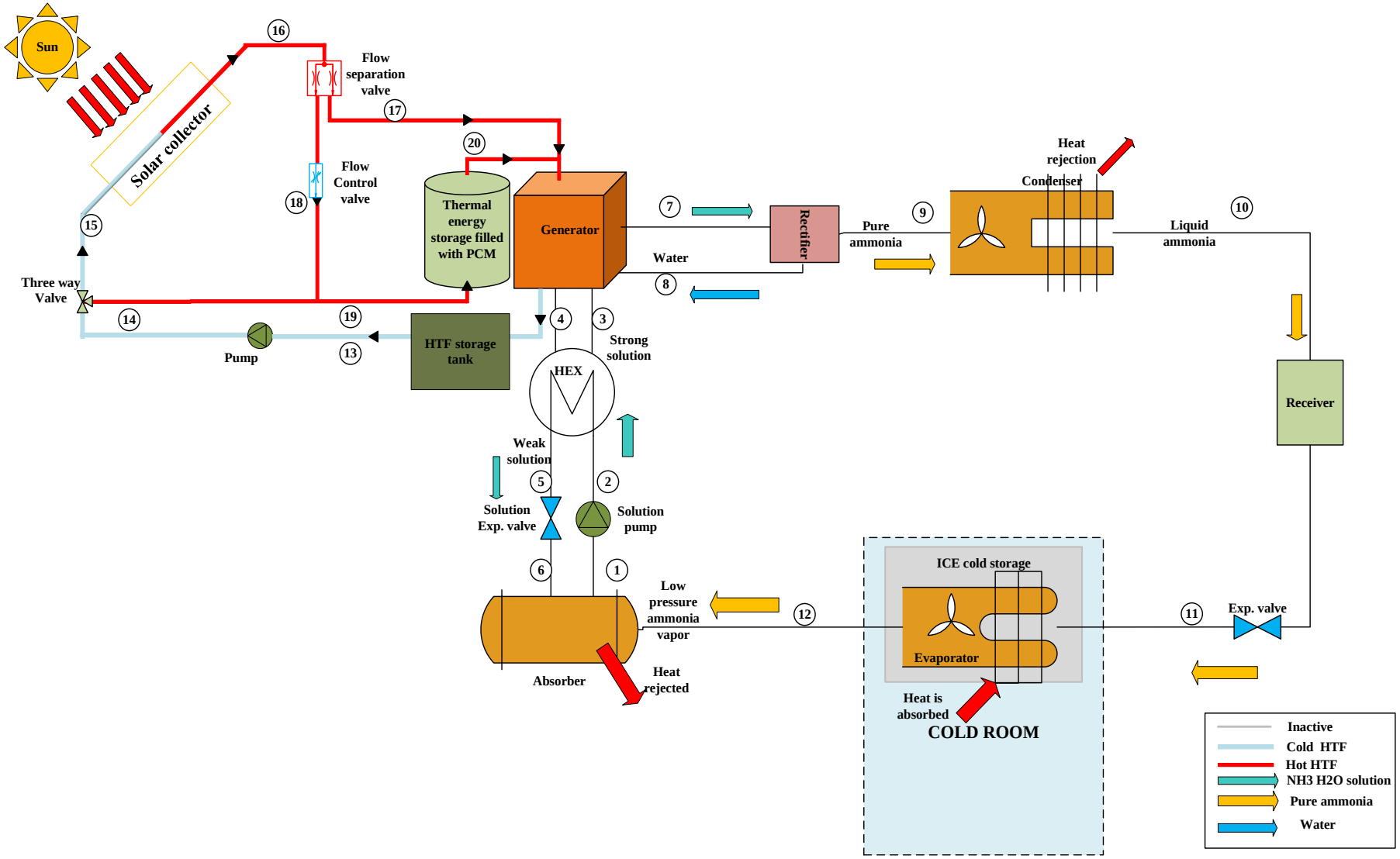

Figure 6-1 Vapor absorption refrigeration system powered by solar collector integrated with charging hot storage PCM

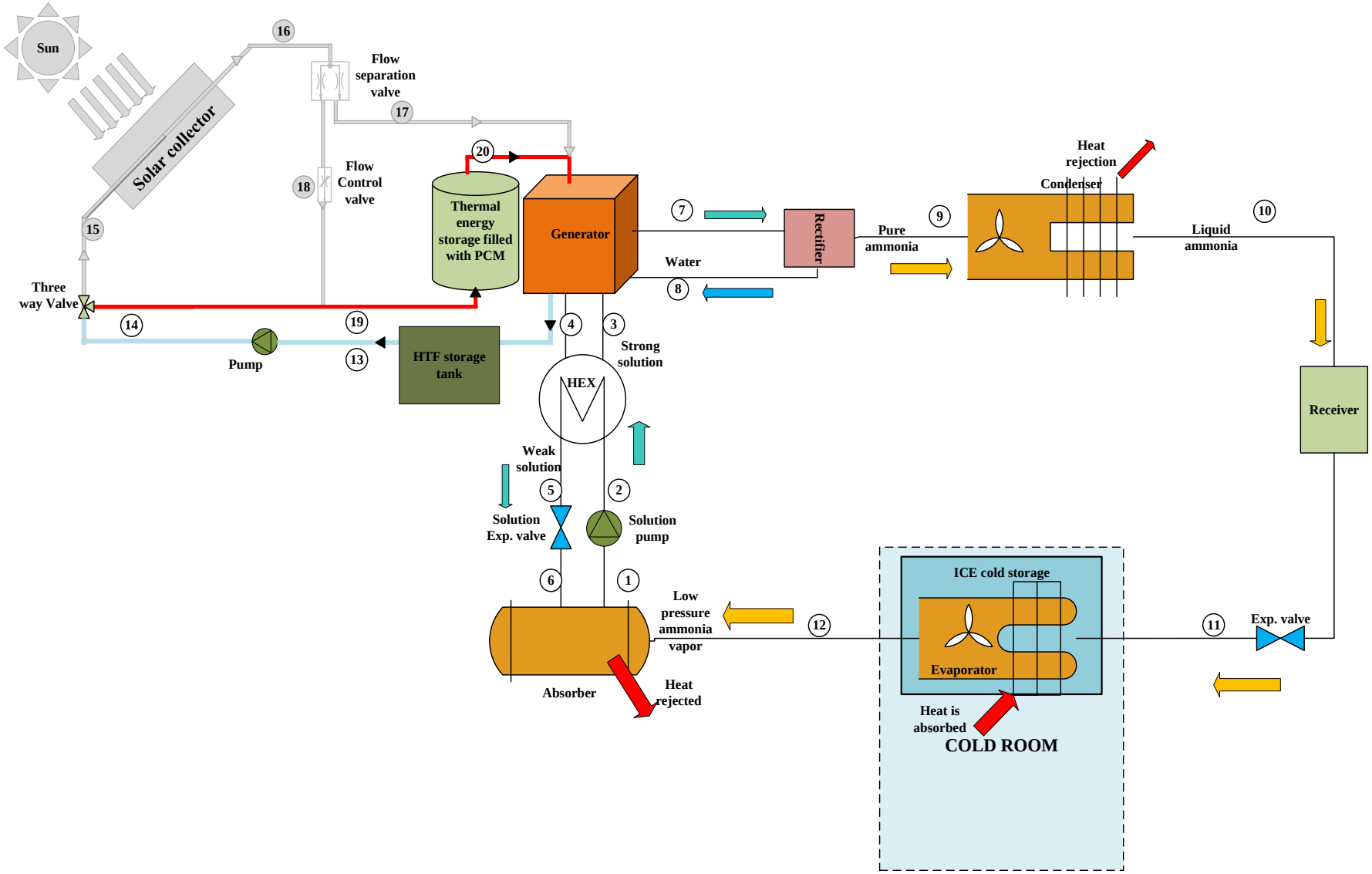

Figure 6-2 Vapor absorption refrigeration system powered by discharging of PCM storage

6.2 Design of Solar Collector

Prior to selecting the solar collector's size and doing a performance study, the kind of solar collector has to be established.

6.2.1 Selection of Solar Collector Type

According to the literature, the compound parabolic collector (CPC) with evacuated tube is the most suitable solar collector for the research's temperature range because it can create processing heat effectively. In order to surpass the 100oC limit, the employment of an evacuated tube is crucial, and conjugating it with a concentrating trough results in greater levels [59]. CPC collector has and advantage of high concentration ratio over than ETC [60] therefore for this study CPC collector is selected.

6.2.2 Sizing of CPC Collector

The compound parabolic concentrator uses sun radiation to gather energy. The HTF that passes through the absorber is heated by a receiver by absorbing the heat reflected from the collector. The heated HTF is transferred from the receiver to the storage through the charging pipe. The quantity of energy consumption and the availability of solar radiation should be taken into consideration while determining the size of the compound parabolic solar concentrator.

6.2.2.1 Geometric Sizing

A Cartesian plane is used to calculate and create parabolic solar collectors, and the two primary components of the geometry are drawn there as a curve and a parabola based on the absorber tube's size. Equations were provided for limiting the form of CPC solar collectors in respect to angle by turning the absorber tube counterclockwise from the positive x-axis. These formulas may be used to determine the coordinate plane geometry of CPC solar collectors as well as their curves for portions in the plane and parabolas. [61].

$$X = r(-\varphi cos\varphi + sin\varphi) \quad (6.1)$$

$$Y = -r(\varphi cos\varphi + sin\varphi)$$

To $$0 \leq \varphi \leq \frac{\pi}{2} + \theta_{max}$$

$$X = r(-A^{*}\varphi cos\varphi + sin\varphi)$$

$$Y = -r(\varphi cos\varphi + A^{*}sin\varphi)$$

To $$A^{*} = \frac{\frac{\pi}{2}+\theta_{max}+\varphi-\cos(\varphi-\theta_{max})}{1+\sin(\varphi-\theta_{max})}$$

To $$\frac{\pi}{2} + \theta_{max} \leq \varphi \leq \frac{3\pi}{2} - \theta_{max}$$

Where r is absorber radius, φ an angle to be determined and θ_{max} maximum acceptance half-angle. Since in this paper the full CPC collector is considering $\varphi = 2\theta_{max}$. As seen, a two-dimensional CPC is made up of two separate parabolas that are positioned so that one parabola's focus is on the other. The acceptance angle max is the angle formed by the CPC's axis and the line that runs from one parabola's focus to the aperture is the acceptance angle θ_{max} edge. The CPC optical axis is parallel to the slope of the parabolic reflector surface at the entry aperture. As a result, the sun rays that are directed at the absorber's surface at the concentrator's maximum acceptance angle are tangentially reflected.

The concentration ratio (C) is given

$$\frac{A_{ap}}{A_a} = C = \frac{1}{sin\theta_{max}} \qquad 6.2$$

The focal length $f = A_{ap}(1 + \sin\theta_{max})$

Area of coverage of CPC collector or aperture area is given $A_{ap} = WL$, Where L is length of the collector and W is collector width.

The height of concentrator of CPC (H) is given as

$$H = \frac{W \times (1 + sin\theta_{max})}{2\tan\theta_{max}} \qquad 6.3$$

Sizing of absorber

Radiation reflected from the solar concentrator is captured by the receiver at this the concentration ratio is used to compute the receiver's (absorber's) size. The area of absorber can be determined by:

$$A_a = \frac{A_{ap}}{C} \qquad 6.4$$

From absorber lateral surface area (cylindrical absorber) $A_a = \pi \times D_o \times L$ where D_o is the external diameter of absorber tube can be determined.

Dr. Subhi et al. shows the area of the concentrator or reflector A_{con}, is related with the area of the apertures A_{ap}, as

$$A_{con} = A_{ap}(1 + sin\theta_{max}) \quad 6.5$$
$$* \left[\frac{cos\theta_{max}}{sin^2\theta_{max}} + \ln \left\{ \frac{(1 + sin\theta_{max}) + (1 + cos\theta_{max})}{sin\theta_{max} \left\{ cos\theta_{max} + (2 + 2sin\theta_{max})^{1/2} \right\}} \right\} \right.$$
$$\left. - \frac{\sqrt{2}cos\theta_{max}}{(1 + sin\theta_{max})^{3/2}} \right]$$

Dr. Subhi et al. also shown that the average number of reflection n, passing through a CPC inside is acceptance angle is given as

$$n = \frac{1}{2sin\theta_{max}} \left(\frac{A_{con}}{A_{ap}} \right) - \frac{(1 + 2sin\theta_{max})(1 - sin\theta_{max})}{2sin^2\theta_{max}} \quad 6.6$$

According to this design's concentration ratio (C) of 3.8 and external absorber tube diameter (Do) calculation of 0.042 m, the half acceptance angle (θ_{max}) was discovered to be 15.26°. By substituting the aforementioned values (D, θ_{max}) in equation (3), the height of the CPC (H) can be determined and will be 3.47 m. CPC will be 4 meters long and 1.5 meters wide, respectively. The receiver tube's inner diameter is set at 0.038 m.

As Dr. Subhi et al. mentioned the reflectivity (ρ) of the reflector is selected to be (97.4%) (SolaReflex thick foil material). The glass cover's transmissivity has been set at 0.95. The absorber's absorptivity is set to 0.95 and its emissivity to 0.9. The glass cover's interior and external diameters are chosen to be (0.05m) and (0.054), respectively. Assume that the CPC collector was pointed south and that its slop (β) is 0 degrees.

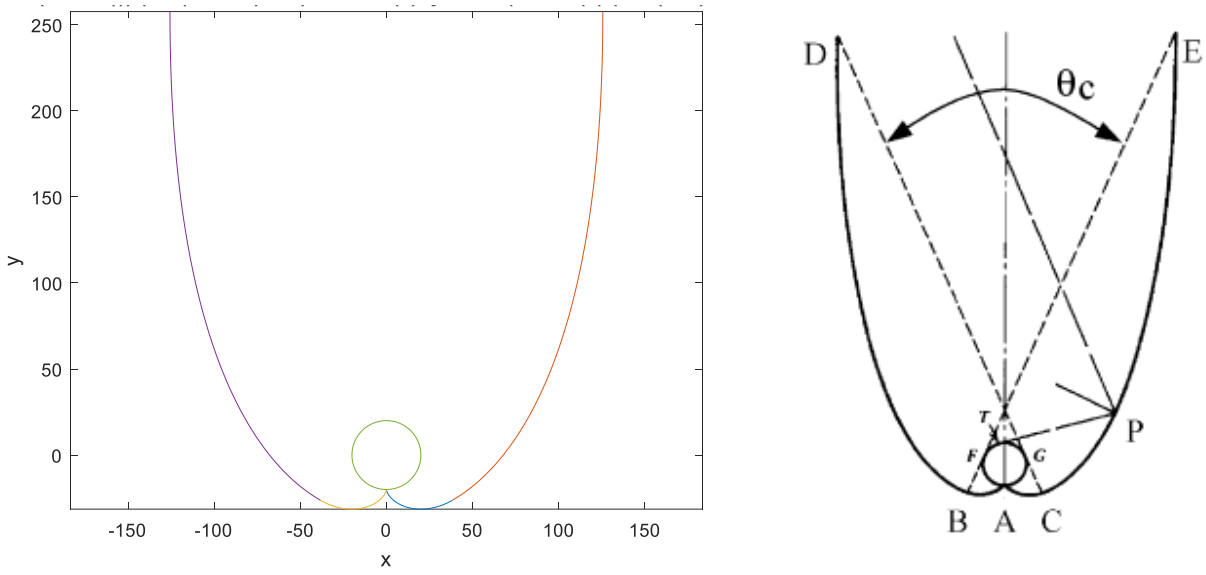

Figure 6-3 Schematic diagram of a compound parabolic collector.

Mathematically planned and built CPC solar collectors with a Security glass covering hide the reflecting surface and safeguard the environment. A resin-coated polystyrene insulation material was utilized for strength and protection. A special adhesive was used to adhere the polystyrene to the reflective foil. A stainless steel absorber tube is coated in matte black selective absorbers. The cover was made of security glass and fastened to a framework with an aluminum frame that encircled the solar collector's edges. It needs to be placed in a fixed location before being tested.

6.2.2.2 Optical Efficiency

The goal of optical analysis of the sun's rays is to determine the heat output of the inspected collector. Under ideal conditions, the concentrators fully reflect incident solar energy. However, due to optical losses, there is no perfect mirror of solar light in reality. The optical performance of CPCs is influenced by a number of factors, including tracking error, geometry error, and mechanical failure.

According to the materials, optical efficiency for solar collector construction was estimated. The solar radiation in the absorber tube may be calculated using this approach. The estimated optical efficiency and relationship are as follows [61].

$$\eta_{op} = \tau_{cpc}\rho r^{n}\alpha_{a}p \qquad 6.7$$

Where τc crosses the cover. αa is the absence of adsorbent. p is the reduction coefficient of the opening. Its formula (1 − g/2πro) in the formula the thickness of the gap is g (here, g = 1.00 cm was considered). ρrn is the effective transmission of the CPC solar collectors. Here, ρ is the solar reflection of the reflective material of the CPC solar collectors. In Formula (10), the average number of reflections is obtained from the following equation:

The effective transmissivity of CPC, τ_{CPC}, accounting for reflection loss inside the CPC depends on the specula reflectivity, ρ, of CPC wall and the average number of reflections ,n, and is given as

$$\boldsymbol{\tau_{\mathrm{CPC}} = \rho^{n}} \qquad 6.8$$

6.2.2.3 Thermal Efficiency

On a premise put out by several writers, the study of CPC solar collectors the mathematical framework was developed. The heat transfer fluid (HTF) circulating through the tube then absorbs the concentrated solar radiation and transforms it into thermal energy.

A transparent cover is often placed over a compound parabolic concentrating (CPC) collector, which is oriented with its long axis in the east-west direction and slanted towards the south. The CPC is angled so that it receives radiation from both beams within the acceptance angle (θ_{max}). The broad acceptance angle of a CPC allows it to receive both diffuse and beam radiation. The absorber or receiver can be of any shape, but often tubes that are joined to the bottom and selectively coated are utilized, as illustrated in Figure 6-4.

The useful energy $Q_u$can be calculated as was done earlier if we know the absorbed energy I_a and U_L.

The insolation, I_{CPC} within the acceptance angle of CPC with concentration ratio, C, is given as

$$I_{\mathrm{CPC}} = I_T - \left(1 - \frac{1}{C}\right) I_d \qquad 6.9$$

Where I_T and I_d are the total and diffuse radiation respectively on the aperture plane. Now the absorbed radiation I_a in terms of I_{CPC} is

$$I_a = I_{CPC}\tau_{cover}\tau_{CPC}\alpha_r = I_T\tau_{cover}\tau_{CPC}\alpha_r\gamma = 1 - \left(1 - \frac{1}{C}\right)\frac{I_d}{I_T} \qquad 6.10$$

Where τ_{cover} = transmissivity of cover τ_{CPC} =effective transmissivity of CPC α_r = absorbtivity of receiver γ = correction factor for diffuse radiation.

The empirical expression of U_L for a CPC with tubular absorber coated with selective coating, covered with concentric glass cover [62], space evacuated and the entire collector covered with a transparent cover is given as

$$U_L = (0.18 + 16.95\varepsilon_r)[0.212 + 0.00255T_a + (0.00186 + 0.000012T_a)(T_r - T_a)] \qquad 6.11$$

Where, T_a = ambient temperature, ºC T_r = absorber temperature, ºC ε_r = emissivity of absorber surface U_L = collector heat loss coefficient, W/m^{2}K of absorber area.

6.2.3 Physical Modeling of CPC Collector

The physical modeling of CPC collector is performed on SOLIDWORK work space using the calculated dimensions.

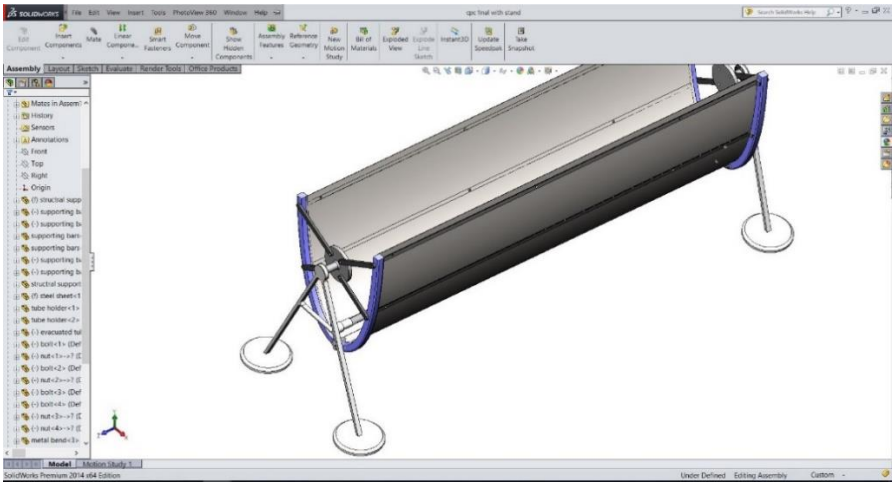

(a)

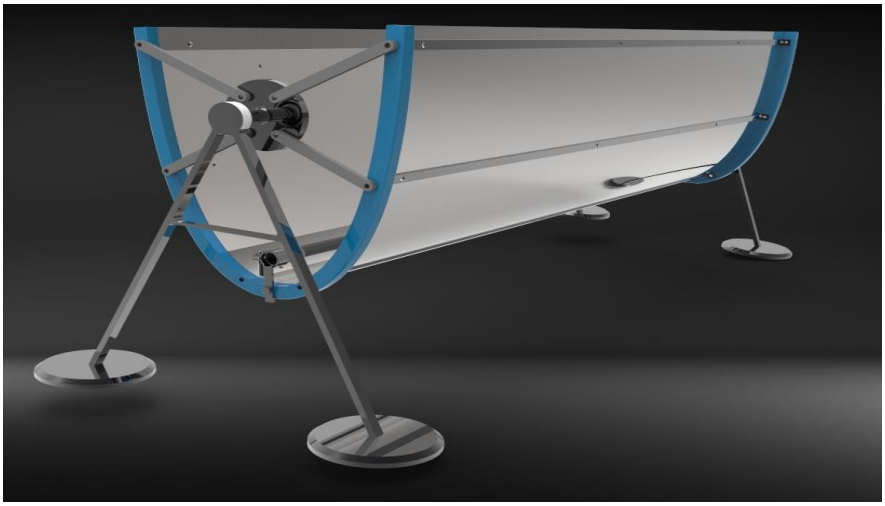

(b)

Figure 6-4 Both a & b 3D Design of CPC collector

6.2.4 Thermal Resistance model of CPC Collecting Elements

The network's Figure 6-5 depicts the heat transfer methods used by CPC solar collectors. The analysis of solar collectors has been recommended for this network. The temperature of the absorber tube in the solar collector rises as a result of solar energy being absorbed there. The heat transmission method in the illustration has five primary temperatures. The fluid, adsorbent, coating, reflector, and environment all have these temperatures.

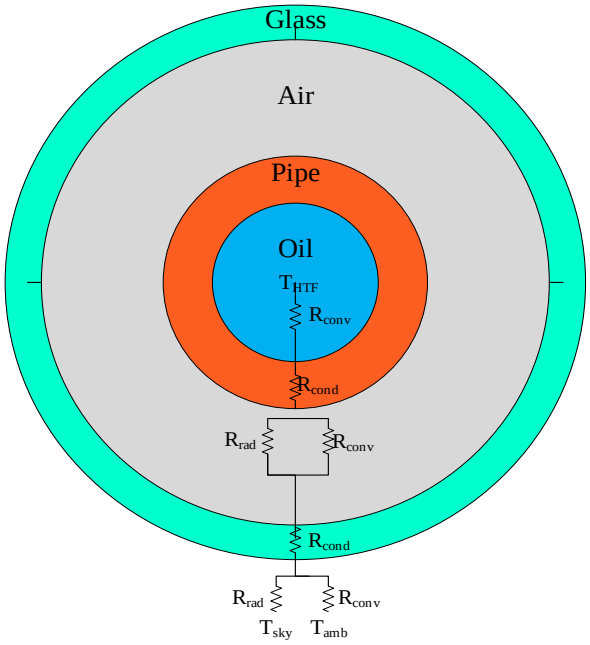

Figure 6-5 Heat transfer network of CPC solar collector

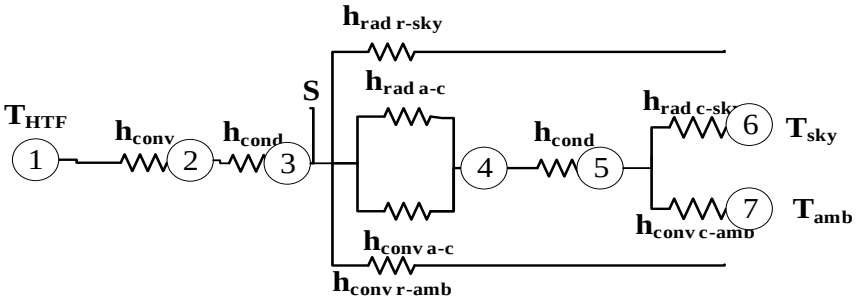

Each node of temperature represents HTF, absorber tube inner surface, absorber tube outer surface, glass tube inner surface, glass tube outer surface, surrounding air and sky respectively

Figure 6-6 Heat transfer network of CPC solar collectors for mathematical modeling

6.2.4.1 Heat Transfer Interaction Analysis in a CPC Collector

A. Heat transfer between the glass cover and the surrounding environment

Convection transfers heat from the glass cover to the ambient air around it, while radiation transfers heat from the glass cover to the sky as a result of temperature differences.

1. Heat transfer through convection

The convection heat transfer is calculated using

$$q_{cover,c-amb} = h_{conv,c-amb}(T_c - T_{amb}) \quad 6.12$$

The aforementioned calculations show the convective heat transfer coefficient between the environment and the glass covering expressed with $h_{conv,c-amb}$ and is calculated from the following formula.

$$h_{conv,c-amb} = \frac{A_c}{A_a}(3.8V + 5.7) \quad 6.13$$

In the formulas, the wind speed is *V* in *m/s*.

2. Heat transfer via radiation

Assume that the sky is represented as a big blackbody cavity, with the glass envelope acting as a little gray convex inside it. The glass container and the sky's radiative heat transmission are provided by

$$q_{rad,c-amb} = h_{rad,c-sky}(T_c - T_{amb}) \quad 6.14$$

The radiant heat transfer coefficient between the cover and sky is given by

$$h_{rad,c-sky} = \varepsilon_c \sigma({T_c}^2 + {T_{sky}}^2)(T_c + T_{sky})(\frac{A_c}{A_a}) \quad 6.15$$

Where ε_c is the external surface of cover glass emittance, σ is the Stephen Boltzmann's constant ($5.67 \times 10^{-8} W/m^2K^4$), T_c is the glass coating temperature, and T_{sky} is the sky temperature. The sky temperature is 6 degrees Celsius lower than the ambient temperature.

$$T_{sky} = T_{amb} - 6℃$$

B. Heat transfer between the reflector and the glass cover, as well as between the reflector and the atmosphere

Heat is also transferred from the parabolic reflector of the collector in and outside of the reflector by convection and radiation.

1. Heat transfer through convection

The convective heat transfer from the reflector to glass cover and to atmosphere is given in the following equations:

$$q_{conv,r-c} = h_{conv,r-c}(T_r - T_c) \quad 6.16$$

$$q_{conv,r-amb} = h_{conv,r-amb}(T_r - T_{amb})$$

Where the heat transfer coefficients are

$$h_{conv,r-c} = (3.25 + 0.0085)\left(\frac{T_c - T_r}{4r_o}\right) \quad 6.17$$

$$h_{conv,r-amb} = \frac{A_r}{A_a}(3.8V + 5.7)$$

2. Heat transfer via radiation

The radiated heat transfer from the reflector of the CPC collector to the glass cover and to the atmosphere is given as

$$q_{rad,r-c} = h_{rad,r-c}(T_r - T_c) \quad 6.18$$

$$q_{rad,r-sky} = h_{rad,r-sky}(T_r - T_{amb}) \quad 6.19$$

$$h_{rad,r-c} = \frac{\sigma({T_r}^2 + {T_c}^2)(T_r + T_c)}{\frac{(1-\varepsilon_c)}{\varepsilon_c} + \frac{1}{F_{c-r}}\left(\frac{A_c}{A_r}\right)\frac{(1-\varepsilon_r)}{\varepsilon_r}}\left(\frac{A_r}{A_a}\right) \quad 6.20$$

Where

$$F_{c-r} = \left(\frac{1}{2}\right)\left[\frac{A_r}{A_c} - \frac{(1-\sec\theta_{1/2})(1+\ 2\sec\theta_{1/2})}{\sec\theta_{1/2}}\right]$$

$$h_{rad,r-sky} = \varepsilon_c\sigma({T_r}^2 + {T_{sky}}^2)(T_c + T_{sky})\left(\frac{A_r}{A_a}\right) \quad 6.21$$

$$h_{rad,a-r} = \frac{\sigma(T_r^2 + T_a^2)(T_r + T_a)}{\frac{(1-\varepsilon_r)}{\varepsilon_r} + \frac{1}{F_{a-r}} + \left(\frac{A_r}{A_a}\right)\frac{(1-\varepsilon_a)}{\varepsilon_a}} \quad 6.22$$

$$F_{a-r} = \left(\frac{A_r}{2A_a}\right)\left[1 - \left(\frac{A_c}{A_r}\right)\frac{(1-\sec\theta_{1/2})(1+\ 2\sec\theta_{1/2})}{\sec\theta_{1/2}}\right]$$

C. Transfer of heat between the receiver tube and the glass cover

Convection and radiation mechanisms transfer heat between the receiver tube and the glass cover.

1. Heat transfer through convection

$$q_{cover,a-c} = h_{cov,a-c}(T_r - T_c) \quad 6.23$$

Where the convective heat transfer coefficient is *hcov, a-c* and is calculated

$$h_{cov,a-c} = (3.25 + 0.0085)\left(\frac{T_a - T_c}{4r_{ao}}\right) \quad 6.24$$

Given that the input of the current collector is considered to be fully developed, the outer diameter of the receiver tube of the solar collector is r_o

2. Heat transfer via radiation

The radiation heat transfer between the receiver tube and the glass cover is calculated as follows:

$$q_{rad,a-c} = h_{rad,a-c}(T_a - T_c) \quad 6.25$$

Where the radiation heat transfer coefficient between the absorber tube and the glass envelope is expressed as follows

$$h_{rad,a-c} = \frac{\sigma({T_r}^2 + {T_c}^2)(T_r + T_c)}{\frac{1}{\varepsilon_c} + \left(\frac{A_c}{A_r}\right)\left(\frac{1}{\varepsilon_a} - 1\right)} \quad 6.26$$

D. Heat is transferred by conduction through the receiver tube and similarly through the trough glass cover.

The Fourier's equation of conduction through a hollow cylinder, which makes the assumptions that there is no thermal resistance and that the thermal conductivity of the glass is constant, is used to calculate the conduction heat transfer through the receiving tube wall.

$$q_{cond,ri-ro} = \frac{2\pi k_r(T_{ri} - T_{ro})}{\ln(\frac{D_{ro}}{D_{ri}})} \quad 6.27$$

Where: k_r is receiver tube thermal conductivity of receiver tube at the average temperature $\frac{T_{ri}+T_{ro}}{2}$ $(W/m℃)$

The same formula is used for conduction through the receiver tube wall and conduction through the glass cover.

E. Transfer of heat between the HTF and the absorber tube

Convectional heat transfer from the inside surface of the receiver tube to the HTF is calculated using Newton's equation of cooling.

$$q_{u-f} = \pi D_{ri} h_{conv,f-a}(T_a - T_f) \quad 6.28$$

The convection heat transfer coefficient at the inside pipe diameter

$$h_{conv,f-a} = Nu_f \frac{k_f}{D_{ri}} \quad 6.29$$

Where Nu_f is Nusselt number based on inside diameter of pipe and D_{ri} is inside diameter of pipe

The Nusselt number calculated using the Gnielinski correlation (Lamrani et al., 2018).

Laminar flow occurs in the receiver tube and the Nusselt number is constant while the Reynolds number is less than 2300. Assuming a constant heat flux, the constant value for pipe flow.

For $Re_f < 2300$ $\quad Nu_f = 4.36$

For $Re_f > 2300$ $\quad N_u = 0.023\, Re^{0.8} {p_r}^{0.4} = \frac{D_{abs,i} h_{conv,fi}}{K}$

F. Collector heat removal factor

The usable energy acquired in relation to the energy gained if the entire absorber were at the heat transfer fluid's input temperature is known as the heat removal factor. It is a measurement of the thermal resistance that solar radiation that has been absorbed must overcome in order to reach the collecting fluid, and it is stated as

$$F_R = \frac{MC_f}{A_r U_L}\left[1 - exp\left(-\frac{A_r U_L F'}{MC_f}\right)\right] \quad 6.30$$

Where A_r is the receiver area (m2) and F' is the collector efficiency factor is given by

$$F' = \frac{{}^{1}/_{U_L}}{\frac{1}{U_L} + \frac{dU_L}{N\pi D_{abs,i} h_{ci}}} \quad 6.31$$

Where k_f is thermal conductivity of the working fluid (W/m K), D_{ro} is receiver tube inner diameter D_{ri} is receiver tube outer diameter, h_{fi} is convective heat transfer coefficient inside the receiver tube [W/m^{2}K] and U_L is the thermal loss coefficient and given by

$$U_L = \left\{\left(h_{tot,c-amb}^{-1}\right) + \frac{h_{tot,a-c}^{-1}\left[h_{tot,r-amb}^{-1}\left(h_{tot,r-c}^{-1} + h_{tot,a-r}^{-1}\right)^{-1}\right]}{h_{tot,a-c}^{-1} + h_{tot,r-amb}^{-1}\left(h_{tot,r-c}^{-1} + h_{tot,a-r}^{-1}\right)^{-1}}\right\}^{-1} \quad 6.32$$

$$= (0.18 + 16.95\varepsilon_r)[0.212 + 0.00255T_a + (0.00186 + 0.000012T_a)(T_r - T_a)]$$

Where the total heat transfer coefficients are

$$h_{tot,c-amb} = h_{conv,c-amb} + h_{rad,c-sky}$$

$$h_{tot,r-amb} = h_{conv,r-amb} + h_{rad,r-sky}$$

$$h_{tot,a-r} = h_{conv,a-r} + h_{rad,a-r}$$

$$h_{tot,a-c} = h_{conv,a-c} + h_{rad,a-r}$$

G. Thermal efficiency

The ratio between the heat flux received by the concentrator and the usable heat gain by the HTF is known as the thermal efficiency of a solar CPC. It is crucial to note that, because these collectors are imaging collectors with a particular picture of the sun in the receiver, only the beam radiation may be utilized from the CPC. (Chahine et al., 2018). The instantaneous thermal efficiency given by

$$\eta_{th} = \frac{Q_{ua}}{A_{ap} I_b} \quad 6.33$$

The useful energy Q_{ua} can be calculated as was done earlier if we know the absorbed energy I_a and U_L.

$$Q_{ua} = I_a A_c - A_a U_L (T_a - T_{amb}) \quad 6.34$$

$$Q_{uf} = A_a F_R \left[I_a - \frac{U_L}{C} (T_{f,i} - T_a) \right] \quad 6.35$$

The outlet fluid temperature is calculated from equation as:

$$T_{f,o} = T_{f,i} + \frac{Q_{uf}}{MC_f} \quad 6.36$$

Mean temperature of fluid,

$$T_{f,m} = \frac{T_{f,i} + T_{f,o}}{2} \quad 6.37$$

The receiver temperature will be,

$$T_r = T_{f,m} + \frac{MC_f (T_{f,o} - T_{f,i})}{h_{ci} \pi D_{r,ext} L} \quad 6.38$$

6.2.4.2 Transient Analysis of CPC Collector

The following hypothesis are considered to analyze the thermal behavior of the CPC solar collector:

- Continuous heat transfer.
- The non-specific permeability of low iron glass coating is 0.90.
- One-dimensional flow is taken into account.
- The reflector sheets are made of steel and have a 0.9 reflection coefficient.
- The corrosion-resistant steel used as the collector adsorbent has an absorption coefficient of 0.95.
- CPC solar collectors have perfect geometry due to flawless production.
- The thermodynamic characteristics, heat flows, and all temperatures are homogeneous around the CPC solar collector.
- The heat resistance of an absorber tube for a solar collector is insignificant and unconsidered.

A. Energy balance of glass cover

On the collector cover, heat transmission between the glass and the outside environment takes place as a result of a number of separate sources of heat transfer, including convection and radiation, which results in a significant amount of heat loss. On the composite parabolic collector glass cover, the formula for the instantaneous energy balance is as follows:

$$G(\alpha_c) + q_{rad,r-c} + q_{conv,r-c} = q_{conv,c-amb} + q_{rad,c-amb} + C_c \frac{dT_c}{dt} \qquad 6.39$$

Where the CPC solar collector glass cover is absorbed by the absorption coefficient α_c and $G(\alpha_c)$ is the amount of radiant solar energy.

B. Energy balance of absorber tube

Internal heat transfer is the heat transfer that occurs between the radiation receiver tube and the heat transfer fluid (HTF), and its value is calculated using the receiver tube's instantaneous energy balance formula.

$$G(\tau_c \alpha_r) = Q_{ua} + q_{conv,r-c} + q_{rad,r-c} \qquad 6.40$$

Where $G(\tau_c\alpha_r)$ is the solar energy passing through the glass coating and τ_c is the absorption coefficient of the glass coating and α_r is the absorption coefficient of the receiver.

C. Energy balance of heat transfer fluid

The energy balance for heat transfer fluid circulating in the absorber tube is stated as

$$m_f C_f \frac{\partial T_f(x,t)}{\partial t} + \dot{m} C_f (T_f(x + \Delta x, t) - T_f(x,t) = Q_{uf} \qquad 6.41$$

Where $\dot{m}$ is a flow rate working fluid flows inside the absorber, $Q_{uf}$is useful heat transfer to the working fluid by convection.

6.2.5 Sizing and Configuration of Solar Fields Using CPC Collector

Determining a set of characteristics that affect solar field performance is the initial stage in the design of a CPC solar field. These variables include the orientation of the solar collectors, the day of the The design point, the direct solar irradiance and ambient air temperature for the chosen date and

time, the location of the plant site (latitude and longitude), the total thermal output power that will be provided by the solar field, the temperatures of the solar field's inlet and outlet, the working fluid for the solar collectors, and the working fluid flow rate.

To produce the needed nominal thermal power output at design point in a typical CPC field, numerous collectors are linked in series to form a row, and several rows are connected in parallel. The number of series-connected collectors in each row is determined by the desired temperature rise between the row's input and output. The number of parallel-connected collectors in a single row was chosen based on the absorption process's requirement for thermal power.

$$Number\ of\ collector = \frac{Thermal\ power\ demand}{The\ power\ delivered\ by\ single\ collector}$$

The power delivered by single collector averagely at minimum irradiance is available for the given size of CPC collector is calculated as 790.92W. The thermal power demand to operate the absorption system using the hot storage PCM is 13.04 kW of energy is required. Therefore for this case the number collector is 17. When the maximum solar irradiance is available the power delivered by single collector calculated as 1601.1 W. therefor for this case the number collector that satisfies the mentioned system power requirement is 8 collectors.

6.3 Sizing of Phase Change Material and Performance Analysis

6.3.1. Material selection of PCM

Material selection is one of the important part in the methodology. The mass flow rate of the heat transfer fluid and the operating temperature are the two main factors that affect PCM's usefulness in solar collectors. The operating temperature aids in choosing the PCM with the proper melting point, and the heat load, combined with the mass flow rate of the heat transfer fluid, determines how long the heat storage system needs to charge and discharge. Solar absorption systems inherently require a thermal storage to deliver heat throughout the night since their heat source is intermittent.

6.3.1 Selection of Phase Change Material

A suitable PCM with a melting point within the range of the generator temperature (81.5°C) is identified. Since the temperature of the heat source (solar collector) is estimated to be more than 130°C and allowing a temperature difference of 20°C, the candidate PCM should have a temperature of 101.5°C as a melting point for the application.

Numerous candidate PCMs are considered for the LHS in the range of 93°C and 120°C [29], [33], [63], [64]. Table 6-1 provides some the PCMs identified in the literature for the required temperature range.

Table 6-1 Thermal and physical properties of selected PCMs

PCM NAME	TYPE	MELTING POINT [°C]	HEAT OF FUSION [kJ/kg]	THERMAL CONDUCTIVITY [W/m.K]	DENSITY [kg.m^3]	HEAT CAPACITY [kJ/kg.K]
Xylitol	Alcohol	93	280	n.a	n.a	n.a
Alpha napthol	Alcohol	96	163	n.a	1096	n.a
Glutaric acid	Fatty acid	97.5	156	n.a	1429	n.a
Oxalic acid	Fatty acid	105	356	n.a	1900	1.62
Erythritol	Alcohol	117	344	0.73/0.326	1450/1300	1.38/2.25
Methyl fumarate		102	242	n.a	1046	n.a
MgCl2.6H2O	Salt hydrate	116.7	168.9	0.704/0.57	1570/1450	2.25/2.61

From Table 6-1 PCMs identified have the required melting point; they are not all well documented for some of relevant properties needed for the sizing of the LHS. One example is Methyl fumarate in Table 5.1 that has a melting point of 102°C, information regarding its thermal conductivity and heat capacity were not available. If more than one PCM is identified based on the melting point, secondary comparisons (in literature review) are considered to select the best candidate PCM.

Since the optimized generator temperature is 81.5^{o}C. Therefore, with in this range by considering the above criteria the selected PCM is **ERYTHRITOL**, which is alcohol in the family of organic PCM. Previous studies revealed that, erythritol possess a latent heat of fusion close to 344 kJ/kg with melting point of 117^{o}C, which is higher value than other materials in this family [29]. Its thermal conductivity is 0.326 (liquid, 140 °C) and 0.733 (solid, 20 °C) as [65] determines.

6.3.2 Selection of Heat Transfer Fluid

The HTF is used as working fluid that passes heat energy gained from solar collector to the PCM storage and generator. The heat transfer fluid have to be taken the temperature of solar collector therefor it should reach greater than 100°C to satisfy PCM temperature and simultaneously generator temperature. Liquid phase of heat transfer fluid is required, in order to use single pump on the system. Liquid heat transfer has several benefits, including less expensive installation and operation. Eliminating large-diameter pipelines, safety valves, steam traps, and water treatment facilities lowers capital costs. Low maintenance needs and decreased makeup save operating costs. Every Eastman Therminol heat transfer fluid is capable of performing well in the liquid phase. Therminol D-12, LT, 55, 59, 68, 72, 75, VP-1, and VP-3 fluids need system pressures larger than their vapor pressures to operate in the liquid phase to their maximum bulk temperature ratings when above their typical boiling temperatures.

A HTF selected in this case was Therminol-55 (Appendix B) the selection is applied based on the catalog and the availability on the simulation software. Therminol liquid phase heat transfer fluids operate over a broad temperature range of –175° to 750°F (–115° to 400°C) and most can be used in non-pressurized systems. It is ideal for heating and cooling and user-friendly in environmental applications. Therminol-55 presents a low odor and has a high flash point; it is a hydrocarbon blend (Awasthi, et al. 2019).

6.3.3 Selection of PCM Storage Tank Material

The PCM is efficiently charged and discharged as necessary consider to the size and material type storage tank. The most prevalent kind of storage unit for (PCM) is a shell and tube heat exchanger, with PCM on the shell side [65].

The selection of a material for the tube heat exchanger depends on several criteria. Among them are thermal conductivity, corrosion and cost. Copper has a thermal conductivity of 386 W/m^{o}C at room temperature (20^{o}C) with the density of 8795 kg/m^{3} [64].

6.4 Sizing of Phase Change Material

From the calculation an absorption refrigerator machine requires optimum value of 1.789 kW as heat input to the generator while the pump work is very less. The cooling load of this machine at night time that requires PCM is 1.137 kW at a temperature level of 0°C (evaporator). With those requirements, the coefficient of performance of the refrigerator is 0.64.

The main goal is to determine the dimension of the PCM storage in terms of the inner and outer diameter of PCM, number of PCM capsules, volume of PCM, mass of the PCM, type of PCM and the appropriate HTF.

The design requirements of the PCM storage to be achieved are:

- Provide 100% solar heat to the domestic ARS;
- The minimum and maximum temperature of HTF entering the generator of the ARS required are fixed at 101°C and 110°C respectively;
- The storage system needs to be able to supply continuously the optimum thermal energy of 1.789 kW to the generator for a period of 18 hours;
- The storage system needs to be safe and non-toxic;
- Selected PCM has to have high latent heat of fusion since there is a constraint of space

To determine the design of PCM thermal storage, the amount of energy demand used for the generator on the absorption system and the mass flow rate of HTF circulates to the system should be known. The optimum temperature desirable for the generator operation should be justified.

Since the Erythritol was selected for the model and its property have been determined in the above section. The cylindrical, aluminum-made capsule is filled with PCM. The capsule's entire length is 0.5m. To stop the melted PCM from escaping out, this capsule is completely sealed on both sides. Aluminum was chosen as the material for the capsule due to its resistance to corrosion and its suitability for the sealing idea.

The amount of PCM is determined by energy demand. Which is $Q_g = 1.789$ kW of energy but by considering the thermal loss at HTF inlet and out let the storage material should 10% more than the required energy that is 1.9679 kW approximately 2kW of energy should store inside PCM, the mass of PCM required can be given as:

$$Q_{pcm} = \int_{Ti}^{Ts} m_{pcm} C_{ps}\, dT + m_{pcm} a_m \Delta h_m + \int_{Tm}^{Tl} m_{pcm}\, C_{Pl} dT \qquad 6.42$$

The energy stored in the PCM capsule is given:

$$Q_{pcm} = mC_p(T_m - T_i) + ma_m \Delta h_m + C_{pl}(T_f - T_m) \qquad 6.43$$

Where, m is mass of PCM, C_{ps} specific heat capacity of PCM for solid state, C_{Pl} specific heat capacity of PCM for liquid state, Δh_m enthalpy of phase fusion and a_m is the fraction melted.

Form the above equation the volume of PCM thermal storage can be determined as

$$V_{st} = \frac{E_{store,in\ pcm}}{\int_{Ti}^{Tm} \rho_{pcm,s}(1-\varepsilon) C_{ps}\, dT + \rho_{pcm}(1-\varepsilon)\Delta h_m + \int_{Tm}^{Tl} \rho_{pcm,l}\,(1-\varepsilon) C_{Pl} dT} \qquad 6.44$$

Therefor the volume of PCM was obtained as $V_{PCM} = 0.5228\ m^3$. Taking 10% change in Erythritol volume during solid liquid transition, the total PCM volume was $V_{PCM} = 0.575 m^3$.

The mass of PCM storage is given by:

$$m_{PCM} = \rho_{PCM} V_{st} (1-\varepsilon) \qquad 6.45$$

$$m_{PCM} = 372.159 kg$$

The diameter of the storage is determined as a function of length of storage defined as:

$$D_{st} = \sqrt{\frac{4V_{st}}{\pi L_{st}}} = 1.712m \quad 6.46$$

Assuming the diameter of PCM capsules is 150 mm, number of PCM capsules required for storage can be given as,

$$n_{PCM,capsules} = \frac{6(1-\varepsilon)V_{st}}{\pi {d_{PCM}}^3} = 195.37 \cong 196 \quad 6.47$$

Where, d_{PCM} is diameter of PCM.

The detail specification of the designed hot storage PCM is presented on Table 6-2 below.

Table 6-2 specification of the designed PCM unit

PCM selected	ERYTHRITOL
Melting point	117°C
Latent heat of fusion	344 kJ/kg
Heat Transfer Fluid	THERMINOL-55
Tube material	Copper
Inlet temperature of fluid	100°C
Mass flow rate	0.02 kg/s
Number of capsule	196
Tank diameter	1.712m
Tank volume	0.958 m^3
Volume of PCM	0.575 m^3
Storage period	18 hrs.
Mass of PCM	372.159 Kg

5.5 Physical Modeling of Hot Storage PCM and CPC collector

The physical modeling of PCM and solar collector are developed on SOLIDWORK benchmark. Basically it represents the designed PCM as shown in figure below.

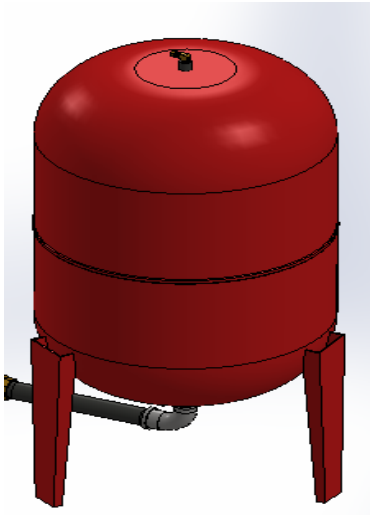

Figure 6-7 3D Design of Hot Storage PCM

6.5 Mathematical Modeling of PCM

The energy balance of the PCM material during energy storage (charge) and discharge is mathematically modeled in this section. An elongated tank with a PCM tube serves as the storage container. During the charging and discharging procedures, the heat transfer process between the HTF and the PCM tube is examined.

The HTF is flowing axially around the tube while the device is charging as shown Figure 6-8. Heat is exchanged between HTF and PCM through the tube when HTF passes through the storage system. The temperature of HTF is maintained throughout discharge procedure.

The following simplifications underpin the model:

- HTF is incompressible and can be thought of as a Newtonian fluid
- Inlet velocity and inlet temperature are constant
- Initial temperature of the latent heat storage unit is uniform, and the PCM is in the solid phase for melting or in the liquid phase
- All natural convection effects are ignored by disregarding any gravitational forces
- Applying constant values liquid PCM density

- PCM is homogeneous and isotropic
- Initial temperature of the PCM is also expected to be known

To establish time-dependent spatial temperature distributions, one-dimensional two-phase energy equations may be used to simulate heat transfer between the air and PCM capsules during charging and discharging.

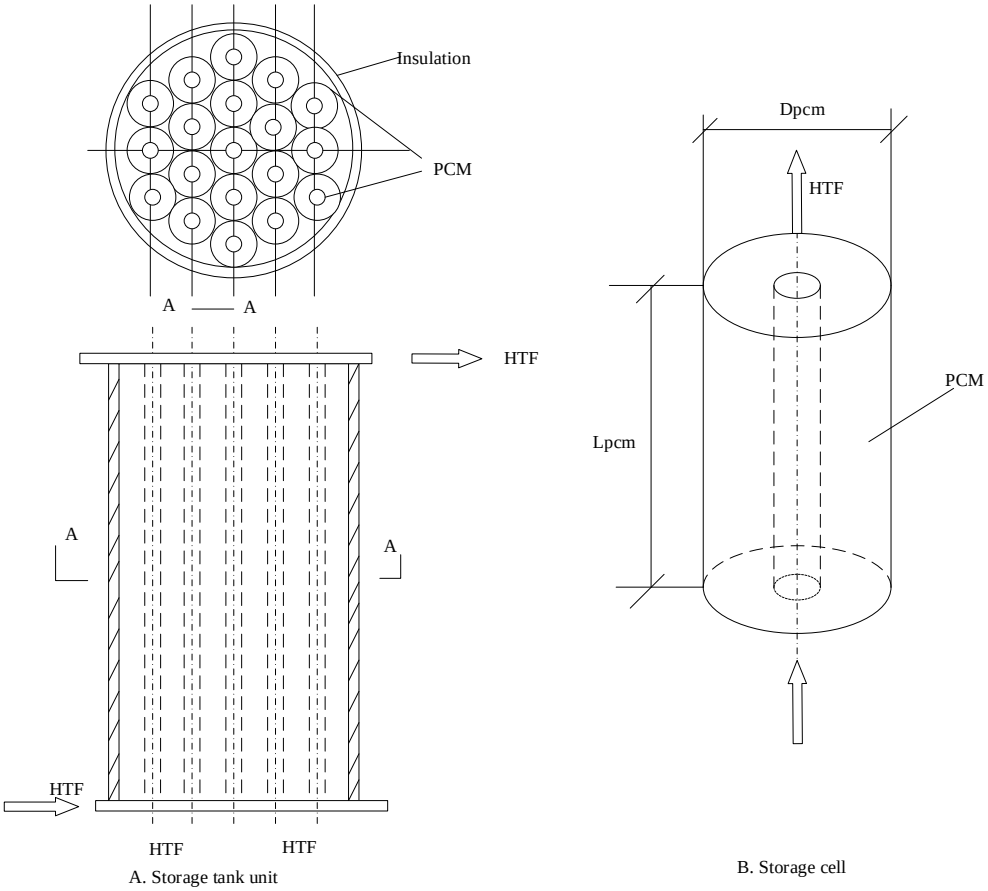

Figure 6-8 Diagram illustrating the geometry of cylindrical hot storage PCM

Transient heat transfer equation for HTF

The partial differential equation for the therminol-55 is given as:

$$\varepsilon A_{cx}\rho_{HTF}C_{p,HTF}\frac{\partial T_{HTF}}{\partial t} + h_v A_{cx}(T_{HTF} - T_{PCM}) + \dot{m}C_{p,HTF}\frac{\partial T_{HTF}}{\partial x} + U_{wal}PL(T_{HTF} - T_{amb}) = 0 \quad 6.48$$

It should be noted that ε (porosity) is the volume fraction of HTF (Therminol-55) whereas 1-ε is the volume fraction of PCM. Where, P is perimeter of the storage tank and L is the length of storage.

Transient heat transfer equations for solid PCM capsule

Heat addition through convection from HTF to PCM capsules and the net heat transfer in the axial direction are used to calculate the temperature change of PCM capsules with time (from PCM capsules beneath and above) .

$$(1-\varepsilon)A_{cs}\rho_{pcm,s}C_{p,pcm,s}\frac{\partial T_{PCM}}{\partial t} - h_v A_{cs}(T_{HTF}-T_{PCM}) - \frac{\partial}{\partial x}\left(k_{PCM}A_{cs}\frac{\partial T_{PCM}}{\partial x}\right) = 0 \quad 6.49$$

Governing equation for melting fraction in the latent heat section

Heat transfer model from the PCM's solid-to-liquid phase transition zone may be done by combining the molten fraction with time difference. The molten fraction is determined by and used to forecast the quality of a liquid PCM.

$$\gamma = \frac{m_{liq,PCM}}{m_{total}} \quad 6.50$$

Where, γ is the molten fraction of PCM

After the temperature exceeds the phase-change level, the energy provided to the PCM is stored as latent heat in the material. eq. (6.51). The heat produced by PCM is what causes the change in enthalpy:

$$\frac{dH}{dt} = \dot{Q} = \frac{d(\rho V h)}{dt} \quad 6.51$$

$$\rho_{PCM}V_{PCM}\frac{d\gamma h}{dt} = \dot{Q} \quad 6.52$$

$$\rho_{PCM}V_{PCM}\frac{d(\gamma c_{p_{PCM}}T + \gamma h_L)}{dt} = \dot{Q} \quad 6.53$$

Where: h_L is the latent heat of PCM (J/kg), ρ_{PCM} is density of PCM (kg/m^3), V_{PCM} is volume of the PCM tube (m^3), $c_{p,PCM}$ is specific heat of PCM (J/kgK), γ is liquid volume fraction (-).

$$\rho_{PCM}V_{PCM}\left[c_{p_{PCM}}\frac{dT}{dt} + \frac{d\gamma h_L}{dt}\right] = \dot{Q} \quad 6.54$$

In mushy phase, there is no temperature change, and the temperature's first derivative is zero.

$$\frac{dT}{dt} = 0 \quad 6.55$$

$$\rho_{PCM}V_{PCM}h_L\frac{d\gamma}{dt} = \dot{Q} \quad 6.56$$

The liquid fraction gamma is calculated from Eqs. (21):

$$\frac{d\gamma}{dt} = \frac{\dot{Q}}{\rho_{PCM} V_{PCM} h_L} \quad 6.57$$

And should be in the range $\gamma = [0,1]$

Simplify by dividing both sides by the total volume (void plus PCM).

$$(1-\varepsilon)(\rho h)_{eff,fus} \frac{d\gamma}{dt} = h_v (T_{HTF} - T_{PCM}) \quad 6.58$$

$$\frac{d\gamma}{dt} = \frac{h_v}{(1-\varepsilon)(\rho h)_{eff,fus}} (T_{HTF} - T_{PCM}) \quad 6.59$$

Where $(\rho h)_{eff,fus} = \frac{\rho_{PCM} V_{PCM} h_L}{V_{total}}$

Transient heat transfer equation for liquid PCM capsules

As a result of convective heat transfer from the HTF to the PCM capsules, the temperature of liquid PCM capsules changes with time.

The heat transferred with HTF has an impact on PCM's sensible heat in a manner similar to how heat transfer occurs in the solid state.

$\gamma = 1$ Liquid volume fraction (liquid state)

$$(1-\varepsilon) A_{cs} \rho_{pcm,l} C_{p,pcm,l} \frac{\partial T_{PCM}}{\partial t} - h_v A_{cs} (T_{HTF} - T_{PCM}) = 0 \quad 6.60$$

Where $\rho_{pcm,l}$ and $C_{p,pcm,l}$ are density and specific heat capacity of PCM for liquid region

6.6 Computational Model

The one dimensional two phase heat transfer partial differential equations are discretized with forward difference in time using the finite difference method. The discrete equation that follows is used to approximate Equation (6.61) of heat transfer fluid.

$$\frac{{T_{HTF,i}}^{m+1} - {T_{HTF,i}}^{m}}{\Delta t} = \frac{h_v}{\varepsilon \rho_{HTF} C_{p,HTF}} \left(T^m_{pcm,i} - T^m_{HTF,i}\right) - \frac{\dot{m}}{\varepsilon A_{cs} \rho_{HTF}} \frac{T^m_{HTF,i+1} - T^m_{HTF,i}}{\Delta x} - \frac{U_{wall} P}{\varepsilon A_{cs} \rho_{HTF} C_{p,HTF}} (T^m_{amb,i} - T^m_{HTF,i}) \quad 6.61$$

The partial difference equations of heat transport in PCM capsules during solid phase, or equation (6.62), are generated by employing forward differences for temporal discretization and a central difference scheme for spatial discretization. .

$$\frac{{T_{PCM,i}}^{m+1} - {T_{PCM,i}}^{m}}{\Delta t} = \frac{h_v(T^m_{HTF,i} - T^m_{pcm,i})}{(1-\varepsilon)\rho_{pcm,s}C_{ppcm,s}} + \frac{k_{pcm,s}}{(1-\varepsilon)\rho_{pcm,s}C_{p,pcm,s}}\left(\frac{T^m_{pcm,i+1} - 2T^m_{pcm,i} + T^m_{pcm,i-1}}{\Delta x^2}\right) \quad 6.62$$

The melt fraction is obtained by discretizing equation (6.12) using the forward difference scheme for heat transfer during phase change in the PCM, as shown below.

$$\gamma_i^{m+1} = \gamma_i^m + \frac{\Delta t h_{eff,pcm}}{(1-\varepsilon)(\rho h)_{eff,fus}}(T^m_{HTF,i} - T^m_{pcm,i}) \quad 6.63$$

Where m and m+1 indicate the current and next time step. Also, i and i+1indicates the current and next space step.

The temperature of the PCM during the liquid phase is calculated by discretizing Equation (6.13) in time steps using the forward difference method, as shown in equation (6.17).

$$\frac{{T_{PCM,i}}^{m+1} - {T_{PCM,i}}^{m}}{\Delta t} = \frac{h_v}{\rho_{pcm,l}(1-\varepsilon)C_{p,pcm,l}}(T^m_{pcm,i} - T^m_{pcm,i}) \quad 6.64$$

The temperature of the HTF is updated during recirculation by taking into account the concentrated and absorbed solar radiation, the heat capacity of the absorber, and the heat loss from the receiver.

$$T^{m+1}_{HTF,out} = T^m_{HTF,in} + \frac{\eta_{op}A_{ap}I_b(t)}{\dot{m}C_{p,HTF}} - \frac{A_{ab}U_{rl}(T^m_{ab} - T_{HTF})}{\dot{m}C_{p,HTF}} - \frac{\rho_{ab}V_{ab}C_{p,abs}\left(T^m_{ab} - T^{m-1}_{ab}\right)}{\Delta t\dot{m}C_{p,HTF}} \quad 6.65$$

Similarly, the temperature of the absorber is updated by taking into account the difference between the absorbed energy and the sum of heat loss from the receiver and energy transported by HTF to the thermal storage, as shown in equation. (6.19)

$$T^m_{ab} = T^{m-1}_{ab} + \frac{\left(\eta_{op}A_{ap}I_b(t) - A_{ab}U_{rl}\left(T^{m-1}_{ab} - T_{amb}\right) - \rho_{ab}V_{ab}C_{p,abs}\left(T^m_f - T^{m-1}_f\right)\dot{m}C_{p,f}\right)dt}{\dot{m}C_{p,HTF}} \quad 6.66$$

Balanced energy during night time

Heat is transferred from thermal storage to the absorption system's generator during discharging. The heat transfer rate

$$\dot{Q}_{gen} = \dot{Q}_{PCM} - \dot{Q}_{conv} \quad 6.67$$

Where: $\dot{Q}_{gen}$ is the rate of heat transfer to generator

$\dot{Q}_{PCM}$ is the rate of heat transfer to the HTF = $\frac{T_{sto}-T_{gen}}{R_{th}}$

$\dot{Q}_{conv}$ is the rate of convective heat loss = $hA_{PCM}(T_{sto} - T_{amb})$

Where, R_{th} is thermal resistance of tank, T_{sto} is storage temperature, T_{gen} is temperature of generator, T_{amb} is ambient air, h is convective heat transfer coefficient and A_{PCM} is cross-sectional area of PCM.

From energy balance, the temperature of the generator is obtained as follows, discretizing equation (6.20) with forward difference scheme as follows.

$$T_{gen}^{m+1} = T_{gen}^{m} + \frac{\dot{Q}_{gen}(t) - (\dot{Q}_{PCM}(t) + \dot{Q}_{conv}(t))}{m_{gen}c_{p,gen}}\Delta t \quad 6.68$$

Initial and boundary condition

At time $t = 0$ $\quad T_{pcm}(x,0) = T_{HTF}(x,0) = T_o$

At time $t > 0$ $\quad T_{HTF}(0,t) = T_{inlet}$, $\frac{\partial T_{HTF}(x,t)}{\partial x} = 0, at\ x = L\ and\ \frac{\partial T_{pcm}(x,t)}{\partial x} = 0, for\ x = 0\ and\ x = L$

6.7 Aspen Plus Model for The Solar Thermal System Linking With Matlab

Tools for process design that can be linked into well-known simulation software, such Aspen Plus®, are required due to process intensification and new technologies. As a result, Matlab® simulations of unit operations that are absent from standard Aspen Plus software packages can be incorporated into the Aspen Plus user interface. By doing this, we may utilize all of Aspen Plus's features, including cost estimation, sensitivity analysis, and optimization. By transmitting the pertinent data from Aspen Plus to Excel, which then feeds the data to a Matlab procedure, the interface between Matlab and Aspen Plus is achieved. The data is delivered to Excel and Aspen Plus after being processed by the Matlab function. Designing new and more complex processes thus requires a tool that maintains the entire functionality and numerical capability of Aspen Plus and can incorporate Matlab user models.

In Aspen plus model plat form it has no appropriate model for solar collector and PCM. And also it is not suitable to identify the charging and discharging of PCM and the effect of solar radiation variation on the CPC collector. Therefor user2 model is used in order to link it with MATLAB work space. First this user2 model leads to link with Excel sheet then the excel sheet will be link with MATLAB. The solar thermal and PCM model is modeled on Aspen plus platform as determined in Figure 6-9. The simulation process flow diagram is presented Figure 6-10.

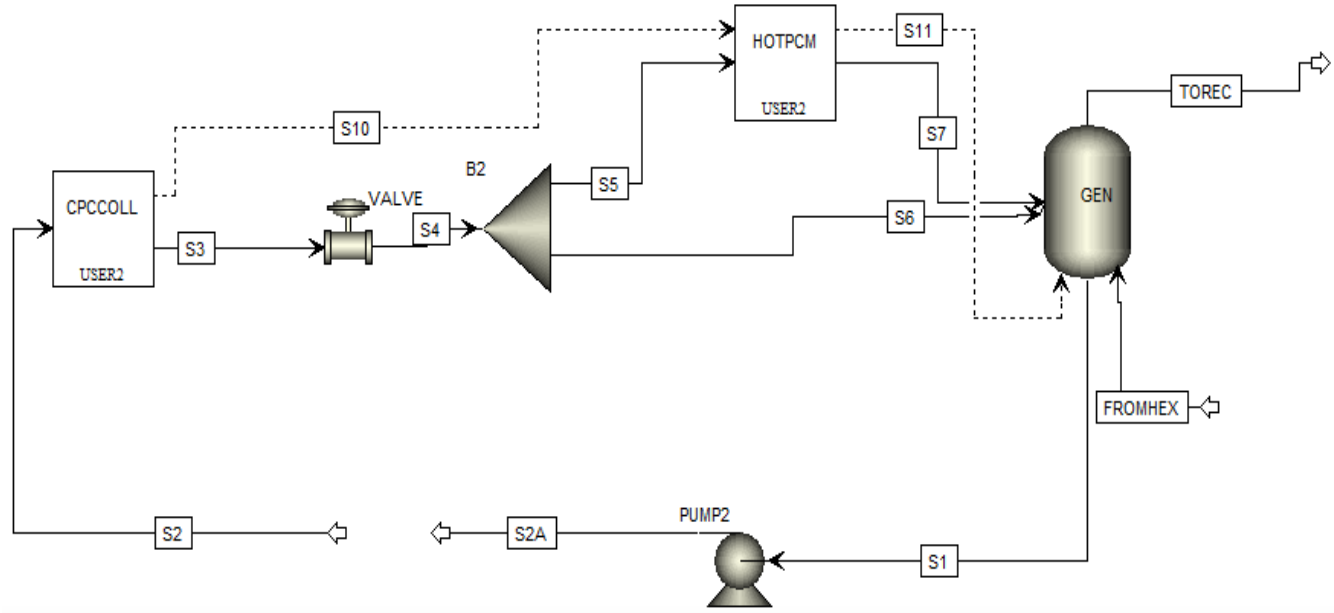

Figure 6-9 Solar thermal with PCM model on Aspen plus

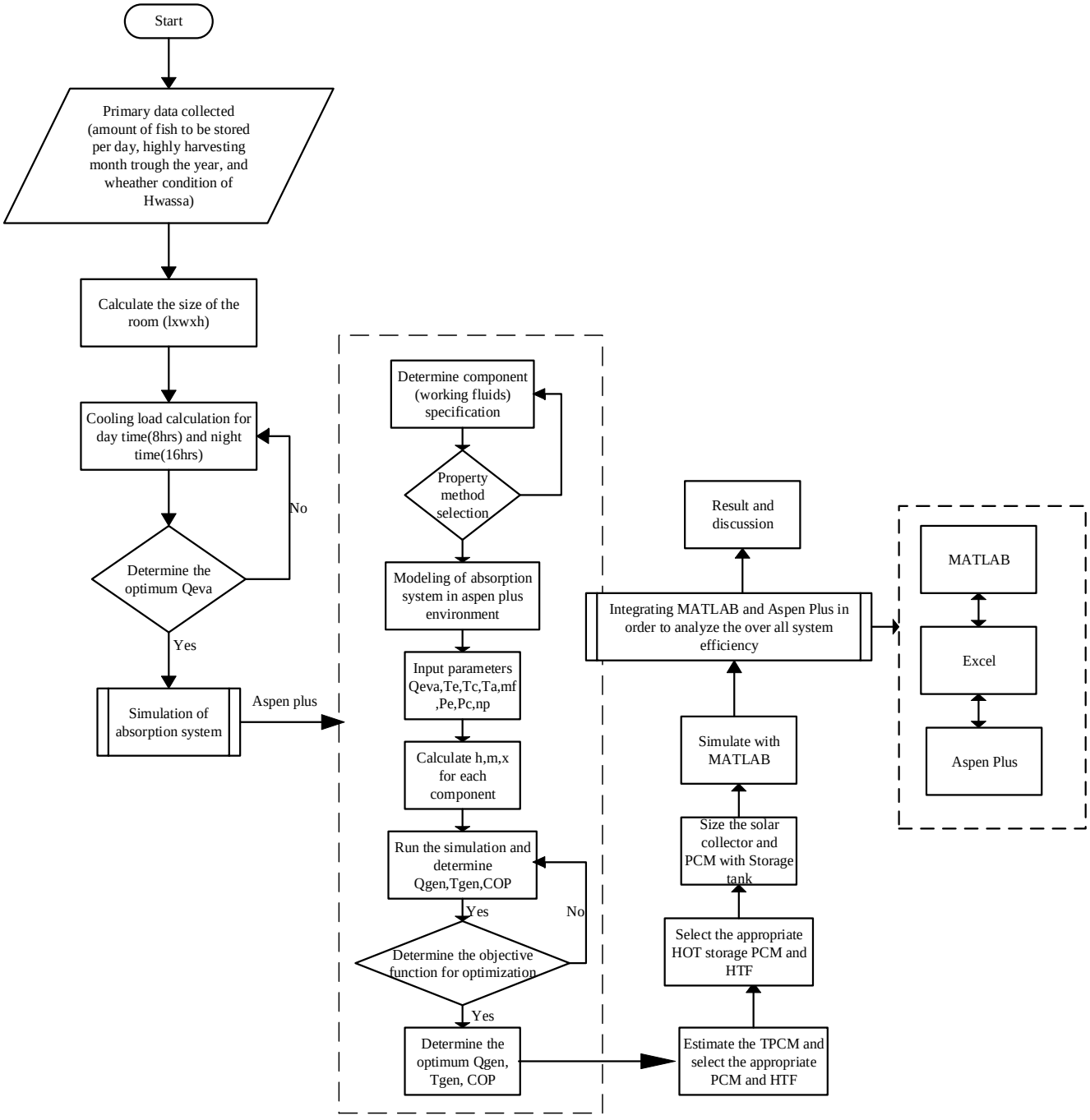

Figure 6-10 Flow chart of process simulation

CHAPTER SEVEN

7. RESULT AND DISCUSSION

7.1 Hourly Beam Incident Solar Radiation on Horizontal Surface

Different input parameters utilized for the thermal and optical analyses of CPC have been simulated from solar radiation model created in Matlab. The solar irradiation, or solar power received during a 24-hour period on representative day of each month mentioned in the previous section. The highest solar energy potential from the winter and spring seasons, respectively, is shown in the months of February and March. The solar radiation levels are highest in March (1024.59 W/m^2) and lowest in July (372.75 W/m^2), respectively. The monthly variations in the incident solar radiation on a horizontal surface are considerable. The maximum and minimum solar data for the hourly beam incident solar radiation on a horizontal surface are depicted in Figure 7-1.

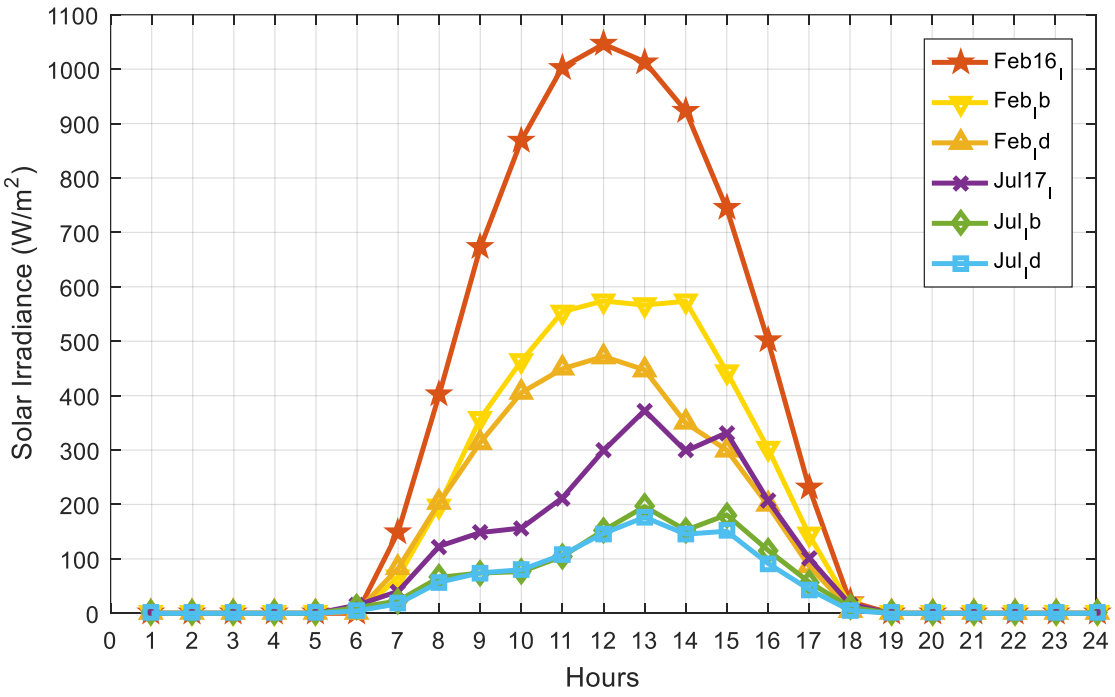

Figure 7-1 Hourly beam and diffused incident solar radiation on Horizontal surface for maximum and minimum solar data

7.2 Variation of Outlet temperature

The transient mathematical model created using Matlab simulates hourly change of heat transfer fluid outlet temperature. The temperature change is dependent on the amount of solar energy available, as seen in Figure 7-2, where the exit temperature from collector can exceed 140^{o}C. Because sunshine hours fluctuate from season to season, the outlet temperature changes with the season.

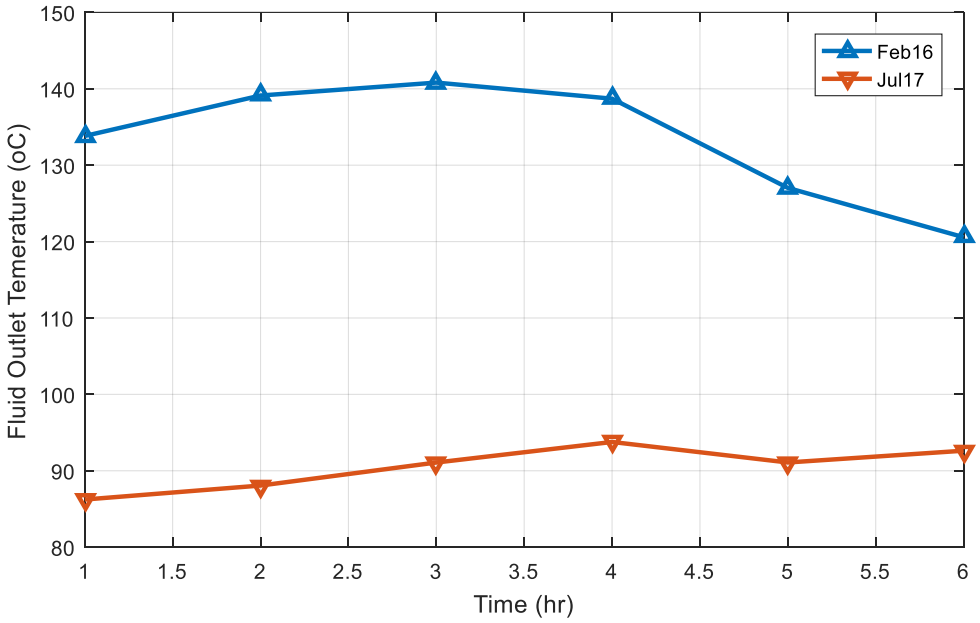

Figure 7-2 Hourly collector HTF outlet temperature for maximum and minimum solar radiation

7.3 Useful heat gained by the collector

Usable heat acquired by a collector that has been computed using the proposed thermal model. The outcome demonstrates that it changes greatly from season to season. The instantaneous usable heat acquired for a particular day is at its highest at solar noon, as shown in Figure 7-3.

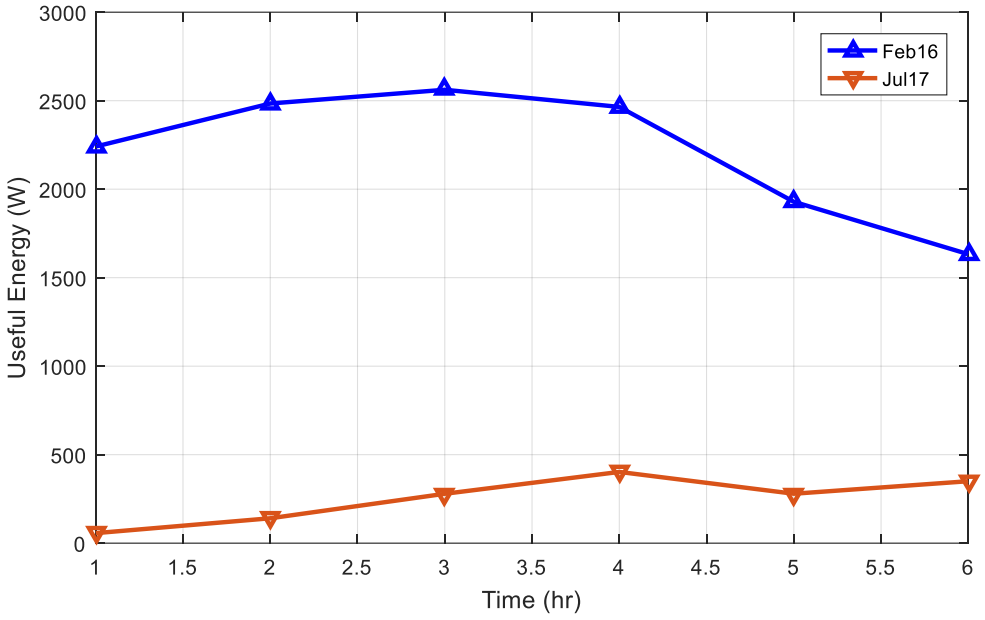

Figure 7-3 Instantaneous useful heat gained for recommended days

7.4 Efficiency of the CPC System

The maximum and lowest thermal efficiencies of collector were estimated using the optical model created in preceding chapter. The lowest and greatest levels of efficiency were recorded in July and March, respectively according to Figure 7-4. The mass flow rate, heat transfer fluid input and outlet temperatures, and solar radiation beam rely on the instantaneous thermal efficiency of the solar collector. Total solar radiation incident instantly on the surface of the collector varies from sunrise to dusk. The Instantaneous thermal efficiency variation throughout the course of a day is depicted in Figure 7-4.

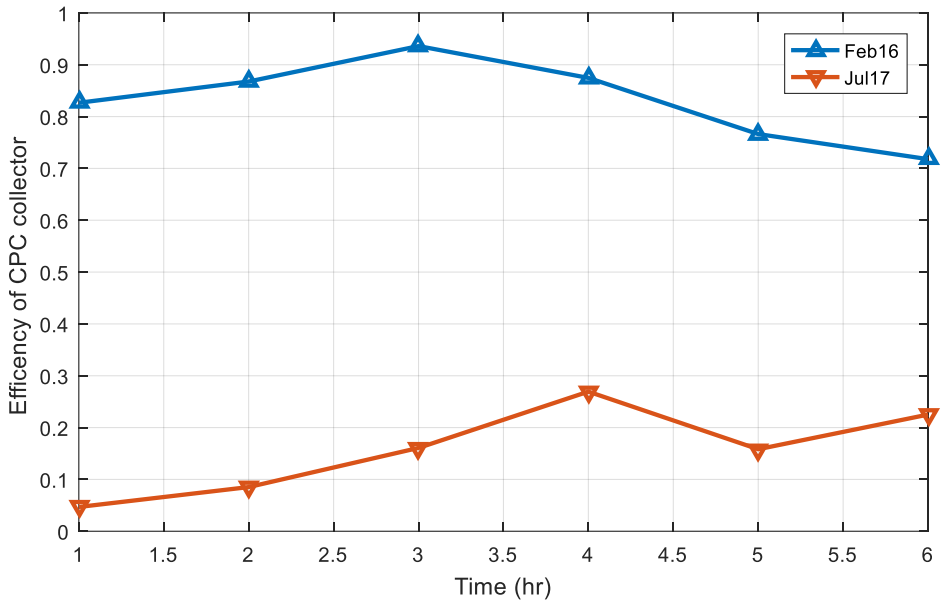

Figure 7-4 Instantaneous thermal efficiency of the collector on March and July

7.5 Temperature Variation of Hot Phase Changing Material during Charging Process

Using the sun irradiation data from Hawassa, simulation was done to forecast PCM thermal storage performance. Therminol oil is needed as heat transfer fluid in an average-sized PCM storage tank with dimensions of 0.5 m in height and 1.253 m in diameter in order to meet the heat requirement of ARS for one nighttime activity. 0.5-meter-long, 0.15-meter-diameter cylindrically enclosed capsule with 0.4-micron porosity. The outcome indicates that 196 capsules were needed overall to store the necessary energy, or 372.2 Kg PCM of Erythirol. The thermal storage was discretized into layers with a thickness of 0.01 m. A 10sec time step was also used. Given are the model's borders and its beginning circumstances. Figure 7-5 indicate that for maximum solar radiation is available at first one hour only sensible heating occurs the left one and half hour is when the phase change process occurs after that for remaining charging hour the temperature increases up to the HTF temperatures reaches.

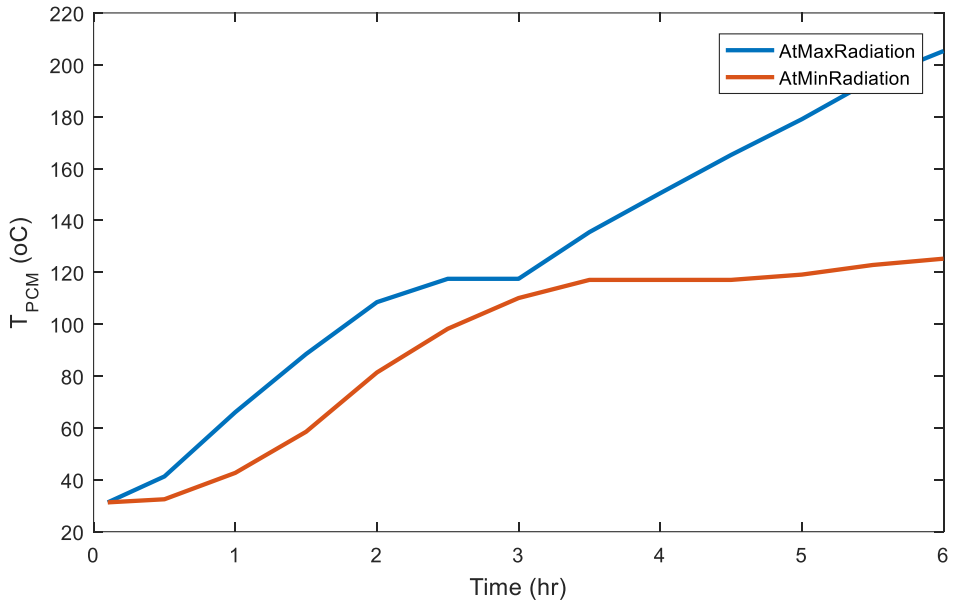

Figure 7-5 Temperature variation of hot PCM during charging for 6 hours for the day of maximum and minimum solar radiation

Figure 7-6 depicts the phase transformation and the melt fraction variation during charging. The PCM was completely melted after 2.5 hours of charging for both highest and lowest solar radiation days.

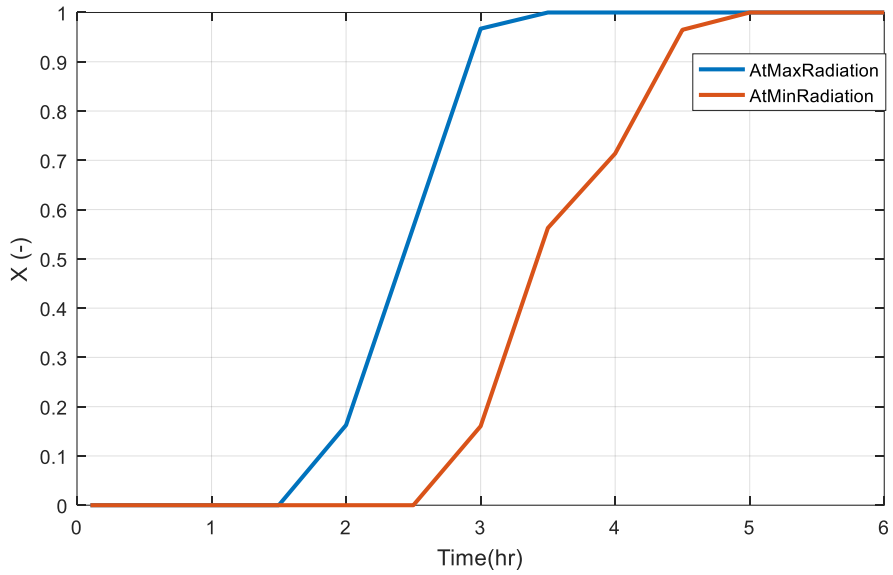

Figure 7-6 Melt fraction of hot PCM versus time during charging for the day of the highest and lowest solar radiation

7.6 Temperature change of hot storage Phase Changing Material during Discharging Process

The heat stored in PCM of thermal storage can be discharged by forced convection using the pump2 indicated on schematic diagram of the system 1. Since the three way valve forced pass way to the solar collector and leads HTF to pass through the PCM after pumping the fluid. The HTF carried heat energy from PCM to the generator for remaining 18 hours at night time. When the minimum solar radiation is available in the recommended day the temperature of the PCM has degraded after discharging for 8.5 hours using 0.02 kg/s mass flow rate of HTF. The generator of ARS requires 81.5^{o}C in order to run the system but after 15 hours the generator temperature decreased slightly. When maximum solar radiation is avail the discharging time will undergo through the night times. Figure 7-7 shows that the temperature variation of thermal storage with respect to time during discharging.

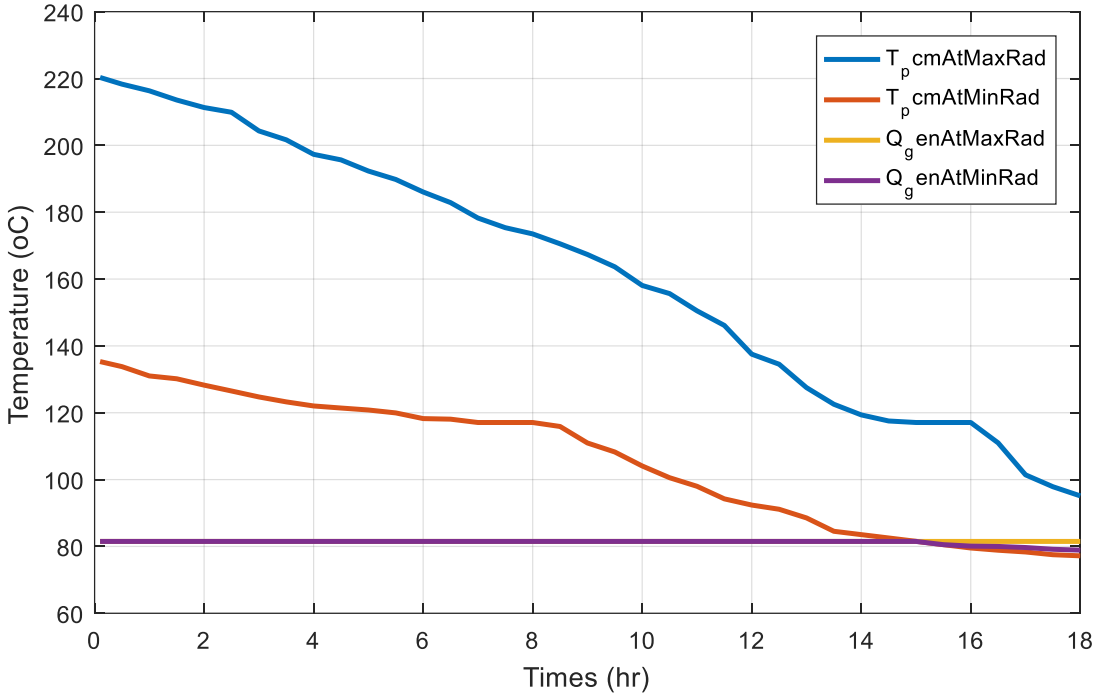

Figure 7-7 Temperature of hot PCM during discharging for highest and lowest solar radiation

Figure 7-8 show the temperature degradation and solidification of the PCM thermal storage after discharge for 16 hours for the day of the highest solar radiation and 8.2 hours for lowest solar radiation.

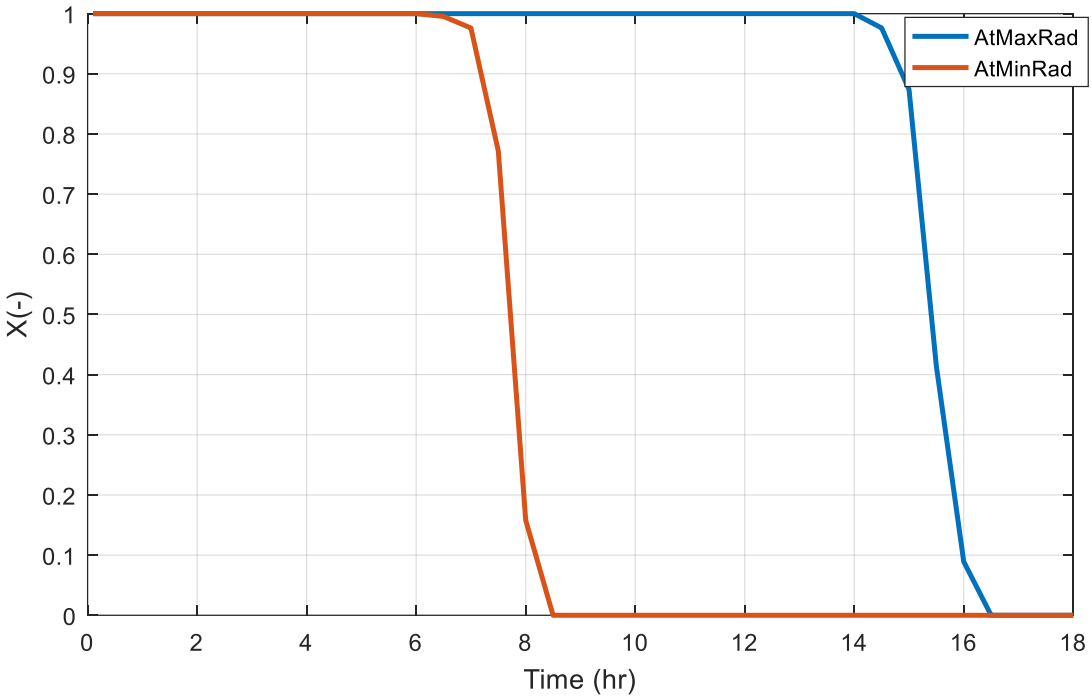

Figure 7-8 Solidification of hot PCM versus time during discharging for highest and lowest solar radiation (X is melt fraction)

CHAPTER EIGHT

8. CONCLUSION AND RECOMMENDATION

8.1 Conclusion

The current work investigates numerical modeling of the solar collector's performance when combined with ARS's latent thermal energy storage. The amount of generator temperature needed for the ARS was determined using the cooling load of ARS for fish storage in the cold room. Utilizing the Aspen Plus software, the process simulation establishes the generator's duty during the day and night. The size of CPC collector and thermal storage devices are developed based on this task.

To analyze the heat transfer in CPC collector and latent thermal energy storage, a one-dimensional model was created. A finite difference approach that was created using Matlab was used to create and solve a transient mathematical model. Excel is used as the data transmitter for the integration of Matlab and Aspen Plus for the entire simulation.

The output temperature from the investigated collector may reach beyond 140°C with a mass flow rate of 0.02 kg/s, according to the results of computer simulations. To meet the cooling requirement throughout the suggested day, 8 CPC collector modules should be employed for hot storage PCM applications at maximum solar radiation and 17 CPC modules for minimum solar radiation available. Performance for ARS utilizing the hot storage application is 0.7, whereas it is 0.6 for the other.

Charging performance of the thermal energy storage was analyzed and the result shows that $372.2kg$ PCM, Erythirol as hot storage needed to store the required energy. The overall efficiency of the system using hot storage PCM is 61.3%.

8.2 Recommendations

According to the study, deep freezing rooms for fish storage applications might be studied in addition to cold rooms. The following points can be suggested for future research based on the findings of this study.

- For other alternative energy source the geothermal energy can be used since the cold room are installed around the lake where geothermal energy is more abounded. In addition to this the cold storage PCM can be used alternative to the hot storage PCM.
- It is necessary to do experimental research to correctly represent the system.
- Next time the cooling load calculation may occurred by varying the daily ambient temperature

REFERENCE

[1] Samrawit Yilma, Heidi Busse, Derese Tamiru Desta, Fikadu Reta Alemayehu "Fish Consumption, Dietary Diversity and Nutritional Status of Reproductive Age Women of Fishing and Non-Fishing Households in Hawassa, Ethiopia: Comparative Cross Sectional Study," Frontiers in Science 2020, 10(1): 7-13

[2] IIR, "The role of refrigeration in worldwide nutrition.," vol. 5th Informatory Note on Refrigeration and Food., 2009.

[3] Gashaw Tesfaye , Matthias Wolff, "The state of inland fisheries in Ethiopia a synopsis with updated estimates of potential yield," Ecohydrology & Hydrobiology 14 (2014) 200–21

[4] Gemechis Tesgera and Kibruyesfa Bayou, "Assessment of Current Practices, Major Challenges andOpportunities of the Fishery of Lake Hawassa, SouthernEthiopia," Int. J. Adv. Res. Biol. Sci. (2021). 8(2): 26-39

[5] M. Kolodziejczyk, K. Smierciew, J. Gagan, and D. Butrymowicz, "Numerical Modelling of Heat and Mass Transfer in Vegetables Cold Storage," *Procedia Engineering*, vol. 157, pp. 279–284, 2016, doi: 10.1016/j.proeng.2016.08.367.

[6] U. Hyginus Ubabuike, "Design and Adaptation of a Commercial Cold Storage Room for Umudike Community and Environs," *IOSRJEN*, vol. 02, no. 05, pp. 1234–1250, May 2012, doi: 10.9790/3021-020512341250.

[7] A. Hmida, N. Chekir, A. Laafer, M. E. A. Slimani, and A. Ben Brahim, "Modeling of cold room driven by an absorption refrigerator in the south of Tunisia: A detailed energy and thermodynamic analysis," *Journal of Cleaner Production*, vol. 211, pp. 1239–1249, Feb. 2019, doi: 10.1016/j.jclepro.2018.11.219.

[8] H.-M. Henning, "Solar assisted air conditioning of buildings – an overview," *Applied Thermal Engineering*, vol. 27, no. 10, pp. 1734–1749, Jul. 2007, doi: 10.1016/j.applthermaleng.2006.07.021.

[9] A. H. Abedin, "A Critical Review of Thermochemical Energy Storage Systems," *TOREJ*, vol. 4, no. 1, pp. 42–46, Aug. 2011, doi: 10.2174/1876387101004010042.

[10] A. Mehari, Z. Y. Xu, and R. Z. Wang, "Thermal energy storage using absorption cycle and system: A comprehensive review," *Energy Conversion and Management*, vol. 206, p. 112482, Feb. 2020, doi: 10.1016/j.enconman.2020.112482.

[11] A. Ghafoor, "Worldwide overview of solar thermal cooling technologies," *Renewable and Sustainable Energy Reviews*, p. 12, 2015.

[12] B. H. Gebreslassie, E. A. Groll, and S. V. Garimella, "Multi-objective optimization of sustainable single-effect water/Lithium Bromide absorption cycle," *Renewable Energy*, vol. 46, pp. 100–110, Oct. 2012, doi: 10.1016/j.renene.2012.03.023.

[13] R. Gomri, "Second law comparison of single effect and double effect vapour absorption refrigeration systems," *Energy Conversion and Management*, vol. 50, no. 5, pp. 1279–1287, May 2009, doi: 10.1016/j.enconman.2009.01.019.

[14] S. Garone, T. Toppi, M. Guerra, and M. Motta, "A water-ammonia heat transformer to upgrade low-temperature waste heat," *Applied Thermal Engineering*, vol. 127, pp. 748–757, Dec. 2017, doi: 10.1016/j.applthermaleng.2017.08.082.

[15] I. Dincer and T. A. H. Ratlamwala, *Integrated Absorption Refrigeration Systems*. in Green Energy and Technology. Cham: Springer International Publishing, 2016. doi: 10.1007/978-3-319-33658-9.

[16] R. Awasthi, S. Chattopadhyay, and S. Ghosh, "Integration of solar charged PCM storage with VAR system for low capacity vegetable cold storage," *J. Phys.: Conf. Ser.*, vol. 1240, no. 1, p. 012070, Jul. 2019, doi: 10.1088/1742-6596/1240/1/012070.

[17] D. N. Basu and A. Ganguly, "Solar thermal–photovoltaic powered potato cold storage – Conceptual design and performance analyses," *Applied Energy*, vol. 165, pp. 308–317, Mar. 2016, doi: 10.1016/j.apenergy.2015.12.070.

[18] "Cold storage design and refrigeration .pdf."

[19] M. U. Arshad, M. U. Ghani, A. Ullah, A. Güngör, and M. Zaman, "Thermodynamic analysis and optimization of double effect absorption refrigeration system using genetic algorithm," *Energy Conversion and Management*, vol. 192, pp. 292–307, Jul. 2019, doi: 10.1016/j.enconman.2019.03.083.

[20] Omer Kaynakil, Kenan Saka, Faruk Kaynakil, "Energy and exergy analysis of a double effect absorption refrigeration system based on different heat source,"2015

[21] K. Faraj, M. Khaled, J. Faraj, F. Hachem, and C. Castelain, "Phase change material thermal energy storage systems for cooling applications in buildings: A review," *Renewable and Sustainable Energy Reviews*, vol. 119, p. 109579, Mar. 2020, doi: 10.1016/j.rser.2019.109579.

[22] H. Selvnes, Y. Allouche, R. I. Manescu, and A. Hafner, "Review on cold thermal energy storage applied to refrigeration systems using phase change materials," *Thermal Science and Engineering Progress*, vol. 22, p. 100807, May 2021, doi: 10.1016/j.tsep.2020.100807.

[23] O. Ketfi, M. Merzouk, N. K. Merzouk, and S. E. Metenani, "Performance of a Single Effect Solar Absorption Cooling System (Libr-H2O)," *Energy Procedia*, vol. 74, pp. 130–138, Aug. 2015, doi: 10.1016/j.egypro.2015.07.534.

[24] M. M. A. Khan, R. Saidur, and F. A. Al-Sulaiman, "A review for phase change materials (PCMs) in solar absorption refrigeration systems," *Renewable and Sustainable Energy Reviews*, vol. 76, pp. 105–137, Sep. 2017, doi: 10.1016/j.rser.2017.03.070.

[25] Yongrui Xu, Zeyu Li Hongkai Chen and Shiliang Lv "Assessment and optimization of solar absorption-subcooled compression hybrid cooling system for cold storage," applthermaleng. 2020, 115886

[26] "Thermodynamic Modeling and Performance Optimization of a Solar-Assisted Vapor Absorption Refrigeration System (SAVARS).pdf."

[27] "Performance assessment of a solar powered ammonia–water absorption refrigeration system with storage units.pdf."

[28] "Thermal Energy Storage Implementation Using Phase Change Materials for Solar Cooling and Refrigeration Applications.pdf."

[29] G. Alva, L. Liu, X. Huang, and G. Fang, "Thermal energy storage materials and systems for solar energy applications," *Renewable and Sustainable Energy Reviews*, vol. 68, pp. 693–706, Feb. 2017, doi: 10.1016/j.rser.2016.10.021.

[30] "Martins et al. - 2015 - New Concentrating Solar Power Facility for Testing.pdf."

[31] D. Schlipf, P. Schicktanz, H. Maier, and G. Schneider, "Using Sand and other Small Grained Materials as Heat Storage Medium in a Packed Bed HTTESS," *Energy Procedia*, vol. 69, pp. 1029–1038, May 2015, doi: 10.1016/j.egypro.2015.03.202.

[32] B. Cárdenas and N. León, "High temperature latent heat thermal energy storage: Phase change materials, design considerations and performance enhancement techniques," *Renewable and Sustainable Energy Reviews*, vol. 27, pp. 724–737, Nov. 2013, doi: 10.1016/j.rser.2013.07.028.

[33] W. Su, J. Darkwa, and G. Kokogiannakis, "Review of solid–liquid phase change materials and their encapsulation technologies," *Renewable and Sustainable Energy Reviews*, vol. 48, pp. 373–391, Aug. 2015, doi: 10.1016/j.rser.2015.04.044.

[34] R. K. Sharma, P. Ganesan, V. V. Tyagi, H. S. C. Metselaar, and S. C. Sandaran, "Developments in organic solid–liquid phase change materials and their applications in thermal energy storage," *Energy Conversion and Management*, vol. 95, pp. 193–228, May 2015, doi: 10.1016/j.enconman.2015.01.084.

[35] N. Sarier and E. Onder, "Organic phase change materials and their textile applications: An overview," *Thermochimica Acta*, vol. 540, pp. 7–60, Jul. 2012, doi: 10.1016/j.tca.2012.04.013.

[36] S. Pincemin, R. Olives, X. Py, and M. Christ, "Highly conductive composites made of phase change materials and graphite for thermal storage," *Solar Energy Materials and Solar Cells*, vol. 92, no. 6, pp. 603–613, Jun. 2008, doi: 10.1016/j.solmat.2007.11.010.

[37] J. M. Khodadadi, L. Fan, and H. Babaei, "Thermal conductivity enhancement of nanostructure-based colloidal suspensions utilized as phase change materials for thermal energy storage: A review," *Renewable and Sustainable Energy Reviews*, vol. 24, pp. 418–444, Aug. 2013, doi: 10.1016/j.rser.2013.03.031.

[38] S. Kuravi, J. Trahan, D. Y. Goswami, M. M. Rahman, and E. K. Stefanakos, "Thermal energy storage technologies and systems for concentrating solar power plants," *Progress in Energy and Combustion Science*, vol. 39, no. 4, pp. 285–319, Aug. 2013, doi: 10.1016/j.pecs.2013.02.001.

[39] D. Zhou, "Review on thermal energy storage with phase change materials (PCMs) in building applications," *Applied Energy*, p. 13, 2012.

[40] S. A. Kalogirou, "Solar thermal collectors and applications," *Progress in Energy and Combustion Science*, p. 65, 2004.

[41] R. Gomri, "Simulation study on the performance of solar/natural gas absorption cooling chillers," *Energy Conversion and Management*, vol. 65, pp. 675–681, Jan. 2013, doi: 10.1016/j.enconman.2011.10.030.

[42] S. Samanta and D. N. Basu, "Energy and Entropy-Based Optimization of a Single-Stage Water–Lithium Bromide Absorption Refrigeration System," *Heat Transfer Engineering*, vol. 37, no. 2, pp. 232–241, Jan. 2016, doi: 10.1080/01457632.2015.1044420.

[43] "Comprehensive thermodynamic and operational optimization of a solar-assisted LiBr water absorption refrigeration system.pdf."

[44] M. Perier-Muzet, J.-P. Bedecarrats, P. Stouffs, and J. Castaing-Lasvignottes, "Design and dynamic behaviour of a cold storage system combined with a solar powered thermoacoustic refrigerator," *Applied Thermal Engineering*, vol. 68, no. 1–2, pp. 115–124, Jul. 2014, doi: 10.1016/j.applthermaleng.2014.03.065.

[45] R. Mansouri, S. Mazouz, M. Bourouis, and A. Bellagi, "Experimental study and steady-state modelling of a," p. 8.

[46] F. Agyenim, "The use of enhanced heat transfer phase change materials (PCM) to improve the coefficient of performance (COP) of solar powered LiBr/H 2 O absorption cooling systems," *Renewable Energy*, vol. 87, pp. 229–239, Mar. 2016, doi: 10.1016/j.renene.2015.10.012.

[47] S. A. M. Said, "Design, construction and operation of a solar powered ammonia-water absorption refrigeration system in saudi arabia," p. 20.

[48] "Y et al. - 2017 - Assessing Sustainable Fishing Yields Using Length-.pdf."

[49] I. J. Adoga et al., "Storage Life of Tilapia (Oreochromis niloticus) in Ice and Ambient Temperature," p. 7, 2010.

[50] Y. Alemu, T. Y, N. J, and B. L, "Assessing Sustainable Fishing Yields Using Length-based Analytical Models: A Case Study with Nile Tilapia in Lake Hawassa (Ethiopia)," *J Fisheries Livest Prod*, vol. 05, no. 04, 2017, doi: 10.4172/2332-2608.1000255.

[51] T. Krishnakumar and Dayanandakumar, "Design of cold storage for fruits and vegetables," 2002, doi: 10.13140/RG.2.2.14335.82082.

[52] E. R. S. Nombrefia, "PROPOSED DESIGN OF A COLD STORAGE STRUCTURE FOR THE TOTAL PRODUCT LOAD OF MUSHROOM," p. 27, 2017.

[53] "kupdf.net_2014-ashrae-handbook-refrigeration-sipdf-1.pdf."

[54] "Performance analysis and evaluation of a commercial absorption–refrigeration water–ammonia (ARWA) system.pdf."

[55] Rajendra Kumar, "DESIGN AND ANALYSIS OF ABSORPTION REFRIGERATION SYSTEM USING H2O + [EMIM] [TFA]," 2015.

[56] C. Somers, "SIMULATION OF ABSORPTION CYCLES FOR INTEGRATION INTO REFINING PROCESSES," p. 106, 2009.

[57] "Modelling and testing the performance of a commercial ammonia water absorption chiller using Aspen-Plus platform.pdf."

[58] Swarna et al., "Multi-objective optimization of vapor absorption refrigeration system for the minimization of annual operating cost and exergy destruction," 2022.

[59] D. K. E. Bellos C. Tzivanidisa, K. A. Antonopoulosa, "Design, simulation and optimization of a Compound Parabolic Collector," 2017.

[60] S. A. Kalogirou, "Solar thermal collectors and applications," *Progress in Energy and Combustion Science*, vol. 30, no. 3, pp. 231–295, 2004, doi: 10.1016/j.pecs.2004.02.001.

[61] H. Shoeibi, A. Jarrahian, M. Mehrpooya, E. Assaerh, M. Izadi, and F. Pourfayaz, "Mathematical Modeling and Simulation of a Compound Parabolic Concentrators Collector with an Absorber Tube," *Energies*, vol. 16, no. 1, p. 287, Dec. 2022, doi: 10.3390/en16010287.

[62] Dr. Subhi S. and Dr. Hameed, "Theoretical Study of the Compound Parabolic Trough Solar Collector," vol. 19, 2012.

[63] Jose et al., "Thermal energy storage for low and medium temperature applications using phase change materials – A review," 2016.

[64] JOSEPH, "MODELLING AND DESIGN OF A LATENT HEAT THERMAL STORAGE SYSTEM WITH REFERENCE TO SOLAR ABSORPTION REFRIGERATION." 2012.

[65] A. Khan et al., "A review for phase change materials (PCMs) in solar absorption refrigeration systems," 2017.

[66] ASHRAE, "text book of," 2009.

APPENDIX

APPENDIX A: CONCENTRATION DIAGRAM FOR AMMONIA WATER SOLUTION

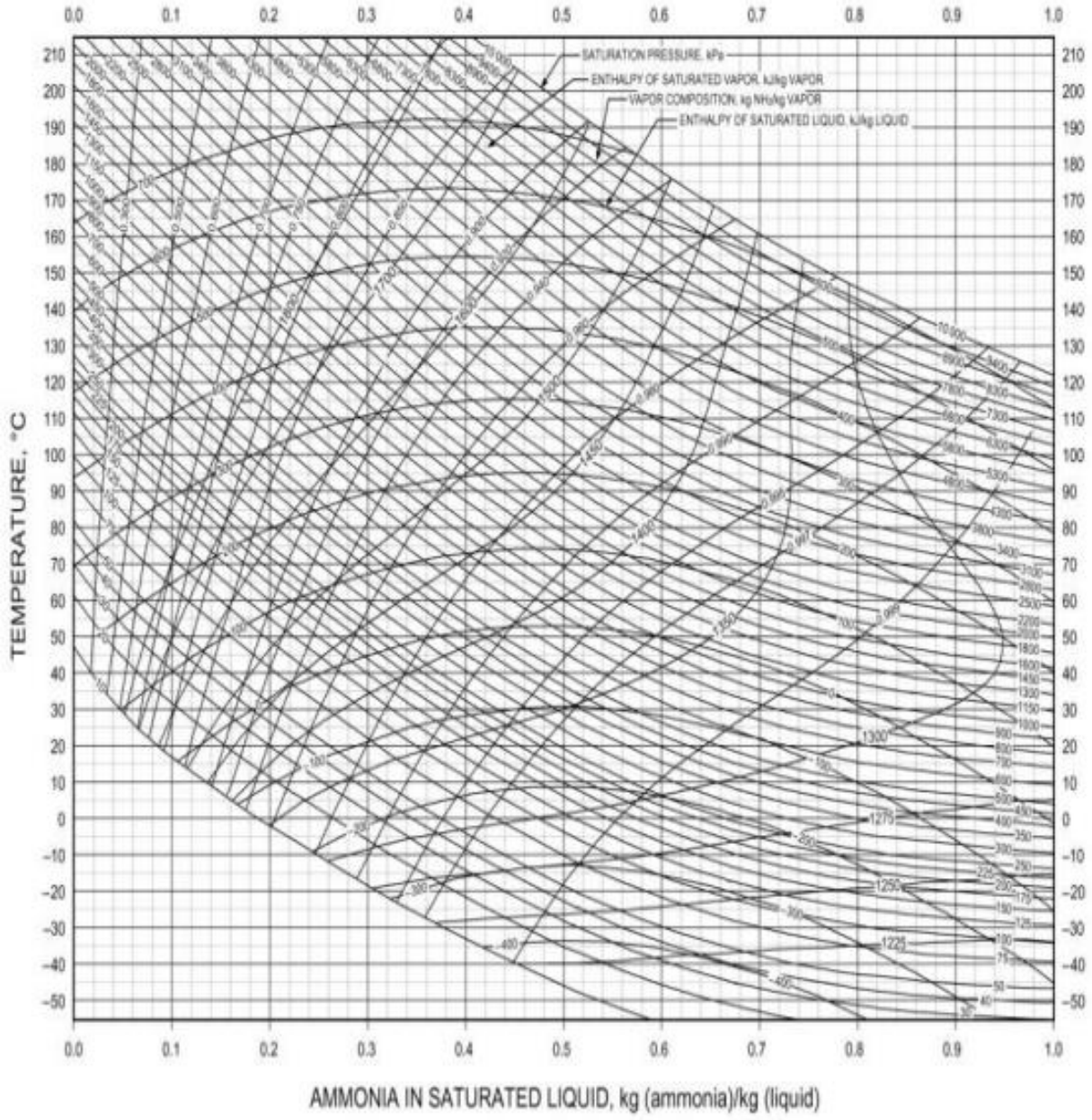

Figure 0-1 Enthalpy-concentration diagram for ammonia-water solutions [66]

APPENDIX B: PROPERTIES OF THERMINOL-55

[Source: http://www.therminol.com]

SI units Liquid phase heat transfer	THERMINOL 54 Economical, medium-temperature-range fluid	THERMINOL 55 Economical, medium-temperature-range fluid
	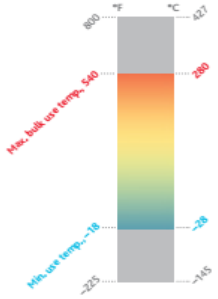	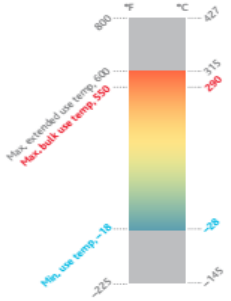
Typical properties[a]		
Appearance	Clear, yellow liquid	Clear, yellow liquid
Composition	Synthetic hydrocarbon mixture	Synthetic hydrocarbon mixture
Maximum bulk temperature	280°C	290°C
Maximum film temperature	310°C	335°C
Normal boiling point	351°C	351°C
Pumpability: at 300 cSt (mm^2/s) at 2000 cSt (mm^2/s)	 −8°C −28°C	 −8°C −28°C
Pour point	< −45°C	−54°C
Flash point, COC	>170°C	177°C
Fire point, COC	>210°C	218°C
Autoignition temperature[b]	> 330°C	382°C (DIN 51794)
Fully developed turbulent flow (Re = 10,000, 3.05 m/s, 2.54 cm tube)	67°C	67°C
Viscosity, mPa·s (cP)	−25°C 1,250 100°C 2.88 200°C 0.75 280°C 0.39	−25°C 1,250 100°C 2.88 200°C 0.75 290°C 0.36
Density at 25°C (kg/m^3)	868	868
Density, kg/m^3	−25°C 902 100°C 818 200°C 748 280°C 688	−25°C 902 100°C 818 200°C 748 290°C 680
Heat capacity, kJ/(kg·K)	−25°C 1.74 100°C 2.19 200°C 2.54 280°C 2.83	−25°C 1.74 100°C 2.19 200°C 2.54 290°C 2.86
Thermal conductivity, W/(m·K)	−25°C 0.134 100°C 0.119 200°C 0.107 280°C 0.098	−25°C 0.134 100°C 0.119 200°C 0.107 290°C 0.097
Vapor pressure, kPa	100°C 0.03 200°C 2.15 280°C 21.3	100°C 0.032 200°C 2.15 290°C 27.2
Geographic availability[c]	Europe/Middle East/Africa	Americas/Asia Pacific

[a] These data are based on samples tested in the laboratory and are not guaranteed for all samples. Contact us for complete sales specifications.
[b] Visit www.therminol.com for additional typical properties and test values. *[c] Check with your local sales office to determine exact availability by country.*

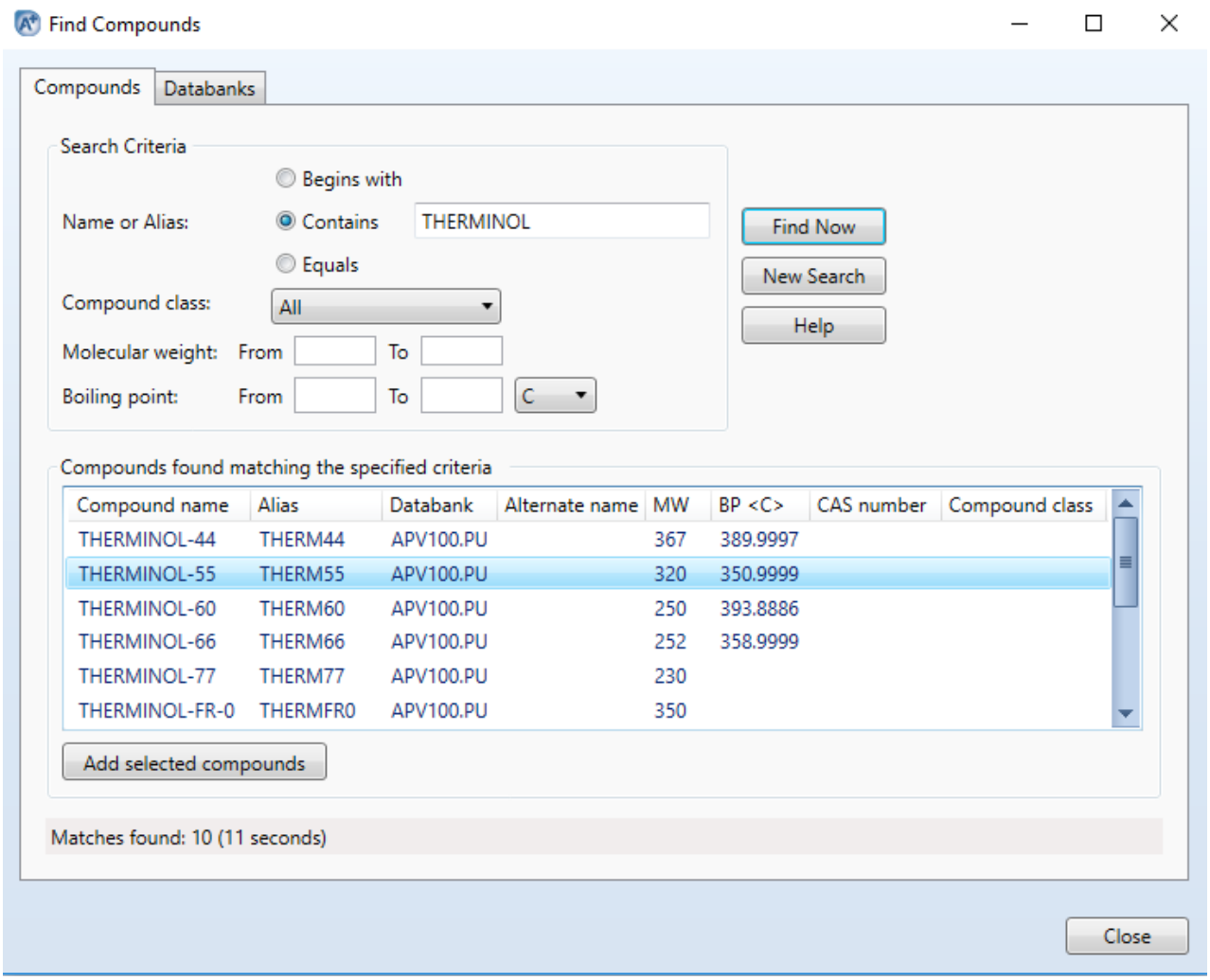
Find Compounds
Compounds
Databanks
Search Criteria
Begins with
Name or Alias:
Contains
THERMINOL
Equals
Compound class:
All
Molecular weight:
From
To
Boiling point:
From
To
C
Find Now
New Search
Help
Compounds found matching the specified criteria
Compound name
Alias
Databank
Alternate name
MW
BP <C>
CAS number
Compound class
THERMINOL-44
THERM44
APV100.PU
367
389.9997
THERMINOL-55
THERM55
APV100.PU
320
350.9999
THERMINOL-60
THERM60
APV100.PU
250
393.8886
THERMINOL-66
THERM66
APV100.PU
252
358.9999
THERMINOL-77
THERM77
APV100.PU
230
THERMINOL-FR-0
THERMFR0
APV100.PU
350
Add selected compounds
Matches found: 10 (11 seconds)
Close

APPENDIX C: SOLIDWORK 3D DESIGN OF OVER ALL THE SYSTEM